INVESTIGATING A ROLE FOR THE ACTIN NUCLEATOR CORDON-BLEU IN BRUSH BORDER ASSEMBLY

By

Nathan Eric Grega Larson

Dissertation

Submitted to the Faculty of the

Graduate School of Vanderbilt University

in partial fulfillment of the requirements

for the degree of

DOCTOR OF PHILOSOPHY

in

Cell and Developmental Biology

December, 2016

Nashville, Tennessee

Approved:

James R. Goldenring, M.D.

Kathleen L. Gould, Ph.D.

Irina Kaverina, Ph.D.

Ryoma Ohi, PhD.

Matthew J. Tyska, Ph.D.

For Allie and Charlie

ACKNOWLEDGEMENTS

discussions. Janice Williams in the Electron Microscopy Core has helped my immensely in the last few years of my time here with various projects, and has always been a pleasure to work with. Also, the CDB staff members who work behind the scenes to students lives run smoothly must also be recognized.

Finally, I must thank my family for the love and support they have given me throughout my life; without them I would not be where I am today. First I must acknowledge to my mom, who passed away just before I started at Vanderbilt, but was always supportive of my love for science and whose immense love I still feel with me today. Also, the love and support I have had from my dad and stepmom in just about every way imaginable during my time in graduate school has been critical in helping me through Graduate School. Lastly, I must thank my wife Allie and son Charlie for bringing me immense joy outside of the lab; this would not have been possible without the two of you; I love you both so much.

TABLE OF CONTENTS

III. CORDON BLEU PROMOTES THE ASSEMBLY OF BRUSH BORDER MICROVILLI

IV. IMPACT OF CORDON BLEU EXPRESSION ON ACTIN CYTOSKELETON
    ARCHITECTURE AND DYNAMICS 67

V. FUTURE DIRECTIONS PART I.
   INITIAL CHARACTERIZATION OF THE INTESTINAL BRUSH BORDER OF THE
   SYNDAPIN-2 KNOCKOUT MOUSE..87

LIST OF FIGURES

LIST OF ABBREVIATIONS

ADP   Adenosine diphosphate

APC   Adenomatous polyposis coli

ARP 2/3 Actin-related protein

ATP   Adenosine triphosphate

BAR   Bin-Amphiphysin-Rvs161/167

BB   Brush border

COBL Cordon-bleu

CC   Coiled-coil

DAD Dia autoregulatory domain

DID   Dia Inhibitory domain

EGFP Enhanced Green Fluorescent Protein

EPS8 Epidermal growth factor receptor pathway substrate 8

ER   Endoplasmic reticulum

F-actin Filamentous actin

FAM65b Family with sequence similarity 65 member B

F-BAR Fes-CIP4 homology-BAR

FH1   Formin homology 1

FH2   Formin homology 2

FLPs finger-like protusions

FMN2 Formin-2

G-actin Globular actin

GTP   Guanosine triphosphate

I-BAR	Inverted- Bin-Amphiphysin-Rvs161/167
IEC	Intestinal epithelial cell
IRSp53	Insulin receptor substrate protein of 53 kDa
INF2	Inverted formin-2
JMY	Junction Mediating and Regulatory protein
KD	Knockdown
KIND	Kinase non-catalytic C-lobe domain
KO	Knock out
LASER	Light amplification by stimulated emission of radiation
LKB1	Liver kinase B1
NPF	Nucleation promoting factor
N- WASP	Neural Wiskott Aldrich syndrome protein
PACSINs	Protein kinase C and casein kinase II interacting proteins
PRD	Proline-rich domain
RBD	Rho GTPase binding domain
SEM	Scanning electron microscopy
SFB	Segmented filamentous bacteria
SH3	Src homology 3
SIM	Structured illumination microscopy
STRAD	STE20-related kinase adaptor
TEM	Transmission electron microscopy
TIRF	Total internal reflection fluorescence
TOCA-1	Transducer of Cdc42-depenent actin assembly protein 1
TRIOBP	TRIO and F-actin binding protein
UtrCH	Utrophin Calponin homology
VASP	Vasodilator-stimulated phosphoprotein
WASP	Wiskott-Aldrich syndrome protein

WH2   Wiskott-Aldrich homology 2

WT   Wild-type

XIRP2   Xin Actin-binding repeat containing 2

CHAPTER I.

Introduction

Cell shape dictates function

During their lifespan, some cells undergo constant changes in shape and location in response to cues from their surroundings, while others maintain complex shapes, depending on the role the cell plays in the body. While cell shape is changing or being maintained, the cell must retain complex intracellular organization in order to perform its specific function in the body. A prime example of rapid and continuous cell shape change is provided by migrating cells, such as immune cells ridding the body of infectious bacteria and dying cells. Conversely, polarized epithelial cells maintain distinct apical and basolateral domains to aid in transport and barrier functions, thereby displaying an exquisite model of a cell's ability to maintain a polarized cell shape over time in order to fulfill its function. When the processes controlling cell shape malfunction, the result is often detrimental. For instance, a hallmark of metastatic cancer cells is that they lose the signals responsible for maintaining their normal cell shape. These cancer cells ultimately migrate from their tissue of origin and colonize a different part of the body, where if left untreated, eventually inhibit the function of the tissues colonized. Only by understanding the molecular mechanisms that control normal cell shape can researchers begin to understand what goes wrong in diseases where normal cell shape is compromised. It is for this reason that understanding how cell shape is controlled is such an active and exciting area of cell biology research.

Cell shape is controlled by three classes of proteins: actin, microtubules and intermediate filaments, that collectively make up the cell skeleton, referred to as the cytoskeleton. This introduction will focus on the actin cytoskeleton, with a specific emphasis on actin cytoskeleton assembly. First, the model system that we use to study the actin cytoskeleton, the intestinal brush border, will be introduced to give rationale for why we study the actin cytoskeleton in this system. Then, seminal studies that provide the basis for our understanding of how actin filaments alone assemble into dynamic units will be discussed. Finally, more complexity will be added by discussing the mechanisms actin assembly factors employ to regulate filament assembly *in vitro* and in several cellular contexts. The overall goal of this introduction is to offer context for why our studies on the actin nucleator cordon-bleu (COBL) have advanced the field of actin cytoskeletal biology and epithelial cell biology.

Intestinal epithelial cells as a model for studying cell shape

The function of an epithelial cell layer is to provide a barrier between the outside world and the organism, while simultaneously allowing for the exchange of molecules between the organism and environment (Guillot and Lecuit, 2013). Intestinal epithelial cells, the majority of which are 'enterocytes', are the sole cell type responsible for nutrient absorption in the body. Enterocytes are born at the base of the Crypts of Lieberkuhn (crypt) from asymmetric cell division of intestinal stem cells; these cells then undergo more rounds of cell division in the transit amplifying zone of the crypt, migrate onto and up the villus, and are ultimately sloughed off into the lumen (van der Flier and Clevers, 2009). Villi are finger-like folds of tissue that protrude into the lumen of the gut, that
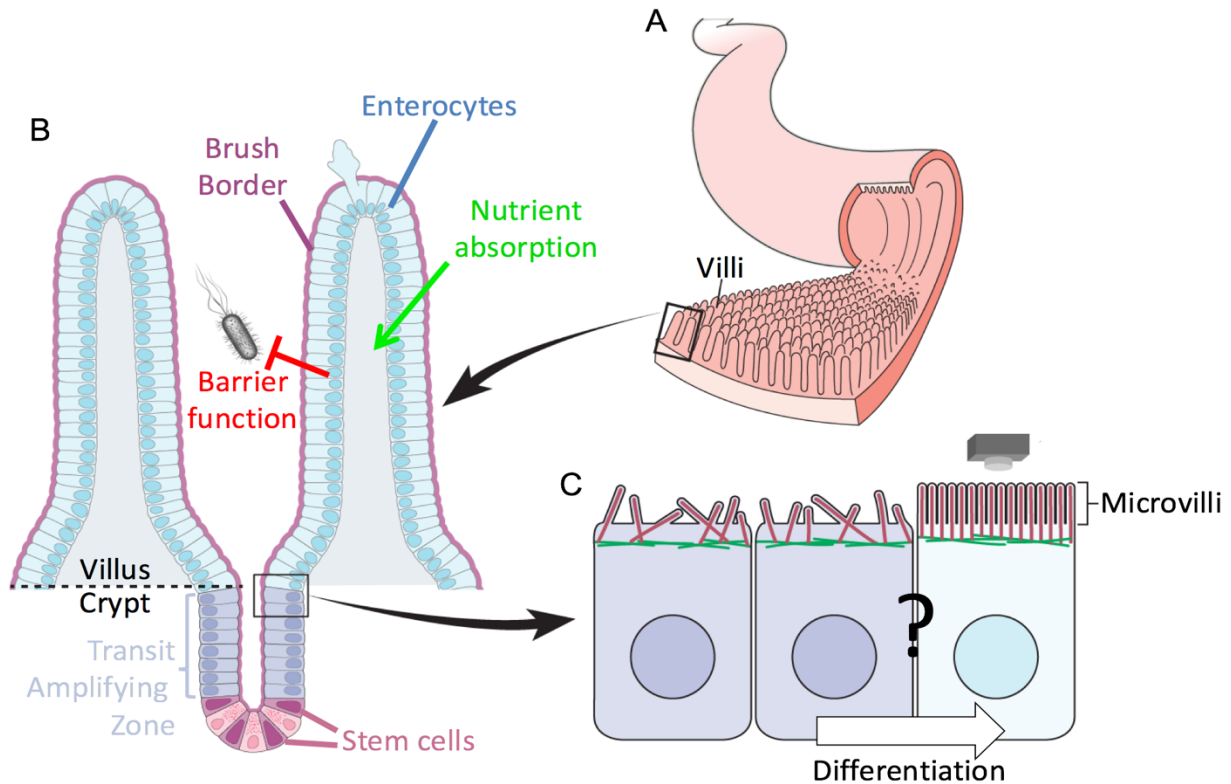
Figure 1-1: Schematic of the intestinal epithelium: A) view of the lining of the small intestine highlighting the villi. B) Cross section of the crypt-villus axis highlighting its functions. C) Zoom of box in B highlighting enterocyte differentiation and brush border assembly as cells move from the crypt to the villus. Adapted from (Crawley et al., 2014a).

function to increase the surface area of the intestine to allow for the maximal uptake of nutrients that pass through the intestine (Fig. 1-1) (Helander and Fandriks, 2014).

Enterocytes provide an excellent model for studying the processes that control cell shape (Crawley et al., 2014a). All epithelial cells are considered 'polarized', that is, they have distinct membrane composition on different sides of the cell termed the basolateral membrane and the apical membrane (Roignot et al., 2013). In the context of the enterocyte, the apical membrane is exposed to the lumen of the intestine, while the basolateral membrane is in contact with basal lamina. This polarized system allows for

transport of nutrients from the lumen, through the cell and underlying mucosa, and ultimately the circulatory system to supply the rest of the body with nutrients.

The apical domain of enterocytes is composed of tightly packed microvilli, finger-like protrusions of membrane of uniform length (1-3 μm depending on location) supported by a core bundle of actin filaments. Collectively, these microvilli make up a domain termed the 'brush border' (BB). The BB serves to further increase the amount of plasma membrane exposed to the intestinal lumen, and is packed with enzymes and transporters that function in nutrient uptake (Maroux et al., 1988). In addition to nutrient absorption, the BB provides a barrier that prevents the bacteria and bacterial products that reside in the gut lumen from entering the host (Peterson and Artis, 2014). Amazingly, the BB acts not just as a passive barrier in this process, but rather actively releases vesicles from the tips of microvilli that are enriched various molecules, including the enzyme intestinal alkaline phosphatase (McConnell et al., 2009; Shifrin et al., 2012). The main role of intestinal alkaline phosphatase is to inactivate lipopolysaccharide found on the surface of bacteria, thereby preventing an immune response from the host and allows for the necessary commensal relationship between the intestinal microbiome and the host (Fawley and Gourlay, 2016).

Despite the critical role that the BB plays in nutrient absorption and host defense, the mechanisms underlying BB assembly are relatively uncharacterized. Therefore, the focus of our lab in recent years has been to uncover the molecular mechanisms employed by enterocytes to assemble and maintain BB structure and function(Crawley et al., 2014b; Crawley et al., 2016; Grega-Larson et al., 2015; Weck, 2016). By studying the normal processes used by enterocytes to assemble microvillar actin bundles, we hope to better

understand what goes wrong in assembling and maintaining BB microvilli in diseases characterized by brush border effacement such as celiac disease, Crohn's disease and microvillus inclusion disease, as well as enteropathogenic *E. coli* infection. Because of the central role actin plays in supporting BB microvilli, my research has focused on how the actin filament bundle that supports microvilli is assembled. To begin to comprehend how microvillar actin filaments are assembled, it is necessary to understand some of the intrinsic properties of actin that govern actin filament formation.

Actin structure and biochemistry

Actin is the most abundant protein in almost all eukaryotic cells and is present in two distinct states, globular (G)- and filamentous (F). ATP binds a cleft in the actin monomer, and ATP bound G-actin is the physiologically relevant G-actin species in cells. The process of F-actin assembly from G-actin is termed actin polymerization, whereby G-actin assembles into a double helical structure through head to tail interaction of individual monomers, resulting in an actin filament with inherent polarity. Because the number of bonds that form between dimers and trimers of actin monomers provide insufficient stability to these small complexes, spontaneous assembly of actin filaments from G-actin monomers is unfavorable; however, once polymerization begins and the filament stabilizes, growth progresses rapidly (Fig. 1-2) (Pollard and Borisy, 2003).

Due to the intrinsic polarity of the actin filament, each end of the filament displays different polymerization rates for ATP-G-actin. This was shown experimentally by incubating short actin filament seeds decorated with the S1 fragment of muscle myosin with G-actin and then visualizing the filaments using electron microscopy (Woodrum et al., 1975). The S1 fragment is composed of the actin binding motor domain of the myosin,
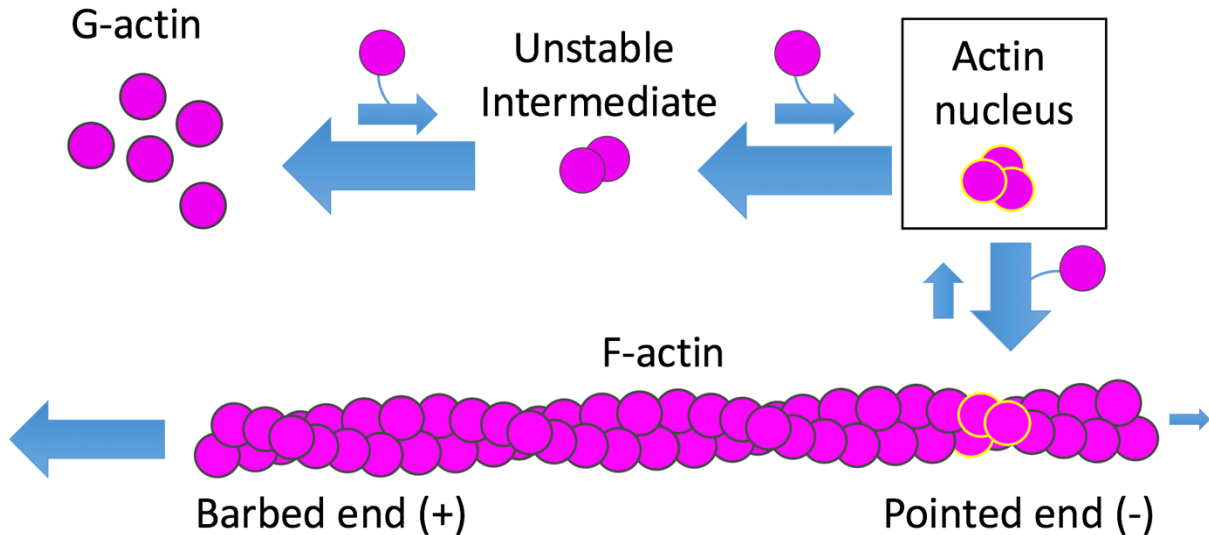
Figure 1-2: **Cartoon depicting the process of actin polymerization**. Box highlights the formation of the actin nucleus, the rate limiting step in the transition from G-actin to F-actin.

and when S1 is bound to actin filaments, the filament appears pointed at one end and barbed at the other end when visualized by negative stain electron microscopy. In these experiments, G-actin addition at the barbed end of the actin filament seed was always 4-8 fold faster than at the pointed end, suggesting polymerization is faster at the barbed end of actin filaments. Since these rates depend on the probability of actin monomers colliding with the ends of the filament, the rates are dependent upon the concentration of actin in solution.

Elegant experiments visualizing actin assembling off of core microvillar actin bundles isolated from intestinal BB samples provided the opportunity for the first measurements of actin polymerization rate constants for each end of the actin filament (Pollard and Mooseker, 1981). In these experiments microvillar actin bundles were incubated with defined concentrations of G-actin, and then the resulting filaments were labeled with the S1 fragment of myosin-2 to mark polarity. Then, by imaging these structures using electron microscopy and measuring filament lengths at fixed time points,

rate constants for actin polymerization were determined. Several years later, this initial study was repeated more rigorously using acrosomal processes from horseshoe crab sperm (Pollard, 1986). Ultimately, by taking the quotient of the dissociation rate and the association rates measured from these assays, the critical concentration, defined as the concentration at which no net growth or shrinkage occurs, was determined for each end of the filament. For ATP-actin, the critical concentration for at the barbed end was found to be 0.12 μM, while the critical concentration at the pointed end was measured as 0.6 μM. Because the critical concentration is lower at the barbed end, polymerization occurs more rapidly at the barbed end than at the pointed end. This also implies that at steady state, monomers will add to the barbed end and dissociate from the pointed end. Satisfyingly, more recently the polymerization of actin filaments was visualized in real time, and this study confirmed the rate constants originally proposed twenty years earlier (Amann and Pollard, 2001).

As mentioned above, the physiologically relevant species of G-actin in cells is ATP-G-actin. G-actin has very low intrinsic ATPase activity, however once incorporated into a filament, conformational changes in actin lead to irreversible ATP hydrolysis approximately 2-3 seconds after incorporating into the filament (Blanchoin and Pollard, 2002; Rould et al., 2006). ADP·Pi persists within the actin filament for much longer (approximately 6 minutes) before the γ phosphate is released leaving ADP-actin. ADP-actin displays lower affinity for its neighboring actin monomers than ATP-actin, making ADP-actin more likely to dissociate from either end of the filament (Pollard, 1986). Ultimately, the rate constants determined for each end of the actin filament, coupled with ATP hydrolysis, predict that at steady state, ATP-actin adds to the barbed end of the actin

filament and ADP-actin dissociates from the pointed end. This process by which these monomers move from the barbed to the pointed end of a filament is termed 'treadmilling.' While treadmilling may be relevant in some instances, it is too slow to explain the actin dynamics seen in many cellular processes, such as cell motility (Pollard and Borisy, 2003). These processes can only be explained by the concerted effort of many different actin binding proteins in cells that modulate intrinsic filament dynamics.

Actin binding proteins that nucleate, elongate, bundle, cap, sever, sequester and regulate actin filaments in various ways in cells are numerous, and the list continues to grow (Pollard, 2016). The controlled interactions of these proteins with actin and each other gives rise to the dynamic actin networks and structures necessary for the function of various cell types. Because my studies have focused on the actin nucleator COBL, the next sections will focus first on the three classes of actin filament nucleators in cells that initiate filament assembly.

Actin nucleation

The process of nucleating actin filaments is highly regulated in cells because although the critical concentration for the assembly of actin filaments from monomers is low, actin filament assembly is energetically demanding (Skau and Waterman, 2015). Because, as discussed earlier, the formation of an actin nucleus is the rate limiting step in F-actin assembly, cells employ proteins termed actin nucleators to catalyze the formation of actin nuclei in cells when and where filament formation is needed.

Intriguingly, the concentration of actin in cells is estimated to be approximately 50 μM (Pollard et al., 2000), much higher than the critical concentration above which all G-actin in solution assembles into filaments. Why then do actin filaments not spontaneously

assemble in cells? The answer is due to the fact that the majority of G-actin in cells is sequestered by proteins that inhibit spontaneous nucleation. The protein thymosin β-4 sequesters ATP-G-actin and prevent actin nucleators from using bound actin monomers for assembly new filaments (Safer and Nachmias, 1994). The profilin family of proteins also sequesters ATP-bound actin monomers and competes with thymosin β-4 for actin monomers (Carlsson et al., 1977); however, profilin also acts as a nucleotide exchange factor for G-actin, thereby maintaining the pool of polymerization favorable ATP-G-actin in cells (Kang et al., 1999). Also, profilin, by binding to proline rich domains of different actin nucleators, also shuttles actin monomers to actin nucleators that are used to build assembly competent actin nuclei when and where filament formation is needed in cells (Paul and Pollard, 2008). The three classes of actin nucleators found in cells are the Arp2/3 complex, formins, and the tandem WH2-domain containing class of nucleators that includes spire and COBL (Fig. 1-3).

Arp2/3 complex

The Arp2/3 complex was the first identified as a profilin interacting protein that promoted actin assembly (Machesky et al., 1997). Shortly thereafter, the complex was purified and shown to be critical a critical factor for motility of the pathogenic bacterium *Listeria monocytogenes* in cell extracts (Welch et al., 1997). It was the first nucleator discovered, and it is also the best characterized nucleator, both biochemically and with regard to its cellular functions.

A multitude of *in vitro* studies have revealed that the Arp2/3 complex binds to the side of a preexisting (mother) actin filament and nucleates the formation of a new

(A) Actin mimics (Arp 2/3 complex)

Nucleation promoting factor

Arp 2/3 complex

G-actin

F-actin

PM

70°

C
A

(B) Formins

1)

FH2

FH1

FH1

FH2

2)

FH1

FH1

FH1

FH2
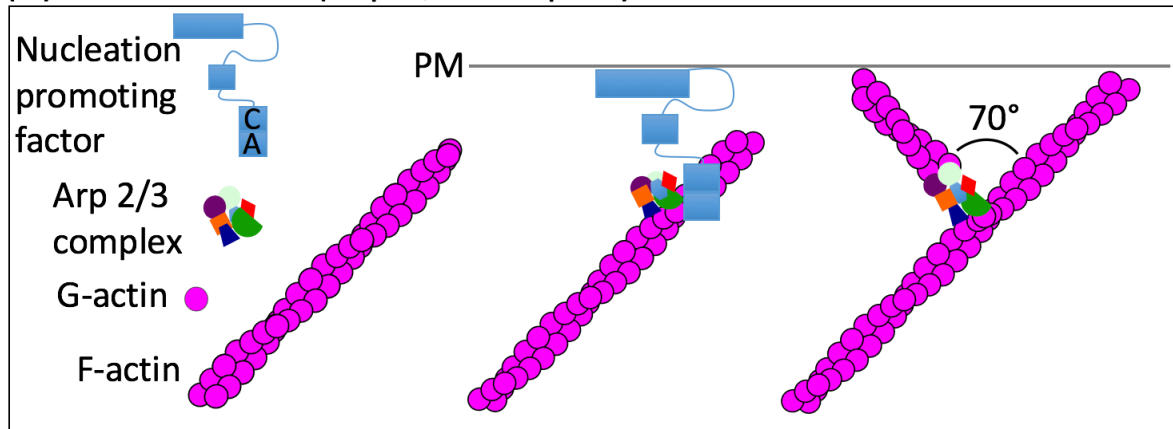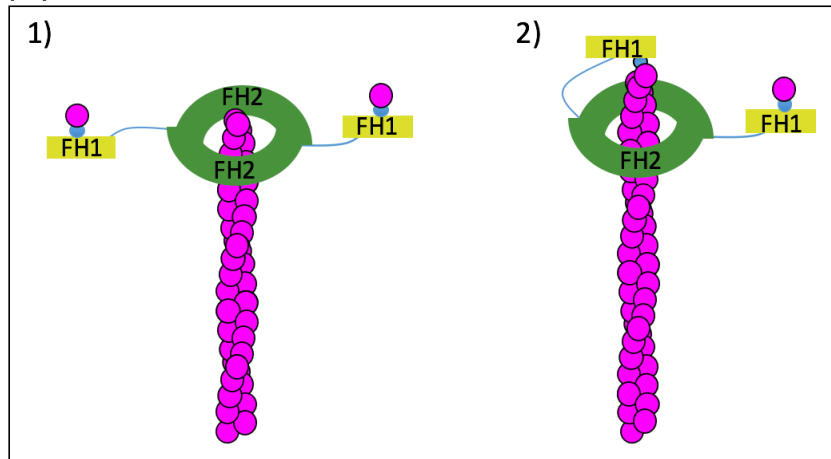
(C) Tandem WH2 domain-based

Spire

COBL

W
W
W
W

W   W
W
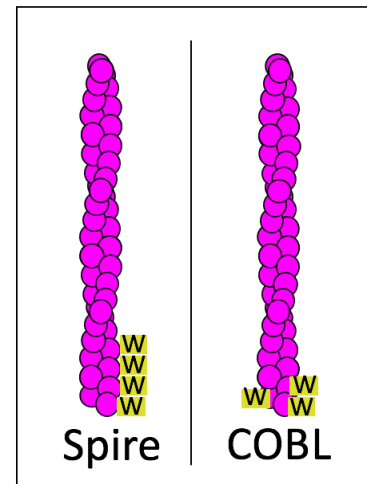
Figure 1-3: **Models of the mechanisms by which the three classes of actin nucleators nucleate actin filaments.** Adapted from (Campellone and Welch, 2010).

(daughter) filament that branches off of the mother filament at a 70° angle (Fig. 1-3A) (Pollard, 2007). The Arp2/3 complex is composed of seven subunits, two of which (ARP2 and ARP3) act as actin mimics, while the other five subunits function to position ARP2 and ARP3 on the mother filament (Rotty et al., 2013). Actin nucleation by the Arp2/3 complex alone is inefficient (Higgs and Pollard, 1999), and nucleation in cells is dependent upon activation by a family of proteins termed nucleation promoting factors (NFPs). NPFs in their inactive state cannot bind to the Arp2/3 complex; but rather are

activated by binding to Rho family GTPases which relieves autoinhibition of the NPF. Once activated, NPFs bind simultaneously to the Arp2/3 complex, priming it for nucleation, and profilin bound ATP-G-actin, which the NPF shuttles to the ARP2 and ARP3 subunits. This creates a complex that mimics an actin nucleus, from which actin polymerization occurs readily.

In cells, the Arp2/3 complex is involved in many processes including cell motility, endocytosis, phagocytosis, vesicle trafficking, junctional complex formation, cytosolic streaming, and podosome and invadopodia formation (Rotty et al., 2013). Thus, it is not surprising that ArpC3 -/- mutant mice, which lack a functional Arp2/3 complex, experience early embryonic lethality at the implantation stage due to defects in trophoblast outgrowth (Yae et al., 2006). The discovery of small molecules that reversibly inhibit the Arp2/3 complex has identified roles for the Arp2/3 complex in processes that can only be visualized in real time (Nolen et al., 2009; Yang et al., 2012; Yi et al., 2011), and will undoubtedly reveal other Arp2/3 dependent cellular processes in the future.

Formins

The second class of actin nucleators discovered are the formin family of proteins. In contrast to the Arp2/3 complex, formins form homodimers that nucleate and elongate linear actin filaments by processively tracking with the barbed ends of growing actin filaments (Fig. 1-3B) (Qualmann and Kessels, 2009). Formin domain structure can be loosely divided into two functional regions, an N-terminal regulatory region and a C-terminal active region (Chesarone et al., 2010). The regulatory region generally consists of a Rho GTPase binding domain (RBD), a Dia inhibitory domain (DID) and dimerization domain. The active region consists of formin homology 1 and 2 (FH1 & FH2) domains, as

well as a Dia autoregulatory domain (DAD), which binds back on the N-terminal DID to provide autoinhibition. As in the case of the NPFs of the Arp2/3 complex, autoinhibtion is relieved upon binding of a Rho GTPase family member to the N-terminal RBD, which elicits conformational changes that expose the active region for nucleation and elongation.

Formins nucleate and elongate actin filaments using the FH1 and FH2 domains, and the FH2 domain dimer is sufficient to nucleate actin filaments *in vitro* (Sagot et al., 2002)*.* Interestingly, the FH2 domain does not bind actin monomers, but is thought to nucleate actin filaments by stabilizing unstable actin dimers and trimers. It is also thought that elements C-terminal to the FH2 domain may play a role in enhancing the nucleation activity of some formins (Lu et al., 2007; Paul and Pollard, 2008). The FH1 domain is unstructured and contains binding sites for profilin; thus, the FH1 domain functions to feed profilin-bound ATP-actin monomers to the growing barbed ends of FH2 bound actin filaments.

One exciting area of research in the formin field involves the crosstalk between mictrotubules and formin assembled actin filaments. Microtubules, like actin filaments, are polarized, with plus and minus ends (Howard and Hyman, 2003). Recent *in vitro* reconstitution work from the Goode Lab has shown that the microtubule binding protein CLIP-170 enhances the rate of actin filament elongation by the formin mDia1 (Henty-Ridilla et al., 2016). CLIP-170-mDia1 complexes bind to the sides of microtubules, however, when the microtubule plus-end protein EB1 was added to the reaction, this complex localized to the plus-ends of microtubules. Remarkably, actin and microtubule dynamics were co-reconstituted *in vitro*, and mDia1 nucleated actin filaments were grown

off the tips of microtubule plus ends, with mDia1-CLIP-170 complexes processively tracking actin filament barbed ends. Clearly, as the authors point out, the next step is to examine where these complexes form *in vivo* and determine if they are required for processes known to require crosstalk between the actin and microtubule cytoskeletons such as directed cell migration and cell division (Rodriguez et al., 2003).

Tandem WH2-domain containing actin nucleators

The most recent class of actin nucleators are the tandem WH2-domain containing actin nucleators (Fig. 1-3C) (Ahuja et al., 2007; Quinlan et al., 2005). This next section will first introduce the general features of WH2 domains, and then discuss what is known about the tandem WH2-domain containing actin nucleators spire and COBL.

WH2 domains are 5 kDa protein stretches that bind G-actin. While these domains are highly variable in sequence, they are generally defined as having one of two functions. (1) A WH2 domain is defined as a sequestering domain if its complex with G-actin is unable to polymerize in filaments. (2) A WH2 domain acts as a functional homologue of profilin, a protein that promotes the addition of G-actin onto filaments, if its complex with G-actin is able to still participate in filament assembly (Didry et al., 2012). Upon binding G-actin, the N-terminus (12-29 AA in length) of the WH2 domain folds into an amphipathic α-helix that binds a hydrophobic cleft between subdomains 1 and 3 of G-actin (Fig. 1-4). The only conserved protein sequence across WH2 domains is a central LKKT/V motif which, when mutated, greatly lowers the affinity of the domain for
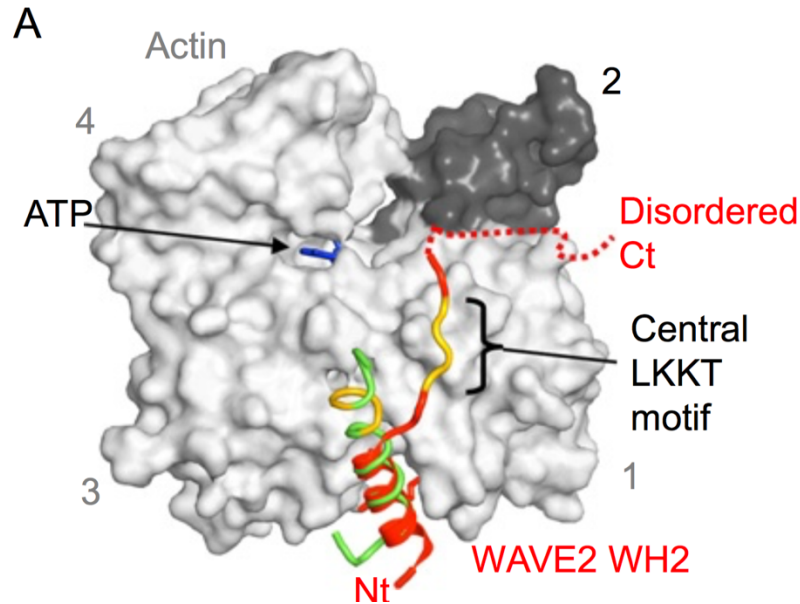
Figure 1-4: **The WH2 domain of WAVE2 in complex G-actin**, highlighting the general features of the interaction. Adapted from (Carlier et al., 2011).

G-actin (Carlier et al., 2011; Chaudhry et al., 2010) (Fig. 1-4). The C-terminal portion of the WH2 domain (4-25 AA in length) imparts either the assembly-promoting or sequestration actions of the WH2 domain. In actin-sequestering proteins, this C-terminal region strongly associates with G- actin. In contrast, WH2 domain containing proteins that promote filament assembly have WH2 domains with C- termini that weakly interact with G-actin (Didry et al., 2012). When WH2 domains are expressed in repeats as in the proteins COBL and spire, WH2 domains function together to modulate filament growth, and/or to nucleate, cap and sever actin filaments (Husson et al., 2011) (Quinlan et al., 2005; Renault et al., 2008). Understanding how protein-specific WH2 domains act differently on actin will lend key insight into our understanding of how the WH2 domain evolved to carry out distinct functions. In contrast to the Arp2/3 complex and formins, relatively little is known about the tandem WH2-domain containing nucleators spire and

COBL; however, the physiological roles that have been identified for these proteins and their mechanisms of actin nucleation are discussed below.

Spire

Spire was first identified in a *Drosophila* mutagenesis screen for female sterility mutations where it was found to be required for both oogenesis and embryogenesis (Manseau and Schupbach, 1989). Later, bioinformatics results combined with yeast two-hybrid analysis identified four sequences in spire with similarity to the WH2 domain of the Arp2/3 NPF N-WASP that bound G-actin (Wellington et al., 1999). Spire was first shown to function as an actin nucleator in pyrene-actin assembly assays, a function dependent on its four WH2 domains and a small actin binding motif conserved among spire proteins (Quinlan et al., 2005). Since its identification as an actin nucleator, several studies have characterized a critical direct interaction between *Drosophila* spire and the fly ortholog of formin-2 (FMN2), cappuccino, that is required to enhance actin filament formation and crosslink actin and microtubules at the oocyte cortex (Dahlgaard et al., 2007; Liu et al., 2009; Quinlan et al., 2007; Rosales-Nieves et al., 2006). Interestingly, mFMN2 and spire-1 have a nearly identical expression pattern during mouse embryogenesis and in the adult brain, suggesting that this complex is evolutionarily conserved (Schumacher et al., 2004).

More recently, several novel roles for formin-spire complexes have emerged. The FMN2-spire complex assembles nuclear actin filaments required for efficient DNA repair (Belin et al., 2015). Additionally, a mitochondria-anchored isoform of spire, spire1C, has been shown to interact with the ER-anchored formin INF2 to regulate mitochondrial division (Manor et al., 2015). Finally, spire2 and FMN2 were shown to interact with

myosin-Va and rab11 on membranes to form a complex thought to regulate the assembly

of F-actin tracks necessary for vesicular trafficking in cells (Pylypenko et al., 2016).

The domain structure of spire is made up of an N-terminal KIND domain which

interacts with the C-terminal tail of formins (Vizcarra et al., 2011), four central WH2
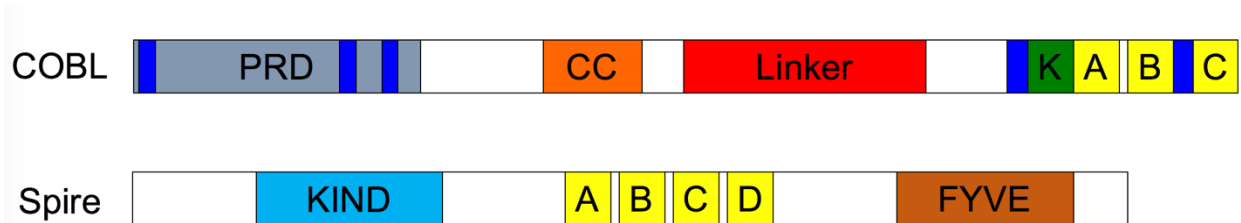
Figure 1-5: Domain diagrams of human COBL and *Drosophila* spire. COBL is 1261 A.A. and spire is 991 A.A. COBL domains include a proline rich domain (PRD, 1-351), a coiled coil (CC, 486-515), a linker (573-821), a lysine rich region (K, 1081-1096), and three WH2 domains (A, B and C, 1109-1261). Spire domains include the KIND domain (90-333), four WH2 domains (A, B, C, and D, 369-482) and a FYVE domain (700-962).

domains which nucleate F-actin (Quinlan et al., 2005), and a C-terminal FYVE domain

which promiscuously interacts with negatively charged lipids (Tittel et al., 2015) (Figure

1-5). Spire, because of the short linkers between its WH2 domains, was first proposed to

nucleate actin filaments by stabilizing a linear array of actin monomers along the long

pitch of an actin filament helix (Quinlan et al., 2005), and an X-ray scattering study of actin

nuclei assembled by the four WH2 domains of spire supports this model (Rebowski et al.,

2008). However, it has also been noted that the stabilized long pitch helix of a double

stranded actin filament is not an efficient way to catalyze nucleation (Sept and

McCammon, 2001). Thus, it is thought that in cells, spire dimerization through its

interaction with formins efficiently nucleates actin filaments by simultaneously recruiting

actin monomers along the two parallel strands of the actin filament (Dietrich et al., 2013).

This hypothesis is supported by the fact that by artificially dimerizing the WH2 domains

of spire, actin nucleation activity is significantly increased *in vitro* (Namgoong et al., 2011). A cellular role for spire independent of formins remains to be found, although if its interaction with formins is required to dimerize spire and turn it into an efficient nucleator, it is likely that spire only acts in complex with formins in cells.

COBL

COBL is the less well characterized of the two tandem WH2-domain containing actin nucleators. COBL was first identified in a gene trap study in mouse embryonic stem cells as a gene that is expressed during early mouse embryogenesis (Gasca et al., 1995). It was noted that the expression of COBL was very similar to HNF3β and sonic hedgehog. Thus, it was proposed that COBL may play an important role in the pathway regulating vertebrate axis formation. The COBL gene was subsequently cloned, revealing that COBL is highly conserved among vertebrates, however no conserved protein domains, except for three WH2 domains at its C-terminus, were identified (Carroll et al., 2003). COBL was identified as an actin nucleator in 2007, a function which required the WH2 domains of COBL, and overexpression or depletion of COBL in cultured neurons resulted in significant increases or decreases in neurite outgrowth and dendritic arborization, respectively (Ahuja et al., 2007). The first essential role discovered for COBL *in vivo* was in the proper assembly of motile cilia in zebrafish, where loss of COBL led to defects in left-right patterning of the embryo due to short, non-functional motile cilia in the Kupffer's vesicle (Ravanelli and Klingensmith, 2011). Subsequently, COBL was shown to be necessary for the appropriate development of ciliated sensory hair cells in zebrafish, futher supporting a role for COBL in building the actin structures necessary for the proper function of ciliated cells (Schuler et al., 2013).

COBL function is dependent on the F-BAR domain containing syndapin family of proteins in several contexts. COBL binds to syndapin 1, 2 and 3 through an interaction between the N-terminal PxxP motifs of COBL and the SH3 domain of each syndapin Figure 1-5) (Schwintzer et al., 2011). Through its membrane-binding F-BAR domain, syndapins are thought to target COBL to sites at cellular membranes where actin nucleation is required. In neurons, syndapin-1 is critical for targeting of COBL to sites of neurite outgrowth, where COBL and the actin binding protein abp1 drive actin assembly in neurites (Haag et al., 2012; Schwintzer et al., 2011). Similarly, the data presented in this thesis shows that syndapin-2 is required to target COBL to sites of nascent microvillar outgrowth in intestinal epithelial cells, where COBL promotes the assembly of intestinal BB microvilli (Chapter III) (Grega-Larson et al., 2015). In contrast, COBL was proposed to target syndapin-2 to microvilli in placental epithelial cells, although clear evidence was lacking in this case (Wayt and Bretscher, 2014).

The mechanism of actin nucleation by COBL is still not clear. It was first thought that because of the 68 amino acid long linker between the second and third WH2 domain, that all three WH2 domains of COBL participate in bringing together a short pitch actin trimer for nucleation (Figure 1-4C and 1-5). When this linker was replaced with a 15 amino acid linker, nucleation activity was abolished when measured by pyrene actin assembly assays (Ahuja et al., 2007). However, a subsequent study showed that nucleation by COBL only required the first WH2 domain and a short lysine-rich sequence immediately N-terminal to the WH2 domains (Husson et al., 2011). The nucleation activity was unchanged when the lysine rich region was included with two or three WH2 domains, suggesting that the same mechanism for nucleation was used for fragments containing

one, two or three WH2 domains and the lysine-rich region. The lysine-rich sequence was also present in the first study; however, its importance was not realized. When the lysine-rich region was not included, the WH2 domains alone only functioned to sequester actin monomers. The major surprise was that COBL fragments containing the lysine-rich region and two or three WH2 domains, in addition to nucleation, also induced actin filament severing, depolymerization, and sequestration of ADP-actin. It is also important to note that the nucleation activity of COBL is lower than formins and spire, suggesting that there may be other factors that enhance the nucleation activity of COBL in cells (Carlier et al., 2011). The studies presented in chapters III and IV of this thesis suggest that filament severing by COBL, in addition to nucleation, may play a functional role in cellular contexts.

Actin nucleation is only the first step in generating the actin filament networks that give cells their shape. While cells organize the actin cytoskeleton in many ways in order to give rise to many different cell shapes, there are two fundamental actin networks that make up the actin cytoskeleton in cells; short, branched networks and linear networks. Generally, branched actin networks are loosely crosslinked and highly dynamic; it is this dynamic actin network that is responsible for cellular motility. In contrast, linear networks are composed of longer actin filaments crosslinked by bundling proteins, and are much more stable in comparison to branched networks. Actin filaments in linear networks can be oriented with their barbed and pointed ends all oriented in the same direction (parallel) that together provide a protrusive force. Conversely, actin filaments can be arranged or in opposite orientations (antiparallel) that provide a substrate that can be acted upon by myosin motor proteins to produce contractile force. Since our studies have focused on

actin based protrusions, the molecular mechanisms involved in controlling the actin dynamics in three types of actin based protrusions will be discussed next.

Control of actin assembly in finger-like protrusions

Filopodia, microvilli, and stereocilia are finger-like plasma membrane protrusions (FLPs) supported by parallel bundles of actin filaments (Figure 1-6). In each of these cases, bundled filaments are oriented with fast growing barbed ends toward the protrusion tip. A general paradigm for actin bundle construction invokes coordinated filament nucleation, elongation, and bundling directly at membrane sites designated for protrusion formation (e.g. the leading edge of a motile cell, or the apical domain of a transporting or mechanosensory epithelial cell). Following assembly, FLP maintenance and lifetime are controlled by factors that regulate actin filament turnover. While the molecules controlling these events in filopodia are well studied, factors governing the assembly and maintenance of microvilli and stereocilia are still poorly understood. This section highlights what we know about actin filament assembly in specific structures and points out gaps in our understanding that require additional investigation.

Filopodia

Filopodia are dynamic FLPs that extend into the extracellular space and allow cells to probe the physical and chemical features of their environment (Fig. 1-6A). These structures are composed of 10-30 bundled actin filaments and can reach up to 10 microns in length (Mogilner and Rubinstein, 2005; Svitkina et al., 2003). In response to extracellular signals, phosphatidyl-inositol kinases such as PIPK1α localize to specific sites on the plasma membrane and generate phosphatidyl inositol-phosphate PI(4,5)P$_2$, a critical signaling lipid involved in filopodia assembly (Tolias et al., 2000). Concurrently,
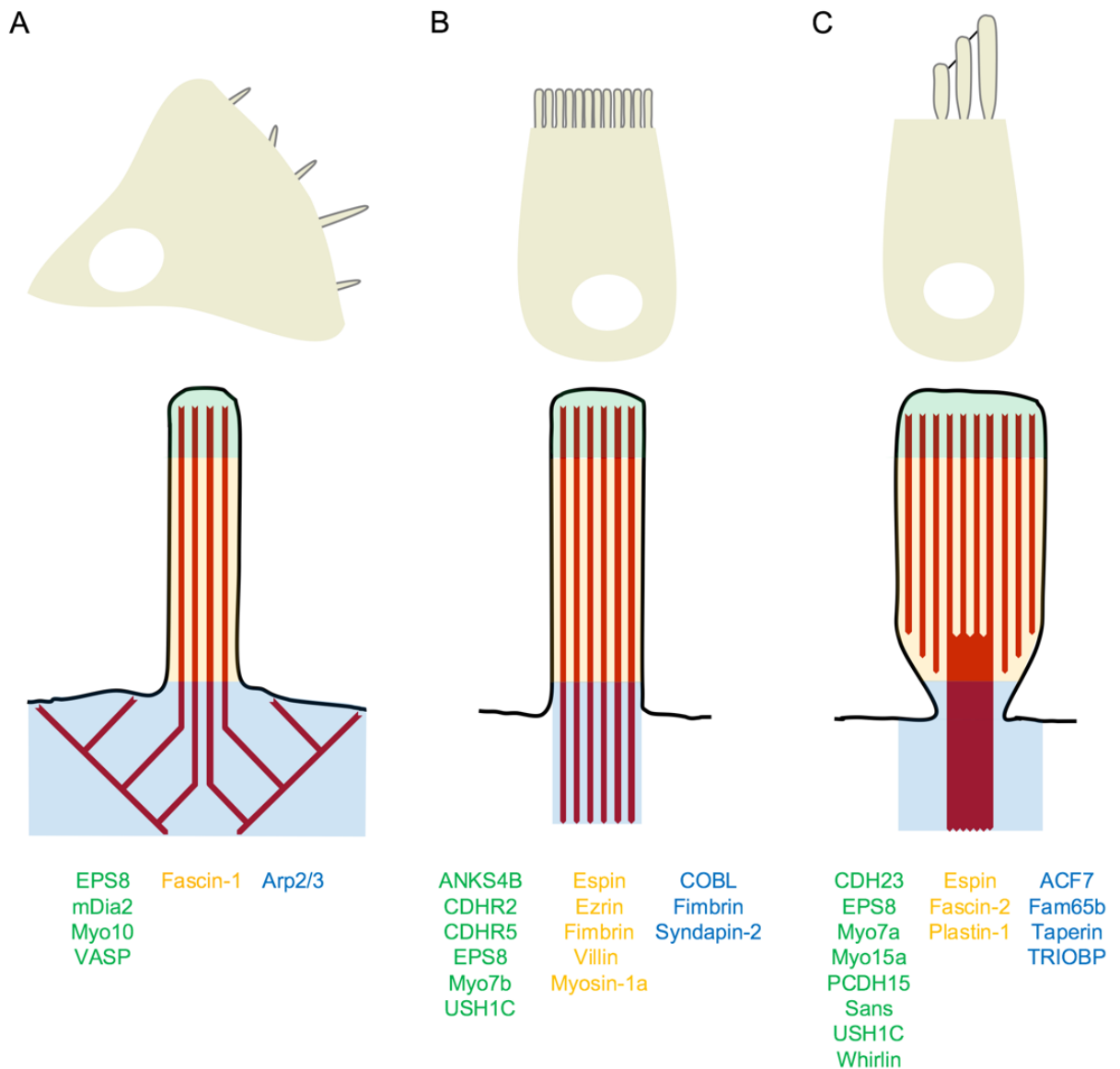
Figure 1-6: Cartoon depiction of the actin networks that support A) filopodia, B) microvilli, and C) stereocilia. Green, orange and blue text depicts molecules that localize to the tip of the protrusion, throughout the protrusion, and at the base of the protrusion, respectively.

the Rho family GTPase Cdc42 binds to newly synthesized $PI(4,5)P_2$ at the plasma

membrane, and this lipid-protein complex activates multiple proteins involved in filopodia

formation such as the Arp2/3 activating proteins WASp and N-WASp (Rohatgi et al.,

1999), formin mDia2 (Peng et al., 2003), the F-BAR protein TOCA-1 (Ho et al., 2004),

and the I-BAR protein IRSp53, which is critical for localizing VASP to nascent filopodia (Disanza et al., 2013). Two models for filopodial assembly have been proposed by different groups, although it should be noted that these models are not mutually exclusive and mechanistic details of assembly are probably cell-type specific. The 'convergent elongation' model suggests that filopodia emerge from a network of branched actin filaments in the lamellipodia, which are initially nucleated by the Arp2/3 complex (Svitkina et al., 2003; Yang and Svitkina, 2011). Following nucleation, a subset of these filaments are protected from capping at their barbed ends through the action of the actin polymerase VASP (Applewhite et al., 2007; Hansen and Mullins, 2010; Lebrand et al., 2004) and formins (Pellegrin and Mellor, 2005; Schirenbeck et al., 2005a; Schirenbeck et al., 2005b), and this promotes their continued elongation. Myosin-X dimers are then able to focus these elongating barbed ends at the membrane in a motor domain dependent manner (Tokuo et al., 2007). Once actin filaments are in close proximity to one another at the membrane, fascin recruitment to these filaments leads to assembly of a parallel actin bundle capable of supporting membrane protrusion (Vignjevic et al., 2006). A second explanation for filopodial assembly is the 'tip nucleation' model (Schirenbeck et al., 2005b). Here, activated formins cluster at the membrane (e.g. mDia2) where they nucleate and elongate actin filaments which are subsequently bundled in parallel by fascin. In both cases, actin monomers incorporate at the tips of the forming filopodial actin bundles and then treadmill through the bundle to the base at a rate of a few microns per minute (Mallavarapu and Mitchison, 1999). There, the actin depolymerization factor cofilin, which preferentially disassembles fascin bundled actin filaments, mediates the recycling of filopodial F-actin back into the cytosolic G-actin pool (Breitsprecher et al.,

2011). Now that the general players in filopodial actin assembly have been determined, future studies must focus on mechanistic differences that give rise to filopodia in different cell types.

Microvilli

Microvilli are FLPs that extend from the apical surface of epithelial cells that line hollow organs (e.g. gut, kidney, lung, inner ear, and gall bladder), and the initial assembly of the actin filaments in microvilli is the focus of this thesis. Although much of what we know comes from studies of intestinal microvilli, factors relevant in this system probably control actin assembly in other types of microvilli as well. A single microvillus is supported by a parallel bundle of 30-40 actin filaments (Fig. 1-6B) (Ohta et al., 2012), which terminates in a subapical network of intermediate filaments known as the 'terminal web' (Hirokawa et al., 1982). Microvillus length can be remarkably uniform within and between cells (0.5-3 μm depending on the tissue); recent studies also suggest this parameter might be regulated by intermicrovillar adhesion (Crawley et al., 2014b; Crawley et al., 2016). While the mechanisms involved in microvillar assembly have been the subject of research for over forty years (Tilney and Cardell, 1970), molecules involved in the nucleation of microvilli were not known until recently. Research presented in this thesis shows that a protein complex containing the F-BAR domain containing protein syndapin-2 and the actin nucleator cordon-bleu may initiate microvillar growth (Grega-Larson et al., 2015; Grega-Larson et al., 2016; Wayt and Bretscher, 2014). However, the molecules that control the elongation of actin filaments in microvilli remain largely unknown and must be the subject of future studies. In this system, espin (Bartles et al., 1998), fimbrin/plastin (Bretscher and Weber, 1980), and villin (Bretscher and Weber, 1979) contribute to actin filament bundling

in a regionalized manner. While villin and espin localize throughout the microvillar actin bundle, fimbrin is enriched in the terminal web where, in addition to bundling actin filaments, it is thought to link the microvillar actin bundle with keratin-19 in the terminal web, eliciting further stabilization of microvilli (Grimm-Gunter et al., 2009). Interestingly, mice lacking all three bundling proteins can still form microvilli, providing strong evidence for additional players (Revenu et al., 2012). The actin binding protein EPS8 is found at the tips of microvilli where it may bundle and cap actin filaments and play a role in controlling length (Croce et al., 2004; Tocchetti et al., 2010). Experiments in cultured polarized epithelial cells show that microvillar F-actin treadmills slowly, with actin incorporating at bundle tips and disassembling at the base (Loomis et al., 2003; Tyska and Mooseker, 2002), but the development of new model systems may allow investigators to revisit these measurements in primary cultures derived from mice or *in vivo* (Sato et al., 2009).

Stereocilia

Stereocilia are large microvillus-derived protrusions arranged in rows of graded height on the apical surface of cochlear and vestibular epithelial cells (also known as 'hair cells') (Fig. 1-6C). These protrusions range from 1 micron in length at the proximal end of the cochlea to 100 microns in length in the vestibular epithelium (Prost et al., 2007). During hair cell differentiation, stereocilia progress through phases of widening and elongation of their core F-actin bundle to ultimately achieve their final shape. A single mature stereocilium is supported by a bundle consisting of hundreds of actin filaments, which tapers at its base, creating the flexural rigidity required for mechanosensory function. The pointed ends of actin filaments in stereocilia bundles are embedded in an actin-rich

meshwork referred to as the 'cuticular plate', which functions to anchor stereocilia (Pollock and McDermott, 2015). Specifically tropomyosin, α-actinin, and XIRP2 function to tightly crosslink actin filaments of the cuticular plate (Francis et al., 2015; Scheffer et al., 2015; Slepecky and Chamberlain, 1985), whereas ACF7 links cuticular plate actin with the underlying microtubule cytoskeleton (Antonellis et al., 2014). While elegant studies from Tilney described in detail changes in stereocilia morphology during development (Tilney et al., 1992; Tilney and DeRosier, 1986; Tilney et al., 1983; Tilney and Saunders, 1983; Tilney et al., 1988; Tilney et al., 1986) (summarized above), our understanding of the molecules that control these precise changes during development and then maintain these structures is lacking. For example, the molecule(s) involved in the nucleation of stereocilia actin filaments are completely unknown. However a number of factors controlling elongation have been identified, including EPS8 (Manor et al., 2011; Zampini et al., 2011) and espin-1 (Salles et al., 2009). Conversely, the bundling proteins fascin-2 (Chou et al., 2011; Perrin et al., 2013; Shin et al., 2010) and fimbrin (Taylor et al., 2015) are dispensible for assembly but required for maintaining normal stereocilia width and height, and TRIOBP, taperin and Fam65b are required for bundling actin filaments specifically in the taper at the stereocilia base where the bundles terminate in the cuticular plate (Kitajiri et al., 2010; Zhao et al., 2016). Additionally, the actin capping protein twinfilin-2 (Peng et al., 2009) as well as gelsolin (Mburu et al., 2010; Olt et al., 2014), an actin severing and capping protein, serve to restrict the length of stereocilia by inhibiting actin polymerization at the tips. Although an early study suggested that the actin bundle of stereocilia treadmills (Rzadzinska et al., 2004), subsequent studies agree that stereocilia actin bundles are stable and actin turnover occurs only at the tips of core

25

bundle actin filaments, suggesting the presence of molecules that block dissociation at the pointed end (Drummond et al., 2015; Narayanan et al., 2015). With the development of a new system for growing and maintaining hair cells in organoid cultures (Liu et al., 2016), as well as advances in stereocilia proteomic analyses that allow for identification of new low abundance proteins and protein complexes (Morgan et al., 2016), research in the stereocilia field is poised to make key advances in the near future.

Summary

Although filopodia, microvilli and stereocilia are all stabilized by a core actin filament bundle, the mechanisms by which the actin bundle is assembled and maintained in each structure is distinct, and in the case of the microvilli that make up the intestinal BB, there are still significant gaps in our understanding. One goal of this thesis is to shed insight into the molecular mechanisms involved in nucleating microvillar actin filament bundles.

We have identified the actin nucleator COBL as a critical regulator of actin assembly in the BB (Chapter III) (Grega-Larson et al., 2015). Polarized COBL localization to the membrane at sites of nascent microvilli is coincident with actin bundle outgrowth, and microvillar assembly is impaired in intestinal epithelial cells lacking COBL. Conversely, intestinal epithelial cells overexpressing COBL have more microvilli, and these microvilli are longer, straighter, and contain significantly more F-actin than control cells. These data together suggest that COBL promotes the assembly of microvilli, most likely by assembling the actin filaments that support them.

Because the mechanism of actin nucleation by COBL is controversial, and because COBL displays multiple activities *in vitro* (nucleation and severing) (Ahuja et al., 2007; Husson et al., 2011), a second focus of our work was to identify what activities of

COBL are relevant in cells. By performing a structure-function analysis using COBL constructs predicted to have no activity, only nucleation activity, or nucleation and severing activity, we identified that, constructs with functional nucleating and severing activities were the most potent inducers of microvillar outgrowth (Grega-Larson et al., 2015). Furthermore, exogenously expressing COBL in non-epithelial cells that do not normally express COBL induced the formation of dynamic actin bundles in the cytoplasm that assemble and disassemble over the course of minutes. Bundles grew from COBL puncta, and accumulation of COBL on these bundles preceded disassembly. Expressing a COBL mutant with normal nucleation activity but deficient in severing led to the formation of bundles that achieved twice the length of bundles forming in cells expressing wild-type COBL (Chapter IV) (Grega-Larson et al., 2016). These data together suggest that in addition to nucleation, the severing activity of COBL is an important activity for fulfilling physiological functions.

Finally, upon noting the tight localization of COBL at the base of the BB, we sought to determine the mechanism by which COBL targets to the BB. The F-BAR domain-containing protein syndapin-2 localizes similarly to COBL in the BB, and syndapin-1 has been shown to target COBL to sites where actin assembly by COBL is needed in neurons (Chapter III) (Grega-Larson et al., 2016; Schwintzer et al., 2011). As in neurons, knockdown of syndapin-2 in intestinal epithelial cells leads to a loss of COBL enrichment in the BB. Thus, we show that COBL targets to the BB by virtue of its interaction with syndapin-2 (Chapter III). Preliminary data show in mice lacking syndapin-2, intestinal BB microvilli are significantly shorter than wild type microvilli (Chapter V). Interestingly, COBL still targets to the BB in syndapin-2 KO mice, albeit less efficiently than in wild-type control

mice, suggesting that other molecules can aid COBL targeting in the absence of syndapin-2. Additionally, the presence of immune cells on the surface of the intestinal epithelium of syndapin-2 KO mice, along with an increase in the number or segmented filamentous bacteria in the ileum of syndapin-2 KO mice, suggests that the barrier function of the BBs of these mice is perturbed.

Our studies are the first to identify an actin nucleator that functions in the assembly of intestinal BB microvilli. Furthermore, these studies provided insight into the mechanism that COBL employs in cells to assemble actin filaments. Finally, our preliminary data suggest that a COBL/syndapin-2 complex is important for assembling and maintaining intestinal BB microvilli not only in isolated cells, but also in the context of the whole animal.

CHAPTER II.

MATERIAL AND METHODS

Cell culture, transfections and lentivirus production

Ls174T-W4 cells (Baas et al., 2004)(generous gift of Dr. Hans Clevers) were cultured in DMEM with high glucose and 2 mM L-glutamine supplemented with 10% tetracycline-free FBS, G418 (1 mg/ml), blasticidin (10 μg/ml), and phleomycin (20 μg/ml). JEG-3 cells and B16F1 cells (ATCC) were cultured in DMEM with high glucose and 2mM L-glutamine supplemented with 10% FBS. All cells were grown at 37°C and 5% CO_2.

For Ls174T-W4 cells, transient transfections were performed using Lipofectamine 2000 (Invitrogen) according to the manufacturer's instructions. Lentivirus particles were generated by co-transfecting HEK293FT cells (T75 flasks at 80% confluency) with 6 μg pLKO.1 shRNA KD plasmids (Open Biosystems, COBL, TRCN0000005530, TRCN0000005531; Syndapin-2, TRCN0000037982) 4 μg psPAX2 packaging plasmid and 0.8 μg pMD2.G envelope plasmid using FuGENE transfection reagent (Roche). Cells were incubated for two days to allow for lentiviral production. Media containing lentivirus was collected and particles concentrated with the addition of Lenti-X concentrator reagent (Clontech). For COBL KD, separate viruses were prepared and concentrated for each shRNA KD plasmid, and then pooled together before transduction to achieve a suitable KD. Lentivirus transduction of Ls174T-W4 cells and rescue of KD was performed as described previously (Gloerich et al., 2012). Briefly, cells were infected with lentiviral shRNAs targeting human COBL on two consecutive days. Two days after the second infection, cells were seeded overnight in the absence or presence of doxycycline. Cells

were then prepared for microscopy, or for SDS-PAGE and immunoblotting. For rescue experiments, cells were transiently transfected two days after the second infection using Lipofectamine 2000 (Invitrogen), induced with 1 µg/ml doxycycline overnight, and fixed the following morning for immunofluorescence.

One day before imaging, B16F1 cells were transfected in a T25 flask at 80% confluency using Lipofectamine 2000 (Invitrogen, 11668) as described by the manufacturer. On the day of imaging, 35 mm glass bottom dishes (In Vitro Scientific, D35-20-1.5-N) were coated with 25 µg/ml laminin (Sigma, L2020) in PBS. B16F1 cells were plated sparsely on laminin-coated dishes (TIRF) or coverslips (SIM) and allowed to adhere for 2 hours before imaging (TIRF) or fixation (SIM).

Immunofluorescence

For Ls174T-W4 cells, cells were first washed once with warm PBS and then fixed with 4% PFA in PBS for 15 minutes at 37°C. Following fixation, cells were washed three times with PBS and permeabilized with 0.1% Triton X-100/PBS for 15 minutes at room temperature (RT). Cells were then washed 3X with PBS and blocked for one hour at 37°C in 5% BSA/PBS. Primary antibodies anti-COBL (1:100, HPA019033, Sigma), anti-syndapin-2 (1:200, HPA049854, Sigma), or anti-GFP (1:200, Aves, GFP-1020) were diluted in PBS and incubated with cells at 37°C for 2 hours, followed by 4 washes with PBS. Cells were then incubated for one hour with goat anti-rabbit AlexaFluor 488 (Invitrogen, A11008) and AlexaFluor 568 Phalloidin (Invitrogen, A12380), at RT (each at 1:200 in PBS). Coverslips were then washed four times and mounted in Prolong anti-fade mountant (Invitrogen, P36930). Cells or tissue samples were imaged at low magnification using a 40x objective on a TCS SP5 laser-scanning confocal microscope (Leica,

Vanderbilt Cell and Developmental Biology Core), and SIM images were acquired using an Applied Precision DeltaVision OMX (GE Healthcare) located in the Vanderbilt Cell Imaging Shared Resource, and processed using softWorx software (GE Healthcare). High magnification confocal images of Ls174T-W4 cells were acquired on a Nikon A1r confocal microscope equipped with 488 and 561 excitation LASERs and a 100x/1.49 NA Apo TIRF objective.

For SIM of B16F1 cells, cells were first washed once with warm PBS and then fixed with 4% PFA in PBS for 15 minutes at 37°C. Following fixation, cells were washed three times with PBS and permeabilized with 0.1% Triton X-100/PBS for 15 minutes at room temperature (RT). Cells were then washed 3X with PBS and incubated with fluorescent phalloidin (Life Technologies) diluted 1:200 in PBS and incubated with cells at 37°C for 30 minutes. Cells were then washed 4X with PBS and mounted on slides in ProLong Gold (Life Technologies).

OCT-embedded mouse (anti-COBL) or human (anti-syndapin-2) small intestinal tissue was cut to 5 µm thick sections onto Superfrost plus coated slides (Fisher) and stored at -80°C. Paraffin embedded mouse intestinal tissue was cut to 5 µm thick sections by the Vanderbilt Digitcal Histology Shared Resource. For IHC on OCT embedded sections, slides were warmed to RT and OCT was removed with three washes for five minutes each with PBS supplemented with 50 mM EGTA-K; this buffer was used for all subsequent steps. Tissue was then permeabilized with 0.3% Triton X-100 in PBS/EGTA for five minutes at RT.

Paraffin embedded mouse intestinal tissue was cut to 5 µm thick sections by the Vanderbilt Digitcal Histology Shared Resource. For staining, paraffin was removed with

31

2 washes with Histoclear (National Diagnostics) and then sections were rehydrated with

an ethanol series (5 minutes per wash, 100%, 100%, 95%, 90%, 75%, 50%, 30%, water,

PBS 3X). Then, sections were blocked using 10% BSA in PBS overnight at 4°C. Block

was removed with one wash and sections were incubated in anti-COBL (1:50,

HPA019167) or anti-syndapin-2 (1:100, HPA049854) rabbit antibodies in PBS overnight

at 4°C. The following day, sections were washed three times with PBS and incubated for

one hour with goat anti-rabbit AlexaFluor 488 (Invitrogen, A11008) and goat anti-mouse

AlexaFluor 568 (Invitrogen, A12380), at RT (each at 1:200 in supplemented PBS). Tissue

was then washed three times and dehydrated with the reverse of the ethanol wash

described above. Then, tissue was mounted in Prolong anti-fade mountant (Invitrogen,

P36930), and imaged using a Nikon A1r laser-scanning confocal microscope.

Drug treatments

Ls174T-W4 cells were plated on coverslips and allowed to adhere; 30 minutes before

induction with 1 μg/ml doxycycline, cells were incubated with 100 nM Latrunculin A

(Sigma, L5163), 30 µM Cytochalasin B (Sigma, C6762), 250 nM Jasplakinolide (Sigma,

J4580), 50 µM CK-666 (Sigma, SML0006), or 12.5 µM SMIFH2 (Sigma, S4826). After 6

hours of incubation with doxycycline and inhibitors, cells were fixed, washed and stained

with AlexaFluor 488 Phalloidin (Invitrogen, A12379), washed four times with PBS, and

mounted on slides using Prolong Gold Antifade mountant (Invitrogen, P36930). Cells

were imaged as described above.

Light Microscopy

For Ls174T-W4 cells, SIM was performed using an Applied Precision DeltaVision OMX

equipped with a 60x Plan-Apochromat N/1.42 NA objective and processed using softWorx

software (GE Healthcare). Confocal microscopy was performed using either a Leica TCS SP5 laser-scanning confocal microscope (fixed cells) or a Nikon A1r laser-scanning confocal microscope (fixed and live cells). For live cell imaging of Ls174T-W4 cells, one day before imaging, cells were transfected in a T25 flask at 80% confluency using Lipofectamine 2000 as described by the manufacturer (Invitrogen, 11668). The next day, cells were plated on glass bottom dishes and allowed to adhere for 6 hours. Imaging was performed on a Nikon A1r confocal microscope equipped with 488 and 561 excitation LASERs and a 100x/1.49 NA Apo TIRF objective. Doxycycline was added to the media at 1 μg/ml just before image acquisition began. Cells were maintained in a humid environment at 37°C and 5% CO_2 using a stage top incubation system (Tokai Hit). Image acquisition was controlled with Nikon Elements software.

For B16F1 cells, live cell imaging was performed on a Nikon TiE inverted light microscope equipped with 488 and 561 excitation LASERs, a 100x/1.49 NA TIRF objective, and Roper Evolve EM-CCD (Photometrics) and Andor Neo sCMOS detectors. Imaging was performed using near-TIRF illumination, where the incident angle of the LASER was adjusted to increase the depth of penetration of the excitation field, which we estimate to extend up to 400 nm into the cytoplasm. Cells were maintained in a humid environment at 37°C and 5% CO_2 using a stage top incubation system (Tokai Hit). Images were acquired every 5 seconds for 15 minutes, and image acquisition was controlled with Nikon Elements software. SIM images of B16F1 cells were acquired using an Applied Precision DeltaVision OMX (GE Healthcare) equipped with a 60x Plan-Apochromat N/1.42 NA oil immersion objective (Olympus) located in the Vanderbilt Cell Imaging Shared Resource, and processed using softWorx software (GE Healthcare).

Brush border isolation

BBs were collected with a modification of the method of Mooseker and Howe (Mooseker and Howe, 1982). All procedures involving animals were carried out under the auspices of VUMC IACUC. All chemicals were from Sigma-Aldrich unless otherwise noted. Intestines were dissected from 12 adult mice per condition (wild type/syndapin-2 KO), flushed with ice-cold saline (150 mM NaCl, 2 mM Imidazole-Cl, 0.02% Na-Azide) and stirred in sucrose dissociation solution (SDS, 200 mM sucrose, 0.02% Na-Azide, 12 mM EDTA-K, 18.9 mM KH2PO4, 78 mM Na2HPO4, pH 7.2) for 45 min. Released cells were washed with multiple cycles of sedimentation (200 x g for 10 min in a Beckman X-15R) and resuspension in fresh SDS. Cleaned cell pellets were resuspended in homogenization buffer (HB, 10 mM Imidazole, 4 mM EDTA-K, 1 mM EGTA-K, 0.02% Na-Azide, 1 mM DTT, 1 mM Pefabloc-SC, pH 7.2) and homogenized by douncing 10 times. BBs were collected from the homogenate by centrifugation at 1,000 x g for 10 minutes; BB pellets were then washed in solution A (75 mM KCl, 10 mM Imidazole, 1mM EGTA, 5 mM MgCl2, 0.02% Na-Azide, pH 7.2) and sucrose added to 50% final concentration. Samples were overlayed with 40% sucrose and centrifuged at 130,000 x g for one hour at 4°C in a Beckman L8-70M ultracentrifuge. BBs were collected from the 40%/50% interface, resuspended in solution A and stored on ice for subsequent experiments. Protein concentrations were determined using the Coomassie Blue Assay (Pierce).

Electron Microscopy

For SEM, specimens were washed several times in warm PBS, and fixed overnight at 4°C with 3% glutaraldehyde in SEM buffer (0.1 M Sucrose, 0.1 M Na-phosphate, pH 7.4). Samples were then washed in SEM buffer, post-fixed with 1% OsO4 on ice for 1 hour,

and washed in SEM buffer. Samples were then dehydrated in a graded ethanol series, dried with hexamethyldisilazane, mounted on aluminum stubs, coated with gold/palladium in a sputter coater, and viewed on a Quanta 250 Environmental Scanning Electron Microscope.

For TEM of intestinal tissue, specimens were washed several times in warm PBS, and fixed overnight in 2.5% gluteraldehyde in 0.1 M cacodylate buffer, pH 7.4 at room temperature (RT) for 1 hr and then transferred to 4°C and incubated overnight. The samples were washed 3x in 0.1 M cacodylate buffer then incubated for 1 hr in 1% osmium tetraoxide at RT, then washed 3x with 0.1 M cacodylate buffer. The samples were then dehydrated through a graded ethanol series: 30%, 50%, 70%, 80%, 95% and then 3 exchanges of 100% ethanol. Next, the samples were incubated in a mixture of 100% ethanol and propylene oxide (PO) followed by 2 exchanges of pure PO. Samples were then infiltrated with 25% Epon 812 resin and 75% PO at RT. Next, they were infiltrated with 50% Epon 812 resin and 50% PO for 1 hr at RT, then exchanged with new 50% Epon 812 resin and 50% PO and incubated overnight at RT. Subsequently, the samples were put through a 75%:25% (resin:PO) exchange, then exchanged into pure epoxy resin for 4 hr and incubated with pure epoxy resin overnight. Next, the resin was exchanged with fresh, pure epoxy resin and incubated for 3 hr, then embedded in epoxy resin and polymerized at 60°C for 48 hr. Thick sections of 500-1000 nm were cut and imaged on a Nikon AZ100M. Regions of interests were selected and 70-80 nm ultra-thin sections were then cut from the block and collected on 300-mesh copper grids. The copper grids were post-section stained at RT with 2% uranyl acetate and lead citrate. Samples were subsequently imaged on a Philips/FEI Tecnai T12 electron microscope.

Western blots

Samples were diluted with Laemmli sample buffer, heated at 95°C for 5 minutes, and equal volumes loaded on a 4-12% Nu-Page gradient gel (Invitrogen). Proteins were transferred in Towbin buffer, pH 8.3 to nitrocellulose at 10V overnight, which was subsequently blocked for 1 hr in 5% milk-PBS. Primary antibodies against COBL (1:250, Sigma HPA019167), Syndapin-2 (1:250, Sigma HPA049854) and GAPDH (1:1000, Cell Signaling) were diluted in PBS containing 0.1% Tween-20 (PBS-T), and incubated with the membranes overnight at 4°C. Membranes were washed four times with PBS-T, and then incubated with donkey-anti-rabbit 800 IRdye (1:5000, Li-Cor 926-32213) for 30 minutes. Membranes were again washed four times with PBS-T and imaged using a Li-Cor Odyssey infrared imaging system. Images of membrane scans were cropped and contrast adjusted using ImageJ (NIH).

Plasmids and molecular biology

pENTR(tm)221 COBL (Invitrogen, IOH536) corresponding to full-length human COBL was purchased and shuttled into a pEGFP-C1 vector (Clontech) adapted for Gateway cloning using the Gateway conversion kit (Invitrogen) to generate pEGFPC1-COBL and verified by sequencing. PCR was used to generate a full length COBL fragment flanked by 5' XhoI and 3' BamHI restriction sites, which was subsequently ligated into linearized p3x-mCitrine-C1 (a kind gift from K. Verhey), producing p3x-mCitrine-COBL. Using full-length COBL as template, PCR was used to create the truncated fragment KABC (a.a. 1081-1261) with 5' XhoI and 3' BamHI sites, which allowed ligation into linearized pEGFP-C1 to create pEGFP-KABC. To generate pEGFP-WH2*, mutations L1113A and L1166A were introduced to pEGFP-COBL using QuikChange site-directed mutagenesis (Agilent).

QuickChange site-directed mutagenesis was also used to generate mutations L1153A, L1154A, I1157A and L1166A in the full length EGFP-COBL construct to generate EGFP-COBL-sever*. All other EGFP-tagged truncation constructs, 1-1080, 1-KA (a.a. 1-1144), 1-KAB (a.a. 1-1202), KA (a.a. 1081-1144), KAB (a.a. 1081-1202), and Linker (a.a. 573-821) were generated using PCR with the full-length COBL construct described above as template. PCR products were first shuttled into pDONR/Zeo or pCR8/GW/TOPO, and then into a Gateway-adapted pEGFP-C1 vector using Gateway cloning (Invitrogen). To generate a COBL construct refractory to KD, 2 silent mutations per shRNA target were introduced into full-length COBL using site-directed mutagenesis. For COBL shRNA TRCN0000005530, which targets COBL nt 1840-1860, nt 1845 (t→c) and nt 1851 (c→t) were mutated. For COBL shRNA TRCN0000005531, which targets COBL nt 3208-3228, nt 3213 (a→g) and nt 3219 (c→t) were mutated. These silent mutations were also introduced into pEGFP-1-1080 and pEGFP-WH2*. Neither shRNA targeted the KABC sequence. pmCherry-syndapin-2 (mouse) and pmCherry-Eps8 (mouse) were purchased from Addgene (27681 and 27681, deposited by C. Merrifield) (Taylor et al., 2011) as were EGFP- and mCherry-tagged variants of UtrCH (26737 and 26740, deposited by W. Bement) (Burkel et al., 2007). Syndapin-2 was then excised from pmCherry-syndapin-2 using EcoRI and BamHI and ligated into pEGFP-C1 to generate pEGFP-syndapin-2. A full length fimbrin construct was purchased from the mammalian gene collection (MGC, clone 33811). PCR was used to create a full length fimbrin fragment, which was then ligated into linearized pEGFP-C1 to generate pEGFP-C1-Fimbrin. A full length mouse villin-1 was construct was purchased from the MGC (clone 18506). PCR was used to generate a full length fragment which was then cloned into pCR8/GW/TOPO (Invitrogen)

using TOPO cloning, and subsequently shuttled into pmCherry-C1 and pEGFP-C1 vectors adapted for Gateway cloning described above. pTYB12-fascin was a kind gift from Dr. Roberto Dominguez, and was used a PCR template for cloning into pCR8/GW/TOPO as described above, and shuttled into pmCherry-C1 adapted for Gateway cloning. The pmCherry-espin construct (Loomis et al., 2003) was a kind gift from Dr. James Bartles, Quickchange site-directed mutagenesis was used to make mutations L302A, L303A and L312A to generate Espin-WH2*. EspinΔABM (1-385 A.A.) was generated using PCR with pmCherry-espin used as the template. tdTomato-F-tractin was a kind gift from Dr. Alissa Weaver. mCherry-zyxin was a kind gift from Dr. Irina Kaverina. All newly generated plasmids were verified by sequencing.

Image analysis and quantification - Chapter 3

Excluding line-scan analysis, all quantitative data is from at least 3 experiments. For length, straightness, phalloidin intensity, and microvillar coverage, the D'Agostino and Pearson omnibus normality test was performed to determine if the data were normally distributed. Normally distributed data was statistically analyzed using the unpaired *Student's t-tests.* If the data were not normal, the *Mann-Whitney U-test* was used to determine significance*.* Statistical analyses performed are stated in the figure legends. All graphs were generated and statistical analyses performed using Prism v.6 (GraphPad). All image analysis was performed using ImageJ (NIH). For quantification of '% cells with BB,' cells were scored as BB-positive if they displayed polarized F-actin accumulation as visualized using a 40x objective on a Leica TCS SP5 confocal microscope. To perform line-scan analysis, a line was drawn along the microvillar axis using F-actin signal (visualized with phalloidin staining) as a reference; the intensity of the

COBL or syndapin-2 signal along that line was then recorded. Intensities from individual line-scans were normalized such that the maximum value was equal to 1. The length axis from individual scans was also normalized such that the base of the microvillus was set equal to 0 and the distal tip to 1. Normalized line-scans were then plotted together and fit to a single Gaussian using non-linear regression (Prism v.6, GraphPad); the resulting fit parameters revealed the position of peak localization (L_P) along the microvillar axis. For perimeter analysis of live differentiating Ls174T-W4 cells, a line beginning on the opposite side of the cell from where the BB was formed was drawn along the perimeter of the cell, and the COBL and UtrCH intensities were plotted along that line for each time point indicated. To measure intensity over time in differentiating Ls174T-W4 cells, a 2.5 μm^2 ROI was drawn at the center of the base where the BB formed and the average intensity of that area for COBL and UtrCH was plotted over time. Microvillar length measurements were performed on projected SIM images by tracing individual microvillar actin bundles using ImageJ. Microvillar straightness was determined as the ratio between a straight line drawn directly from the base to the tip of a microvillus and the actual length of the protrusion. Microvillar phalloidin intensity was measured in unprocessed images by drawing a line along the length of single protrusion and averaging the intensity along that line. For analyses where individual microvilli were measured, 10 microvillar actin bundles were scored per cell. Microvillar coverage, i.e. fraction of the cell perimeter occupied by microvilli, was determined from projected SIM images using ImageJ. In JEG-3 cells, microvillar number was quantified in ImageJ by tracing an area of a cell, counting the number of microvilli in that area for COBL overexpressing and untransfected cells, and then normalizing the value to microvilli per 100 μm^2. For measuring enrichment of COBL

39

and syndapin-2 at the base of the BB in Ls174T-W4 cells, the base of the BB as determined by phalloidin staining was traced with an 8 pixel wide line and the mean intensity of both signals along that line was determined. The same line was then moved to a region approximately 2 μm below the base of the BB (that did not include the nucleus) and the mean intensity of COBL and syndapin-2 along that line was determined. BB:cytosol enrichment was defined as the ratio of these two mean intensities.

Image analysis and quantification - Chapter 4

For measurements number of protrusions per 10 microns, ANOVA with the Tukey's multiple comparisons HSD test was used to determine significance. All graphs were generated and statistical analyses performed using Prism v.6 or v.7 (GraphPad). All image adjustments (contrast enhancement and smooth function) and analyses were performed using ImageJ (NIH). For line scans in Figure 1, intensities were normalized to the first image of each montage. Kymographs were generated by making a maximum intensity projection of the entire time series drawing a line along the resulting linear actin structure of interest and using the 'Reslice' function in ImageJ. For the graph in Figure 1E, total structure length and total COBL occupied structure length was measured for each time point that the structure was visible and plotted. To perform line scan analysis of linear actin structures, a line was drawn along the structure axis beginning on the side of COBL signal; the intensity of the COBL and Eps8 signal along that line was then recorded. Intensities from individual line scans were normalized such that the maximum value was equal to 1. The length axis from individual scans was also normalized such that the COBL-enriched side of the linear structure was set equal to 0 and the opposite side 1. Normalized line scans for COBL and eps8 were then plotted together and fit to a

single Gaussian using non-linear regression (Prism v.6, GraphPad). Elongation and shortening rates were determined using the slopes of kymographs generated as stated above. The number of protrusions per 10 microns was calculated by first measuring the cell perimeter excluding protrusions and then counting the number of protrusions that the cell contained. The number of protrusions was then divided by the perimeter and multiplied by 10.

CHAPTER III.

CORDON BLEU PROMOTES THE ASSEMBLY OF BRUSH BORDER MICROVILLI

Nathan E. Grega-Larson, Scott W. Crawley, Amanda L. Erwin, and Matthew J. Tyska

Department of Cell and Developmental Biology, Vanderbilt University, Nashville, TN

37240, USA

To whom correspondence should be addressed:

Matthew J. Tyska, Ph.D.
Professor
Dept. of Cell and Developmental Biology
Vanderbilt University
3154 MRB III, PMB 407935
465 21st Avenue South
Nashville, TN 37240-7935
Office: 615-936-5461
Lab: 615-936-5504

Abstract

Microvilli are actin-based protrusions found on the surface of diverse cell types, where they amplify membrane area and mediate interactions with the external environment. In the intestinal tract, these protrusions play central roles in nutrient absorption and host defense, and are therefore essential for maintaining homeostasis. However, mechanisms controlling microvillar assembly remain poorly understood. Here we report that the multi-functional actin regulator, cordon bleu (COBL), promotes the growth of brush border (BB) microvilli. COBL localizes to the base of BB microvilli via a mechanism that requires its proline-rich N-terminus. Knockdown and over-expression studies show that COBL is needed for BB assembly and sufficient to induce microvillar growth using a mechanism that requires functional WH2 domains. We also find that COBL acts downstream of the F-BAR protein, syndapin-2, which drives COBL targeting to the apical domain. These results provide insight into a mechanism that regulates microvillar growth during epithelial differentiation and hold significant implications for understanding the maintenance of intestinal homeostasis.

Introduction

Found on the surface of numerous cell types, microvilli are finger-like membrane protrusions supported by parallel bundles of F-actin. One of the most elaborate arrays of microvilli, known as the brush border (BB), projects from the apex of the intestinal epithelial cell (IEC), where it functions in nutrient processing and host defense (Crawley et al., 2014a). Loss of these protrusions due to genetic causes such as microvillus inclusion disease, or infections with enteric pathogens such as enteropathogenic *E coli*, leads to nutrient malabsorption and osmotic imbalances that cause dramatic dehydration, and in susceptible populations, death (Davidson et al., 1978; Vallance et al., 2002). However, molecular mechanisms controlling the growth of microvilli on the surface of transporting epithelia have yet to be defined.

Given that microvilli are supported by polarized actin bundles, understanding how these bundles form during differentiation and are stabilized thereafter, will be critical for understanding BB assembly and function. Actin-based cytoskeletal structures in general are assembled through the coordinated action of factors that mediate initial filament formation (i.e. nucleation), elongation, capping, bundling, and cross-linking to membranes or other cytoskeletal systems (Chhabra and Higgs, 2007). Factors that bundle actin filaments within microvilli (villin, fimbrin, espin, and EPS8)(Bartles et al., 1998; Bretscher and Weber, 1979, 1980; Hertzog et al., 2010) or link the resulting core bundles to the overlying plasma membrane (e.g. myosin-1a, ezrin)(Bretscher, 1989; Verner and Bretscher, 1985) have been the subject of extensive investigation. However, molecules that control upstream events in microvillar formation, such as actin filament nucleation and elongation, remain poorly understood. Studies on other types of protrusions, such as

filopodia, which extend from the leading edge of crawling cells (Faix et al., 2009), might provide mechanistic clues. The parallel actin bundles that support filopodia are formed by at least two distinct mechanisms. In the first case, bundle formation is driven by elongation and bundling of Arp2/3-nucleated filaments that originate in the dendritic array of the lamellipodium (Svitkina et al., 2003). In the second, filopodial actin bundle formation is initiated at the membrane by barbed-end associated factors such as formins, which are capable of both nucleating and elongating filaments in linear bundles (Schirenbeck et al., 2005b; Steffen et al., 2006). Interestingly, recent studies show that mice lacking ArpC3, an essential component of Arp2/3 complex, still assemble well-organized BBs (Zhou et al., 2015), suggesting branched nucleation is unlikely to play a role in the formation of epithelial microvilli. However, proteomic analyses of isolated BBs also identified formin DIAPH1 and the Wiskott-Aldrich homology 2 (WH2) domain-containing factor COBL, as potential regulators of microvillar formation (McConnell et al., 2011; Revenu et al., 2012), although the extent to which these molecules contribute to BB assembly remains unclear.

The objective of the current study was to identify factors that promote the growth of IEC BB microvilli. Our results indicate that COBL plays an important role in promoting the growth of microvillar actin bundles during intestinal epithelial differentiation. Moreover, a COBL interacting partner, syndapin-2, targets this factor to the apical domain during this process. Importantly, these studies provide a molecular framework for future investigations into the early steps of BB biogenesis. These findings also hold implications for understanding apical morphogenesis in other epithelial systems, such as kidney, lung, and inner ear.

Results

BB assembly requires dynamic turnover of the actin cytoskeleton

To explore the molecular basis of microvillar assembly, we employed a cell culture model that allowed switch-like control over epithelial differentiation. Ls174T-W4 cells are human IECs that stably express myc-LKB1 and an inducible FLAG-STRADα. LKB1 is a serine/threonine kinase and master regulator of cell polarity (homologous to Par-4 in *C. elegans* and *D. melanogaster*)(Martin-Belmonte et al., 2007). STRADα is an LKB1 specific adaptor protein that activates and translocates LKB1 from the nucleus to the cytoplasm (Baas et al., 2003). Exposing Ls174T-W4 cells to doxycycline induces STRADα expression thereby activating LKB1, initiating apical/basal polarity establishment and downstream events such as BB formation (Baas et al., 2004). Uninduced Ls174T-W4 cells exhibit an unpolarized morphology with cortical F-actin labeling (Figure 3-1A). After induction with 1 μg/ml doxycycline for eight hours, ~80% of Ls174T-W4 cells polarize and display a prominent BB on one side of the cell (Figure 3-1B,C). Although the Ls174T-W4 model has been used to study polarity signaling upstream of BB assembly (Gloerich et al., 2012; ten Klooster et al., 2009), we took advantage of the switchable nature of this system to dissect the mechanism of microvillar growth.

We first sought to determine if Arp2/3 complex or formins functioned in assembling microvilli. BB assembly was induced in Ls174T-W4 cells in the presence of CK-666, which inhibits Arp2/3 complex (Nolen et al., 2009), or SMIFH2 (Rizvi et al., 2009), which directly inhibits the FH2 domains of numerous formins from diverse species, and specifically inhibits mouse DIAPH1/mDia1 (Rizvi et al., 2009), the only formin detected in BB
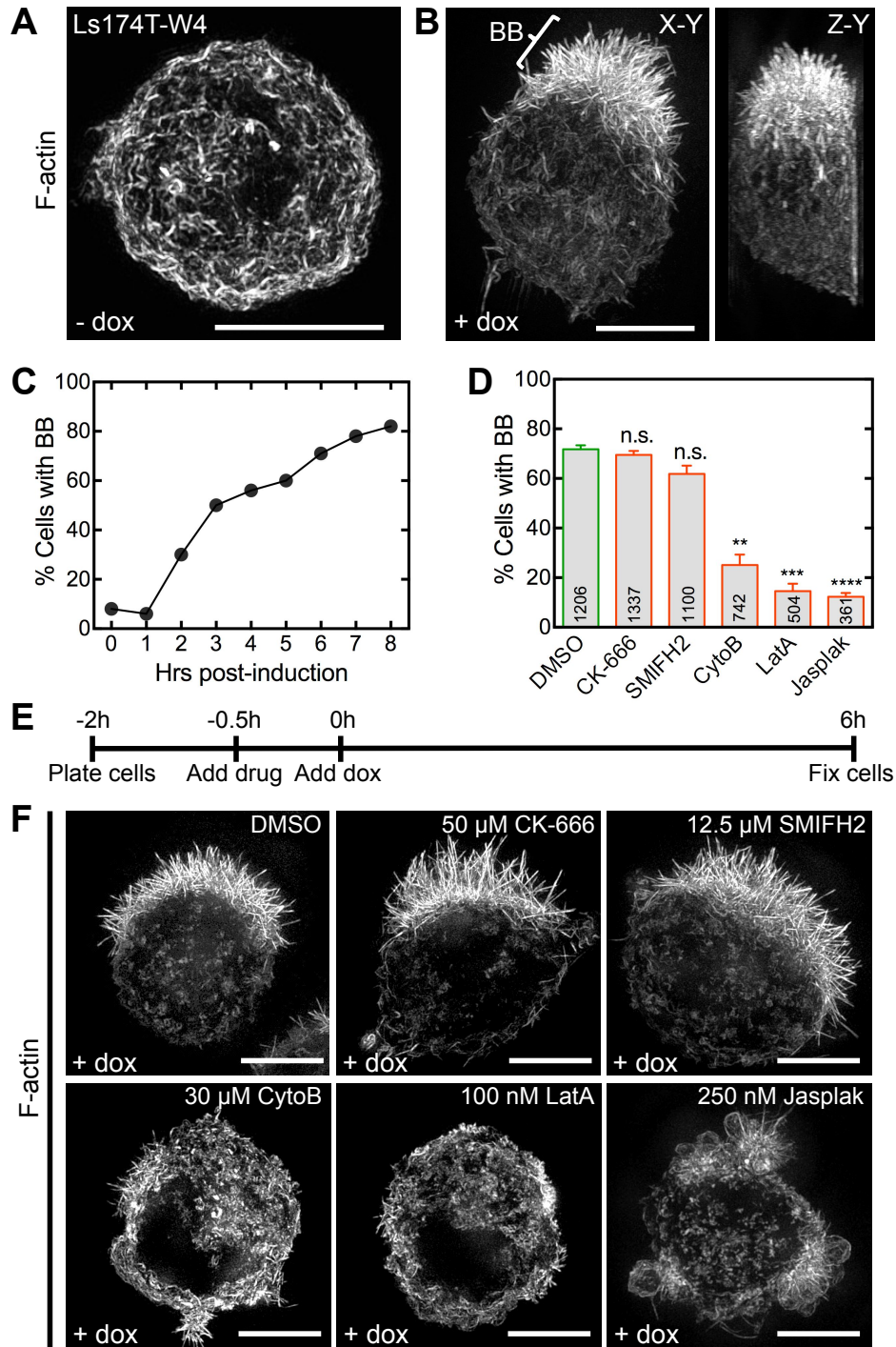
Figure 3-1: Actin dynamics are required for BB assembly. (A) SIM projection of an uninduced Ls174T-W4 cell stained with phalloidin to visualize F-actin (white). (B) En face (left) and lateral (right) SIM projections of an induced Ls174T-W4 cell; bracket highlights the BB. (C) Percentage of BB positive cells at time points indicated. (D) Percentage of BB positive cells from various drug treatments. Mean ± SEM from 3 separate experiments, n per condition listed in bars. (Student's t-test, **$p < 0.005$, ***$p < 0.0005$, ****$p < 0.0001$). (E) Schematic of experimental design and (F) SIM projections of Ls174T-W4 cells treated with drugs during induction. Scale bars are 5 μm.

proteomic studies (McConnell et al., 2011; Revenu et al., 2012)(Figure 3-1D-F;).

Interestingly, these compounds had little impact on the number of BB positive cells after

6 hrs of induction (CK-666, 69.5 ± 1.8%; SMIFH2, 61.8 ± 3.3%; DMSO control, 71.7 ±

1.6%). We did note that microvilli in CK-666 treated cells were slightly, but significantly

longer as compared to control cells (2.40 ± 0.03 μm vs. 2.21 ± 0.03 μm); one possible

explanation is that Arp2/3 inhibition increases the concentration of actin monomers

available for microvillar elongation (Burke et al., 2014; Rotty et al., 2015; Suarez et al.,

2015). In contrast, the fraction of BB positive cells was significantly reduced when barbed-

ends of actin filaments were capped using cytochalasin B (25.1 ± 4.2%), actin monomers

were sequestered with latrunculin A (14.6 ± 3.0%), or filaments were stabilized with

jasplakinolide (12.3 ± 1.5%, Figure 3-1D-F). Although the results of small molecule

inhibition studies should be interpreted with caution, these data are consistent with

previous reports showing that mice lacking functional Arp2/3 complex continue to build

normal BBs (Zhou et al., 2015), and lymphocytes lacking Arp2 or upstream activator

WASP still assemble microvilli (Majstoravich et al., 2004; Nicholson-Dykstra and Higgs,

2008). Together, these results suggest that microvillar growth is driven by the assembly

of new actin filaments that elongate from their barbed-ends, and that Arp2/3 and formins

are not needed for this process.
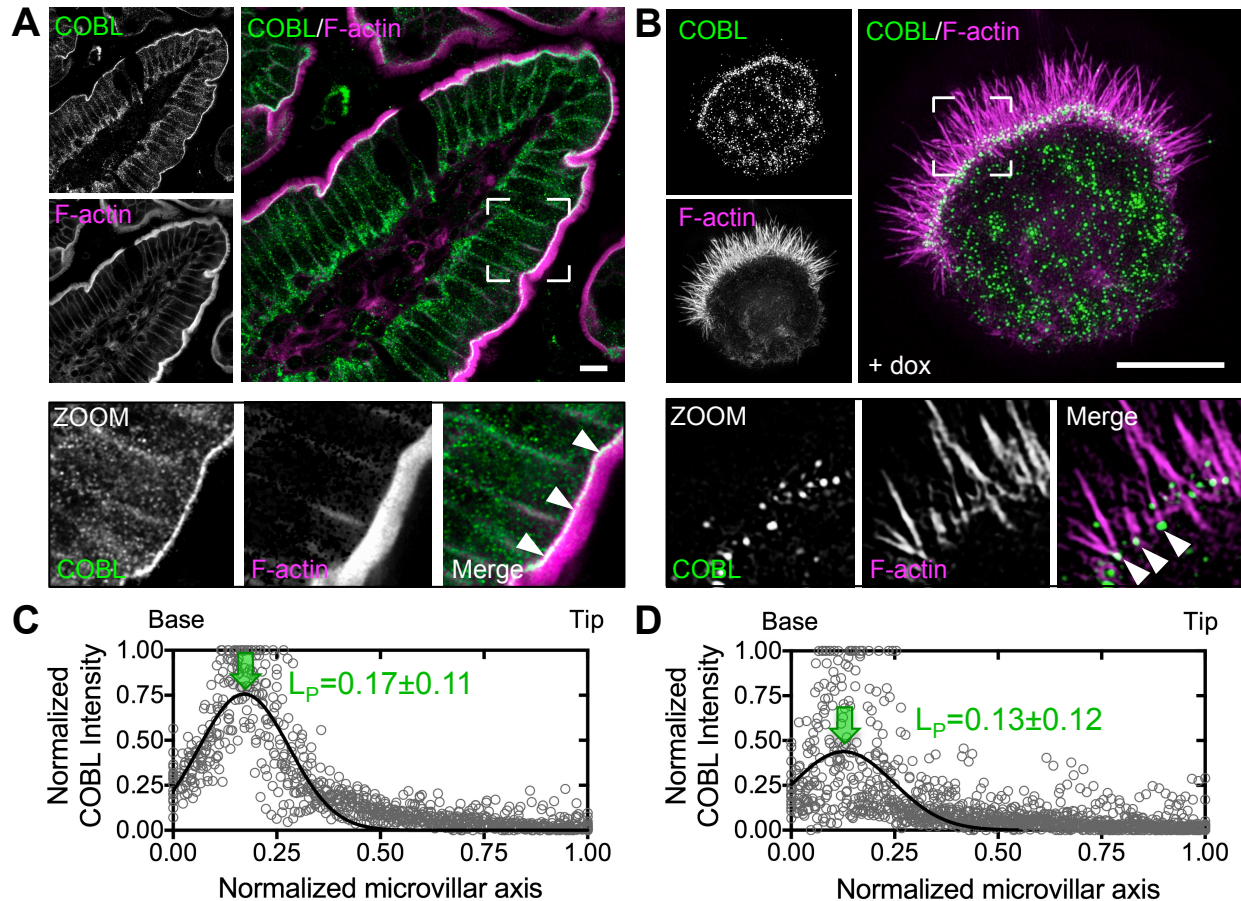
Figure 3-2: COBL localizes to the base of BB microvilli. (A) Endogenous COBL (green) and F-actin (magenta) labeling in a single villus from mouse small intestine. Boxed corners indicate zoom region, which highlights terminal web localization of COBL. (B) SIM projection of an induced Ls174T-W4 cell showing localization of endogenous COBL (green) and F-actin (magenta). Boxed corners indicate zoom region. (C,D) Linescans (n = 25) parallel to the microvillar axis show the distribution of endogenous COBL in mouse small intestine and in Ls174T-W4 cells, respectively. Arrows highlight the peak localization (L_P, mean ± SE) along the normalized microvillar axis. Scale bars are 5 μm.

COBL - a multifunctional actin regulator that localizes to the base of microvilli

Another actin regulator identified in BB proteomic studies is the multi-WH2 domain-containing molecule, COBL (McConnell et al., 2011; Revenu et al., 2012). Individual WH2 domains are G-actin binding modules capable of mediating filament nucleation, severing, and a variety of other activities when linked in tandem (Dominguez, 2009). Since its initial identification as a nucleator (Ahuja et al., 2007), further studies revealed profilin-like

binding to ATP-actin, sequestration of ADP-actin, and filament severing (Husson et al., 2011). How the multiple activities demonstrated by COBL WH2 domains *in vitro* contribute to COBL activity in cells remains unclear. However, COBL has been implicated in neural tube formation (Carroll et al., 2003), neurite outgrowth (Ahuja et al., 2007), assembly of motile cilia in Kupffer's vesicle (Ravanelli and Klingensmith, 2011), and the differentiation of sensory cells (Schuler et al., 2013).

Immunostaining of mouse intestinal tissue revealed that COBL was strongly enriched at the base of the BB (Figure 3-2A, zoom), where the pointed-ends of microvillar actin bundles are anchored (Hirokawa et al., 1982). Structured illumination microscopy (SIM) of endogenous COBL labeling in Ls174T-W4 cells showed a striking enrichment of puncta near or at the base of individual microvillar actin bundles (Figure 3-2B, zoom). This localization is consistent with a previous report on the targeting of EGFP-tagged COBL in the JEG-3 placental epithelial cell line (Wayt and Bretscher, 2014). Linescans revealed peak COBL signal at 0.17 ± 0.11 (tissue, Figure 3-2C) and 0.13 ± 0.12 (Ls174T-W4 endogenous, Figure 3-2D), when plotted as a function of normalized microvillar length (0 = base, 1 = tip). Importantly, overexpressed EGFP-tagged COBL exhibited localization similar to endogenous COBL with peak localization at 0.16 ± 0.15 (Figure 3-3A-C). Moreover, time-lapse imaging of EGFP-COBL in polarizing Ls174T-W4 cells revealed tight temporal and spatial overlap with F-actin, as visualized using mCherry-tagged UtrCH (Burkel et al., 2007), during BB assembly (Figure 3-3D-F). Thus, COBL enriches at the nascent apical domain during polarity establishment, and localizes near or at the pointed-ends of microvillar actin bundles, the expected site of action for a WH2 domain-containing nucleator.
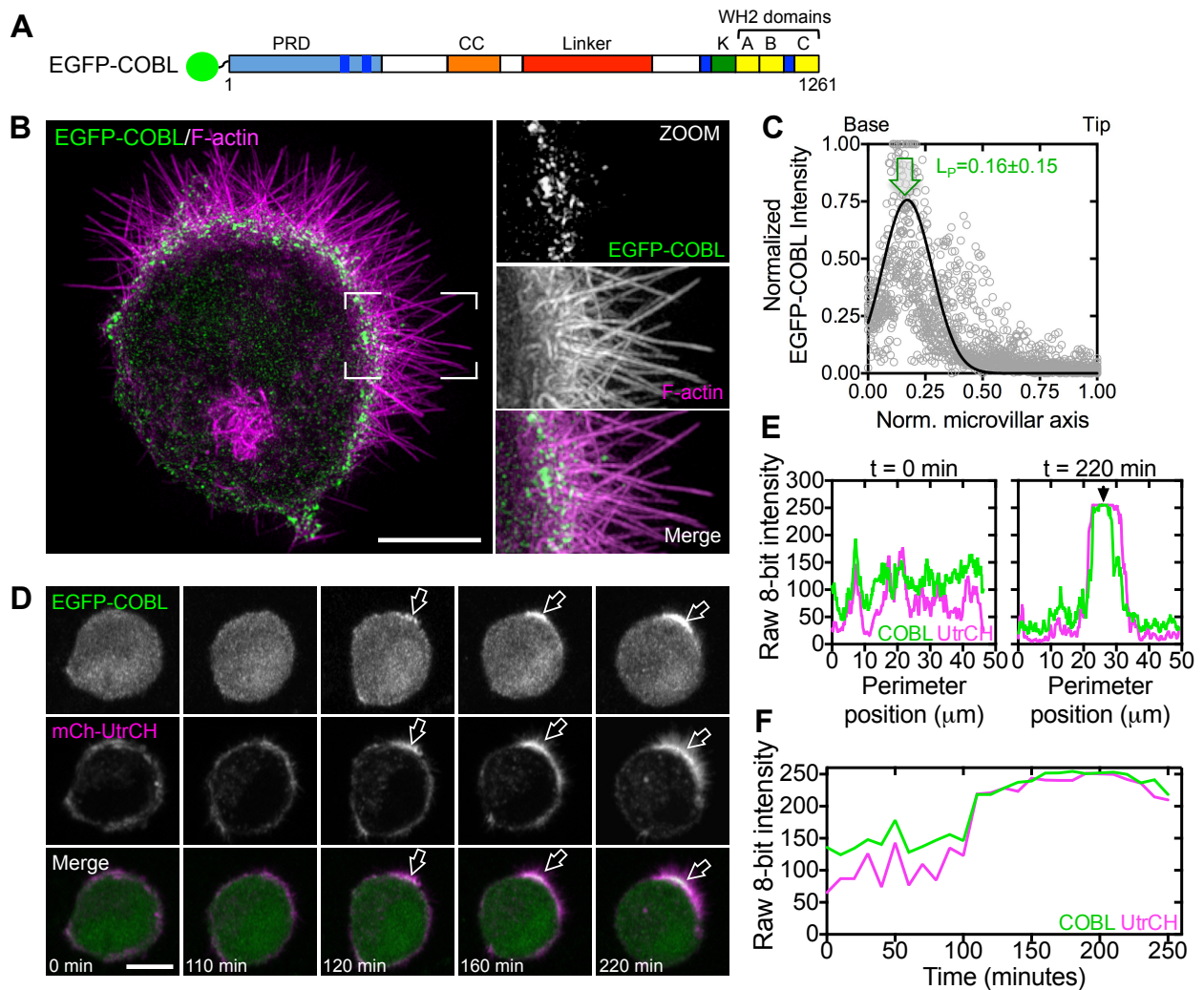
Figure 3-3: COBL localization at the base of the BB coincides with microvillar formation.
(A) Schematic of full-length COBL domain organization; PRD = proline rich domain, CC = coiled-coil, K = lysine-rich region, A, B, and C refer to COBL WH2 domains. (B) SIM projection of an induced Ls174T-W4 cell overexpressing EGFP-COBL (green) and stained for F-actin (magenta). Boxed corners indicate zoom region. (C) Linescans (n = 25) parallel to the microvillar axis show the distribution of EGFP-COBL in Ls174T-W4 cells. Arrow highlights the peak localization. (D) Time series montage of a single Ls174T-W4 cell co-expressing EGFP-COBL and mCherry-UtrCH, undergoing cell polarization and BB assembly. (E) Perimeter line-scan analysis of the cell shown in C at t = 0 and t = 220 min, black arrow in right hand plot marks position of the BB. (F) Intensity profile over time of a 2.5 µm^2 ROI at the base of the forming BB in C. Scale bars are 5 µm.

Overexpression of COBL induces microvillar growth

COBL is comprised of an N-terminal proline-rich domain (PRD), three C-terminal WH2 domains, and intervening predicted coiled-coil (CC) and linker motifs (Figure 3-4A). In Ls174T-W4 cells overexpressing EGFP-COBL, we noted that microvillar actin bundles

A

	PRD	CC	Linker	WH2 domains K $\overbrace{A\ B\ C}$	
COBL	1			K A B C	1261
WH2*				K * * C	1261
1-1080				K	1080
1-KA				K A	1144
1-KAB				K A B	1202
KA			1081	K A	1144
KAB			1081	K A B	1202
KABC			1081	K A B C	1261
Linker		573	821		

B

-24h → 0h → 6h
Transfect cells | Re-plate cells + dox | Fix cells

C

D

Predicted activities

Phalloidin Intensity (au) — Microvillar Straightness — Microvillar Length (μm) — Microvillar Coverage

- EGFP
- EGFP-WH2*
- EGFP-Linker
- EGFP-1-1080
- EGFP-KA
- EGFP-1-KA
- EGFP-1-KAB
- EGFP-KABC
- EGFP-KAB
- EGFP-COBL

None

Nucleation only

Nucleation & Severing

52

Figure 3-4: Overexpression of COBL promotes microvillar growth. (A) Schematic of full-length COBL domain organization and truncated/mutated COBL constructs used in this study; PRD = proline rich domain, CC = coiled-coil, K = lysine-rich region, *refers to point mutations (L1113A and L1166A) that inactivate G-actin binding ability of COBL WH2 domains. (B) Schematic of procedure for overexpression experiments followed by (C) SIM projections of Ls174T-W4 cells overexpressing COBL constructs (green) and stained with phalloidin (magenta). Boxed corners indicate zoom region. (D) Quantification of microvillar phalloidin intensity, straightness, length, and surface coverage for cells overexpressing COBL constructs. Predicted activities listed to the right of the quantification are based off of biochemical experiments published in (Husson et al., 2011). A *student's t-test* (*$p<0.05$, **$p<0.005$, ***$p<0.0007$) was used to determine significance for phalloidin intensity. For straightness, length and coverage measurements, *Mann-Whitney U-tests* (*$p<0.05$, **$p<0.005$, ***$p<0.0004$, ****$p<0.0001$) were used to determine significance. For all graphs, the boxes represent the 25th and 75th percentiles around the median, and the whiskers represent the 5th and 95th percentiles. n = 25 cells/condition, 10 microvilli/cell. Scale bars are 5 µm.

appeared more numerous, longer, and straighter relative to EGFP transfected controls (Figure 3-3B; 3-4C). Scoring of SIM images revealed that microvillar length, straightness, phalloidin intensity (proportional to F-actin content), and the fraction of cell surface covered with microvilli were all significantly increased in cells overexpressing EGFP-COBL (Figure 3-4D). Interestingly, truncation of COBL from the C-terminus, and thus elimination of WH2 domains, had a graded effect on microvillar morphology. Constructs with no WH2 domains showed little impact (1-1080, linker). Constructs with a single WH2 domain, which nucleate actin *in vitro* (1-KA, KA)(Husson et al., 2011), showed a modest effect, whereas constructs with two or three WH2 domains, which nucleate and sever *in vitro* (Husson et al., 2011), elicited the most significant microvillar induction (1-KAB, KAB, KABC, COBL; Figure 3-4C,D). However, a full-length COBL construct with inactivating mutations in the first two WH2 domains (Chen et al., 2013) did not significantly impact microvillar morphology (WH2*, Figure 4C,D). These results suggest that COBL promotes the growth of microvilli using a mechanism that takes advantage of multiple functional WH2 domains.
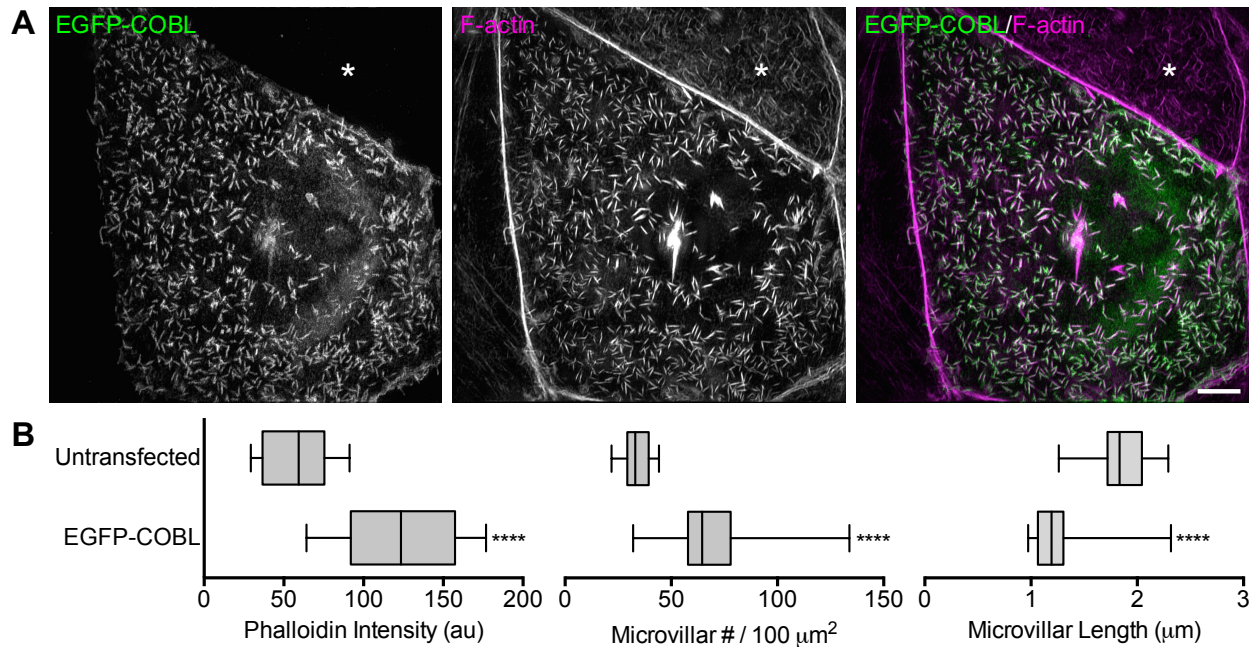
Figure 3-5: COBL overexpression in JEG-3 cells increases microvillar F-actin. (A) SIM projection of a JEG-3 cell overexpressing EGFP-COBL and stained with phalloidin to label F-actin. Note the increase in microvillar phalloidin intensity in a cell overexpressing COBL relative to a non-expressing cell (white asterisk, upper right). Scale bar is 5 μm. (B) Quantification of the effect of overexpression of EGFP-COBL on microvillar phalloidin intensity, microvillar number, and microvillar length in JEG-3 cells. For phalloidin intensity, significance was determined using the Student's t-test (****$p<0.0001$). For microvillar number and microvillar length, significance was determined using the Mann-Whitney U-test (****$p<0.0001$). For graphs, boxes represent the 25th and 75th percentiles around the median, the whiskers represent the 5th and 95th percentiles. n = 17 cells/condition.

A recent study investigating COBL function in the JEG-3 placental cell line reported that overexpression reduced microvillar length (Wayt and Bretscher, 2014). Using SIM we observed that JEG-3 cells overexpressing COBL assembled more microvilli, with higher levels of F-actin in individual protrusions (Figure 3-5A,B), findings that are consistent with our studies in IECs. We did observe shorter protrusions, however, suggesting that in the JEG-3 context, COBL overexpression and the subsequent assembly of numerous microvilli taxes the limited actin pool available for protrusion elongation (Burke et al., 2014). The same study suggested that the linker domain of COBL (Figure 3-4A,B) was necessary and sufficient to target this molecule to the base of

microvilli on the surface of JEG-3 placental epithelial cells (Wayt and Bretscher, 2014).

When we overexpressed this domain in Ls174T-W4 cells, it enriched in the BB, but its

localization was diffuse throughout the microvillus. Our truncation analysis and SIM

imaging revealed that only fragments containing a.a. 1-1080 were enriched at the base

of the BB, in a manner similar to endogenous COBL. Therefore, in addition to the linker

domain, other motifs within the N-terminus are likely required for proper terminal web

targeting.

Loss of COBL function impairs BB assembly

To determine how loss of COBL impacts the formation of BB microvilli, we used shRNA

to knockdown (KD) expression in Ls174T-W4 cells (Figure 3-6). COBL KD significantly

reduced the fraction of cells able to assemble BBs (33.8 ± 3.0% of COBL KD vs. 72.6 ±

1.0% of scramble control cells; Figure 3-6A-D). This perturbation was specific to loss of

COBL as re-expression of a full length COBL construct refractory to KD (COBLr) rescued

BB formation (67.5 ± 1.6%; Figure 3-6D). Moreover, functional WH2 domains were

required for rescue, as a full-length COBL construct with inactivated WH2 domains

(WH2*) or a construct lacking WH2 domains (1-1080) failed to improve the KD phenotype

(27.3 ± 2.7% and 31.4 ± 2.7%, respectively; Figure 3-6D. Re-expression of the KABC

fragment containing all three functional WH2 domains yielded a partial rescue (54.0 ±

3.1%; Figure 3-6D).

COBL KD did not completely abolish BB assembly in Ls174T-W4 cells, despite a

>95% reduction in protein levels, suggesting that other molecules probably contribute to

microvillar formation. This would be consistent with the partial penetrance observed in

studies with KO mouse models lacking major microvillar
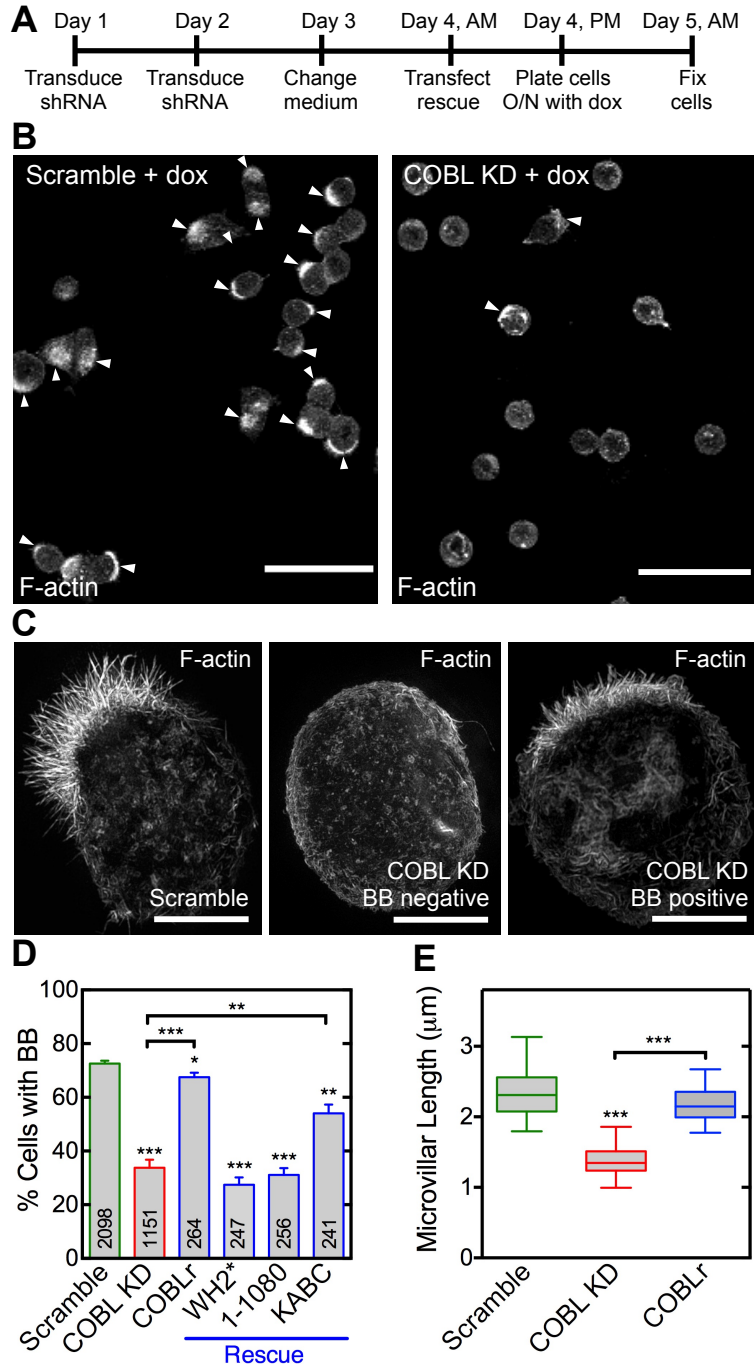
Figure 3-6: COBL is required for microvillar growth. (A) Schematic of experimental design. (B) Images of scramble control or COBL KD cells scored for BB positive cells. Arrowheads highlight BB positive cells. Scale bar = 40 μm. (C) SIM projection images of scramble control cell, COBL KD cell without a BB, and COBL KD cell with a BB stained with phalloidin. Scale bars are 5 μm. (D) Percentage of BB positive cells in KD and rescue experiments. Mean ± SEM from 4 separate experiments, n per condition listed in bars (Student's t-test, *p<0.05, **p≤0.008, ***p≤0.0004). (E) Quantification of microvillar length from scramble, COBL KD, and rescue cells with COBLr that were scored as BB positive cells in D. Boxes represent the 25th and 75th percentiles around the median, the whiskers represent the 5th and 95th percentiles. n = 30 cells/condition. (Mann-Whitney U-test, ***p<0.0005).

structural proteins (Revenu et al., 2012; Saotome et al., 2004; Tyska et al., 2005).

However, when we used SIM to more closely examine COBL KD cells that were scored

as "BB positive" in low magnification fields (Figure 3-6B), their microvilli appeared

significantly shorter than those assembled by scramble control cells (1.39 ± 0.05 μm vs.

2.35 ± 0.07 μm; Figure 3-6C,E). Shorter length was rescued by expression of a full length

COBL construct refractory to KD (COBLr) (2.17 ± 0.05 μm; Figure 3-6E). These loss-of-

function and rescue experiments indicate that COBL is required for normal microvillar

formation and functional WH2 domains are needed for proper function in this context.

COBL targeting to the apical domain requires syndapin-2

The F-BAR domain protein syndapin-1 has been shown to target COBL to sites of neurite

outgrowth in neurons (Schwintzer et al., 2011). In that context, targeting is mediated by

direct binding between the N-terminal PRD of COBL and the C-terminal SH3 domain of

syndapin-1. Whereas syndapin-1 is specific to the CNS and syndapin-3 is only expressed

in skeletal muscle and heart tissue, syndapin-2 is ubiquitously expressed (Quan and

Robinson, 2013). Importantly, COBL has been shown to directly bind all three syndapins

in vitro (Schwintzer et al., 2011). However, the functional implications of interactions

between COBL and syndapins-2 or 3 have yet to be investigated in cells. To determine if

syndapin-2 plays a role in targeting COBL to the apical surface of IECs, we first examined

the expression and localization of syndapin-2 in small intestinal tissue and the Ls174T-

W4 model system. Syndapin-2 was enriched at the base of microvilli in human small

intestine (Figure 3-7A) and in Ls174T-W4 cells (Figure 3-7B). Linescans showed that,

similar to COBL, syndapin-2 localizes near the pointed-ends of microvillar actin bundles

with peak localization at 0.21 ± 0.14 (tissue, Figure 6C) and 0.11 ± 0.10 (Ls174T-W4

cells, Figure 3-7 D) when plotted as a function of microvillar length. Furthermore, endogenous syndapin-2 shows striking colocalization with EGFP-COBL at the base of microvilli in Ls174T-W4 cells (Figure 3-7E). Time-lapse imaging of EGFP-COBL and mCherry-syndapin-2 in polarizing Ls174T-W4 cells also revealed spatial and temporal
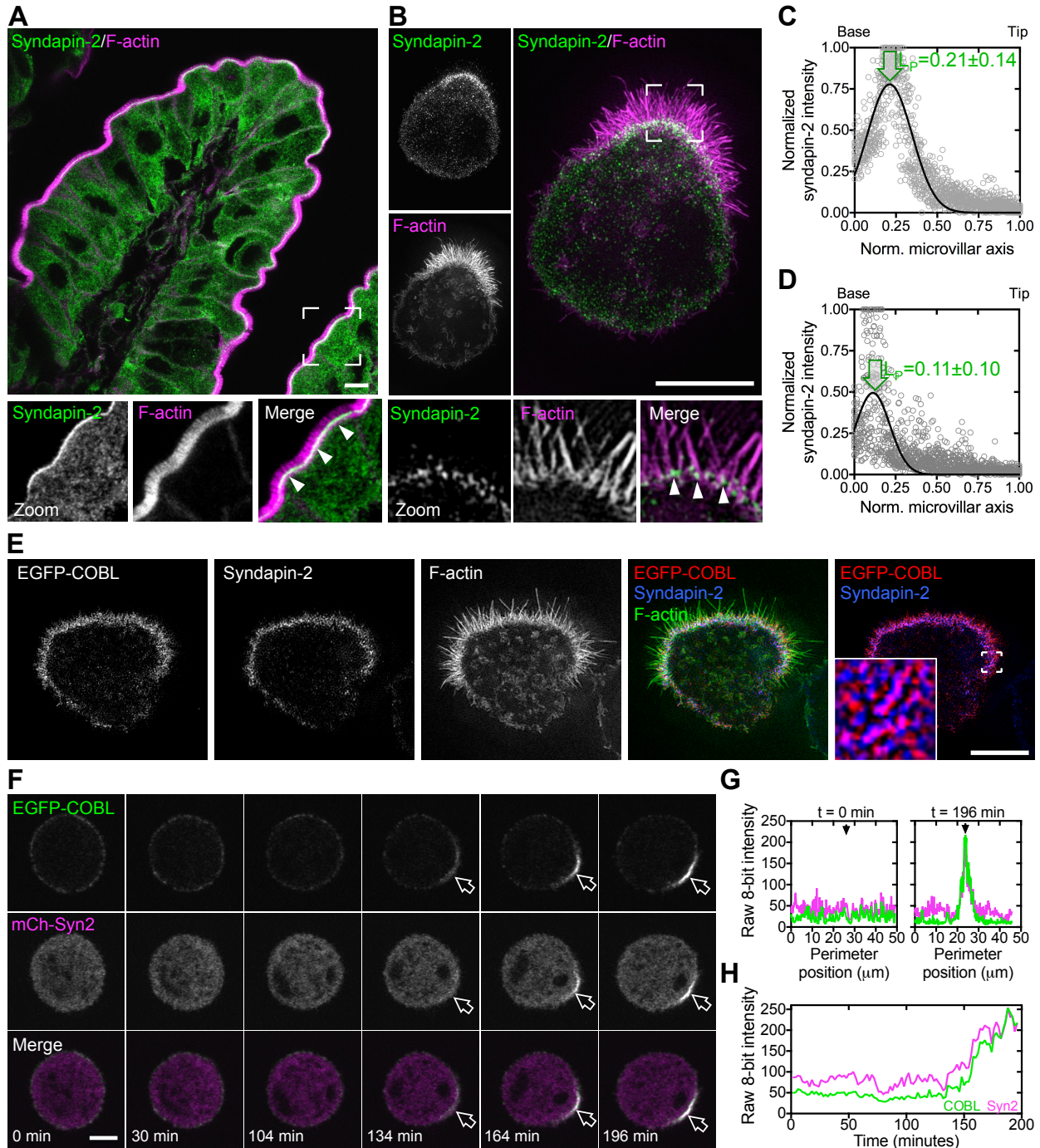
Figure 3-7: Syndapin-2, similar to COBL, localizes to the base of BB microvilli. (A) Endogenous syndapin-2 localization (green) and F-actin signal (magenta) in a villus from human small intestine. Boxed corners indicate zoom region; arrowheads highlight syndapin-2 localization near the base of the BB. (B) SIM projection of endogenous syndapin-2 (green) in an Ls174T-W4 cell reveals enrichment at the base of the BB. Boxed corners indicate zoom region. Arrowheads highlight syndapin-2 localization at the base of the BB. (C,D) Linescans parallel to the microvillar axis (n = 25) show the distribution of endogenous syndapin-2 in human small intestine and in Ls174T-W4 cells, respectively. Arrows highlight peak localization. (E) SIM projection of EGFP-COBL (red), endogenous Syndapin-2 (blue) and F-actin (green) shows colocalization of EGFP-COBL and Syndapin-2 at the base of the BB. Boxed corners in red/blue channel overlay indicate zoom region. (F) Time series montage of an Ls174T-W4 cell co-expressing EGFP-COBL and mCherry-syndapin-2 undergoing cell polarization and BB assembly. (G) Perimeter line-scan analysis of the cell shown in C at t = 0 and t = 196 min, black arrow in right hand plot marks position of the BB. (H) Intensity profile over time of a 2.5 µm^2 ROI at the base of the forming BB in F. Scale bars are 5 µm.

colocalization at the base of forming BBs (Figure 3-7F-H). Thus, syndapin-2 is well positioned to interact with COBL and facilitate its targeting to the apical membrane during epithelial differentiation.

We next sought to determine the impact of syndapin-2 KD on BB assembly and COBL targeting in Ls174T-W4 cells. Similar to COBL KD, syndapin-2 KD resulted in a significant decrease in the percentage of cells capable of forming BBs (40.7 ± 2.4%) relative to controls (73.8 ± 1.2%; Figure 3-8A). This phenotype was rescued by reintroducing a mouse syndapin-2 construct refractory to KD (75.3 ± 4.2%; Figure 3-8A). Moreover, inspection of BB-positive syndapin-2 KD cells revealed a significant loss of COBL localization from the base of microvilli (Figure 3-8B,C). In the reciprocal experiment, COBL KD produced only a minor impact on syndapin-2 signal at the apical domain (Figure 3-8B,D). Thus, these data suggest that in the context of IECs, syndapin-2 functions upstream of COBL and is needed for targeting of this factor to the apical membrane.
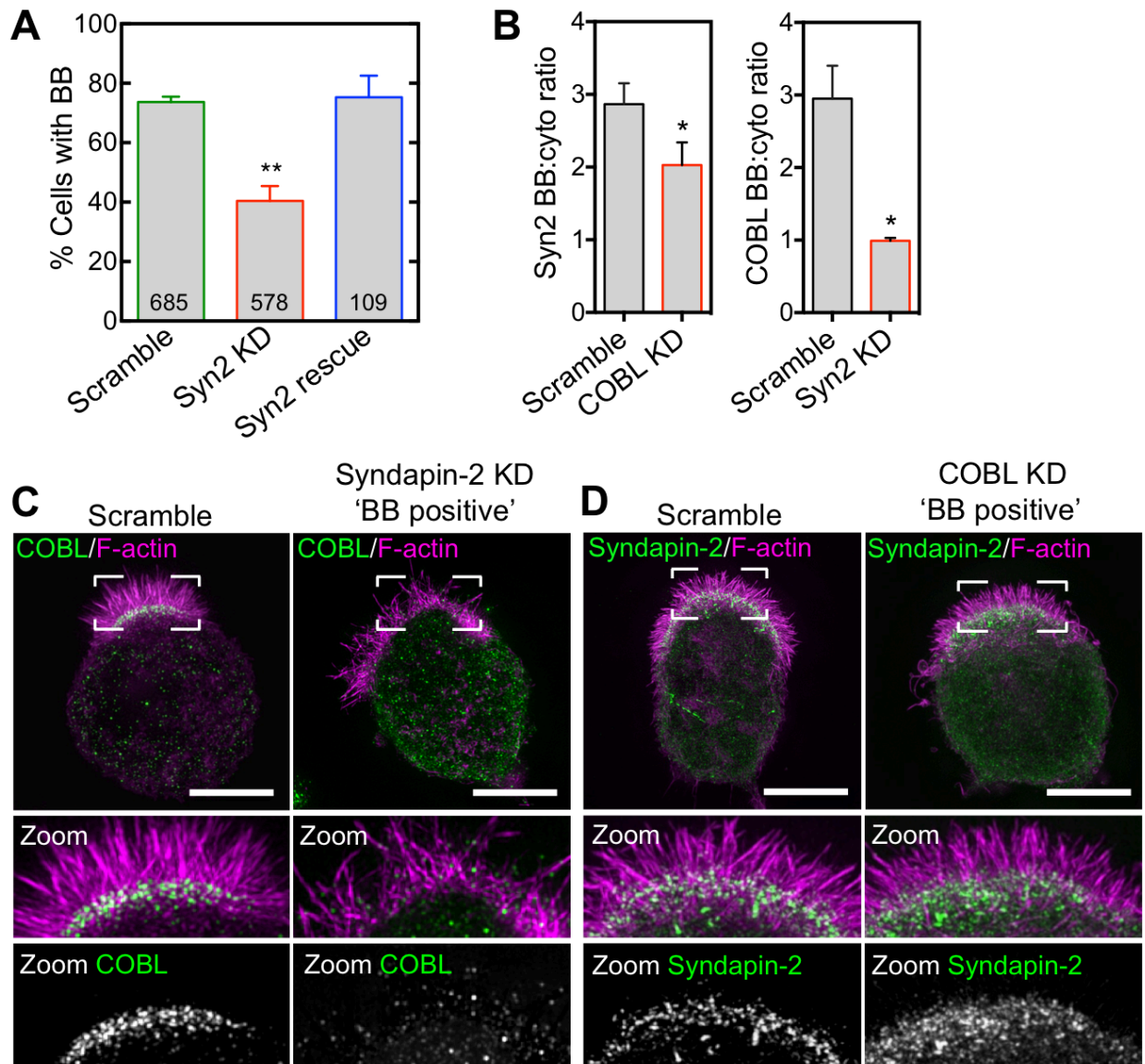
Figure 3-8: Syndapin-2 targets COBL to the base of the BB. (A) BB formation in response to syndapin-2 KD and rescue. Mean ± SEM from 3 separate experiments, n per condition listed in bars. (Student's t-test, **p<0.004). (B) Left, syndapin-2 BB enrichment in scramble and COBL KD cells. Right, COBL BB enrichment in scramble and syndapin-2 KD cells. Data is displayed as mean ± SEM (Student's t-test, *p<0.05). n = 30 cells/condition. (C) SIM projections of COBL immunostaining (green) and F-actin (magenta) in control and syndapin-2 KD cells. Boxed corners indicate zoom region. (D) SIM projections of syndapin-2 immunostaining (green) and F-actin (magenta) in control and COBL KD cells. Boxed corners indicate zoom region. Scale bars are 5 μm.

A recent study examining the localization of over-expressed proteins in JEG-3 cells concluded that COBL is responsible for targeting syndapin-2 to the membrane (Wayt and Bretscher, 2014). This conflict with our observations might suggest that the function of

COBL-syndapin-2 complex is context specific. However, our results are consistent with studies performed in neurons, which revealed that syndapin-1 targets COBL to sites of F-actin assembly during dendritogenesis (Schwintzer et al., 2011).

Discussion

Impact of COBL on microvillar morphology

Our findings indicate that COBL plays a significant role in promoting microvillar growth and BB assembly during the differentiation of cultured IECs. *In vitro* biochemical studies with COBL fragments revealed a range of activities including nucleation, severing of ADP-F-actin, sequestration of ADP-G-actin, and profilin-like binding to ATP-actin (Husson et al., 2011). In our assays, overexpression of COBL and COBL fragments containing multiple active WH2 domains induced striking effects on microvillar growth. Cells transfected with longer fragments of the COBL C-terminus (1-KAB, KAB, KABC), which are predicted to nucleate and sever (Husson et al., 2011), significantly increased microvillar surface coverage (Figure 3-4D). One possible interpretation of this effect is that generating large numbers of microvilli during BB assembly requires cooperation between COBL nucleation and severing activities, both of which would increase the number of elongation-competent filaments.

COBL over-expression also increased phalloidin intensity along the microvillar axis, suggesting more filaments per core bundle (Figure 3-4D). Microvilli were also longer and straighter, which might represent secondary effects of having more filaments per core (Figure 3-4D). Thicker bundles would also exhibit a higher flexural rigidity (Gittes et al., 1993), which could explain their straighter appearance in SIM images. Bundles containing more filaments would also have more force generating barbed-ends pushing against the

apical membrane, which could explain the increased length of COBL-induced microvilli. However, we cannot rule out other potential mechanisms that might influence microvillar length. For example, COBL might recruit elongation/anti-capping factors such as Ena/VASP family members or formins (Chesarone and Goode, 2009), to the apical domain, although our experiments would argue against significant involvement of formins in BB assembly (Figure 3-1D,F).

COBL KD completely inhibited microvillar formation in a large fraction of cells, and stunted microvillar growth in the remaining cells (Figure 3-6). Rescue experiments also revealed that functional WH2 domains, which mediate nucleation and severing (Ahuja et al., 2007; Husson et al., 2011), are needed for these effects. Although COBL KD was greater than 95% effective based on western blots, approximately 35% of COBL KD cells still formed rudimentary BBs suggesting that other pathways compensate for the loss of COBL in this model. Such compensatory mechanisms are expected when we consider that BBs still form in mouse models lacking key structural proteins, including myosin-1a (Tyska et al., 2005), ezrin (Saotome et al., 2004), or villin, espin, and plastin-1 (Revenu et al., 2012).

Significance of COBL localization

Super-resolution analysis of COBL localization in native intestinal tissue and cultured IECs revealed enrichment near, but not precisely at the pointed-ends of microvillar actin bundles. Population averages show that COBL enrichment exhibits a peak at ~15% of total bundle length from the pointed-end (Figures 3-2C,D, 3-3B). Because our SIM images are limited to a lateral resolution of ~110 nm (~diameter of a core bundle), we are unable to determine whether COBL is integrated within mature microvillar actin bundles, binds to

the sides of core bundles, or is merely anchored near bundle rootlets. However, a truncated form of COBL lacking C-terminal WH2 domains targeted to the apical domain, but failed to demonstrate the focused enrichment of full length COBL near the pointed-ends (Figure 3-4C). Thus, direct binding to actin contributes to the precise distribution of COBL observed in our SIM images.

Is COBL localization consistent with a role in generating microvillar actin bundles? Because WH2 domain-containing proteins generate new filaments by creating nuclei that elongate primarily from their barbed-ends, these factors are expected to localize to filament pointed-ends (Ahuja et al., 2007; Quinlan et al., 2005; Zuchero et al., 2009). However, the actin nucleator APC remains bound to the filament it nucleates without inhibiting elongation of the pointed-end (Breitsprecher et al., 2012). As elongation proceeds, APC is left near but not precisely at the pointed-end. A similar mechanism might help explain the localization of COBL: following formation of a COBL-actin nucleus, elongation might proceed from both ends of the nucleus, leaving COBL behind at the original site of nucleation. This model is consistent with a recent structural study, which proposed that COBL-actin nuclei initially elongate from the pointed-end before barbed-end elongation begins (Chen et al., 2013). Biochemical studies have also shown that both ends of microvillar core bundles are uncapped and remain competent for elongation (Mooseker et al., 1982). Enrichment of COBL near the base of microvillar F-actin bundles would also be consistent with a role in binding and severing ADP-F-actin. While it is appealing to interpret COBL localization data only in terms of nucleation and severing activities (Ahuja et al., 2007; Haag et al., 2012; Husson et al., 2011), our experiments do

63

not allow us to rule out other contributions to microvillar formation, such as anchoring core bundles in the terminal web.

Apical targeting of COBL requires syndapin-2

For COBL to function in microvillar growth, it must be targeted to the apical plasma membrane during differentiation. BAR domain-containing proteins are now recognized as membrane targeting factors for actin polymerization machinery (Aspenstrom, 2010). BAR domains are small helix bundles that form dimers capable of sensing and inducing membrane curvature (Peter et al., 2004). Our studies indicate that syndapin-2, which contains an N-terminal F-BAR domain, is required for COBL targeting to the apical domain (Figure 3-8). Because the N-terminal polyproline motifs in COBL interact with the SH3 domains of all three syndapin family members (Schwintzer et al., 2011), this requirement probably reflects direct binding between syndapin-2 and COBL. Consistent with this, the N-terminal region of COBL is sufficient for apical targeting (Figure 3-4). Thus, syndapin-2 likely provides COBL with a physical link to the apical plasma membrane. Interestingly, syndapin family F-BAR domains bind membranes with high positive (i.e. inward) curvature (Quan and Robinson, 2013), such as the plasma membrane found between adjacent microvilli. The intermicrovillar region is also an established site of endocytosis, which is intriguing given that syndapins have been implicated in membrane internalization (Qualmann and Kelly, 2000).
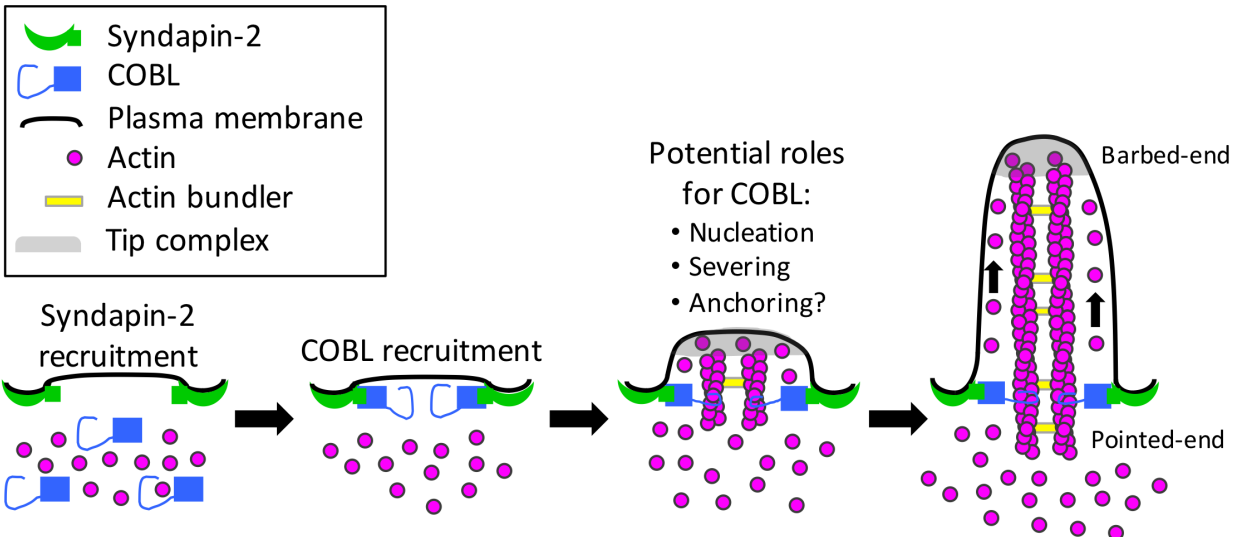
Figure 3-9: Model depicting a role for COBL in the formation of brush border microvilli.

Model and conclusions

Our studies lead us to the following model for microvillar growth during BB assembly (Figure 3-9). We propose that COBL targets to the nascent apical domain of differentiating IECs using the membrane binding capacity of its binding partner, syndapin-2. There, COBL contributes to microvillar formation using one or more of its actin regulating activities including nucleation, severing, and/or anchoring. Following filament formation, new filaments elongate and are bundled by factors such as villin, fimbrin, espin, and EPS8 to generate a core bundle of mature length (~1-3 µm)(Crawley et al., 2014a). While minor elongation may take place off the pointed-ends, the barbed-ends grow much faster. Dynamics at the barbed-ends will be controlled by capping and anti-capping factors, which are likely components of the electron dense 'tip complex' that appears to serve as a membrane attachment site for filaments in both growing and mature microvilli (Burgess and Grey, 1974; Mooseker et al., 1982; Tilney and Cardell, 1970).

In conclusion, our results provide new insight on a COBL-dependent mechanism of microvillar growth during BB assembly. We expect future studies to focus on identifying elongation and capping factors that function in microvillar formation, and determining how syndapin-2-dependent targeting of COBL is controlled by upstream factors that regulate polarity establishment (Gloerich et al., 2012). Future work must also elaborate on the findings presented here by exploring roles for COBL in intestinal diseases characterized by perturbations of BB microvilli (Davidson et al., 1978; Vallance et al., 2002).

CHAPTER IV.

IMPACT OF CORDON BLEU EXPRESSION ON ACTIN CYTOSKELETON

ARCHITECTURE AND DYNAMICS

Nathan E. Grega-Larson, Scott W. Crawley and Matthew J. Tyska

Department of Cell and Developmental Biology, Vanderbilt University, Nashville, TN

37240, USA

To whom correspondence should be addressed:
Matthew J. Tyska, Ph.D.
Professor
Dept. of Cell and Developmental Biology
Vanderbilt University
3154 MRB III, PMB 407935
465 21st Avenue South
Nashville, TN 37240-7935
Office: 615-936-5461
Lab: 615-936-5504

Abstract

Cordon-bleu (COBL) is a multifunctional WASP-Homology 2 (WH2) domain-containing protein implicated in a wide variety of cellular functions ranging from dendritic arborization in neurons to the assembly of microvilli on the surface of transporting epithelial cells. *In vitro* biochemical studies suggest that COBL is capable of nucleating and severing actin filaments, among other activities. How the multiple activities of COBL observed *in vitro* contribute to its function in cells remains unclear. Here, we used live imaging to evaluate the impact of COBL expression on the actin cytoskeleton in cultured cells. We found that COBL induces the formation of dynamic linear actin structures throughout the cytosol. We also found that stabilizing these dynamic structures with the parallel actin bundling protein espin slows down their turnover and enables the robust formation of self-supported protrusions on the dorsal cell surface. Super-resolution imaging revealed a global remodeling of the actin cytoskeleton in cells expressing these two factors. Taken together, these results provide insight as to how COBL contributes to the assembly of actin-based structures such as epithelial microvilli.

Introduction

A major goal in actin cytoskeleton biology is to identify factors responsible for assembling specific subcellular networks and arrays. Investigators have uncovered a vast collection of regulatory factors, which function together to drive the assembly of actin arrays using a range of activities including filament nucleation, elongation, capping, bundling, and severing (Lee and Dominguez, 2010). One functionally diverse class of regulatory factors are the WASP-Homology 2 (WH2) domain-containing molecules, which include Cordon-bleu (COBL), SPIRE, JMY, the bacterial effector proteins VopF and VopL, TARP, Sca2, Leiomodin, and WASP family nucleation promoting factors (Namgoong et al., 2011). WH2 domains are 17-20 amino acid sequences characterized by an amphipathic α-helix, an LKKV motif, and a variable C-terminus (Dominguez, 2016). In isolation, WH2 domains can bind G-actin, but much more complex functions are possible when these domains are linked in tandem.

A prime example is provided by COBL, which is comprised of an N-terminal proline rich region with several PxxP motifs that bind SH3 domain-containing proteins, a central weak coiled coil that may play a role in oligomerization, and three tandem C-terminal WH2 domains. COBL was first identified in a gene trap study in mouse as a novel gene expressed along the midline during embryogenesis (Gasca et al., 1995). Subsequently, it was shown that COBL functions as an actin nucleator, critical for neurite outgrowth (Ahuja et al., 2007). In zebrafish, COBL is important for the proper development of the Kupffer's vesicle (Ravanelli and Klingensmith, 2011), and necessary to form functional ciliated sensory hair cells (Schuler et al., 2013). More recently, COBL was shown to be involved in the assembly of F-actin bundles that support microvilli on the surface of

intestinal and placental epithelial cells (Grega-Larson et al., 2015; Wayt and Bretscher, 2014). In these contexts, COBL targets near the base of microvillar actin bundles, where the pointed ends of actin filaments reside (Hirokawa et al., 1982). Intestinal epithelial cells lacking COBL are deficient in brush border assembly, whereas overexpression of this factor drives microvillar growth and expansion of the brush border (Grega-Larson et al., 2015).

Numerous studies indicate that COBL is a multifunctional regulator of actin dynamics. Based on the spacing between its WH2 domains, COBL was initially proposed to stabilize a short pitch trimeric actin nucleus from which spontaneous filament assembly can occur (Ahuja et al., 2007). However, a subsequent study using purified fragments of COBL showed that only one WH2 domain was necessary for nucleation (Husson et al., 2011). This study also revealed that COBL constructs with at least two WH2 domains exhibit filament severing activity and sequestered ADP-actin in pyrene-actin polymerization assays. In terms of mechanisms underpinning these activities, a crystal structure of the first two WH2 domains of COBL in complex with two actin monomers suggests that a COBL-actin nucleus initially grows slowly in the pointed-end direction because barbed-end growth is blocked (Chen et al., 2013). ATP hydrolysis of bound actin monomers is proposed to induce a conformational change that in turn allows for rapid barbed-end elongation (Chen et al., 2013). Thus, if COBL does nucleate actin filaments in cells, it is expected to enrich near the pointed-ends of the resulting actin filaments. This prediction is consistent with the studies in epithelial cells alluded to above (Grega-Larson et al., 2015; Wayt and Bretscher, 2014).

Whereas COBL activities that impact actin dynamics are localized to its C-terminal WH2 domains, the N-terminal proline rich domain has been implicated in protein/protein interactions and subcellular targeting. COBL polyproline motifs bind the SH3 domain of the F-BAR protein syndapin, which plays a role in targeting COBL to the membrane in neurons and intestinal epithelial cells (Grega-Larson et al., 2015; Schwintzer et al., 2011). Additionally, COBL contains numerous calmodulin binding sites, calcium and calmodulin regulate COBL actin binding, and the effect of COBL on dendritogenesis is dependent on its interaction with calmodulin (Hou et al., 2015).

How COBL contributes to cytoskeletal remodeling in cells remains unclear, in part due to a lack of live cell imaging data. To determine how COBL impacts the dynamics and architecture of the actin cytoskeleton in live cells, we examined the impact of expressing fluorescent protein-tagged COBL in cultured B16F1 mouse melanoma cells. We found that COBL expression induces the formation of dynamic linear actin structures, which associate with COBL-enriched puncta at their pointed ends. Stabilization of these features with the actin bundling protein, espin, allows for the formation of long-lived, self-supporting plasma membrane protrusions that resemble microvilli. Our results reveal that WH2 domain actin regulatory factors such as COBL hold the potential to drive assembly of F-actin-supported finger-like protrusions. These findings also provide insight on how epithelial cells create and maintain the elaborate cellular morphologies that are required for physiological function.
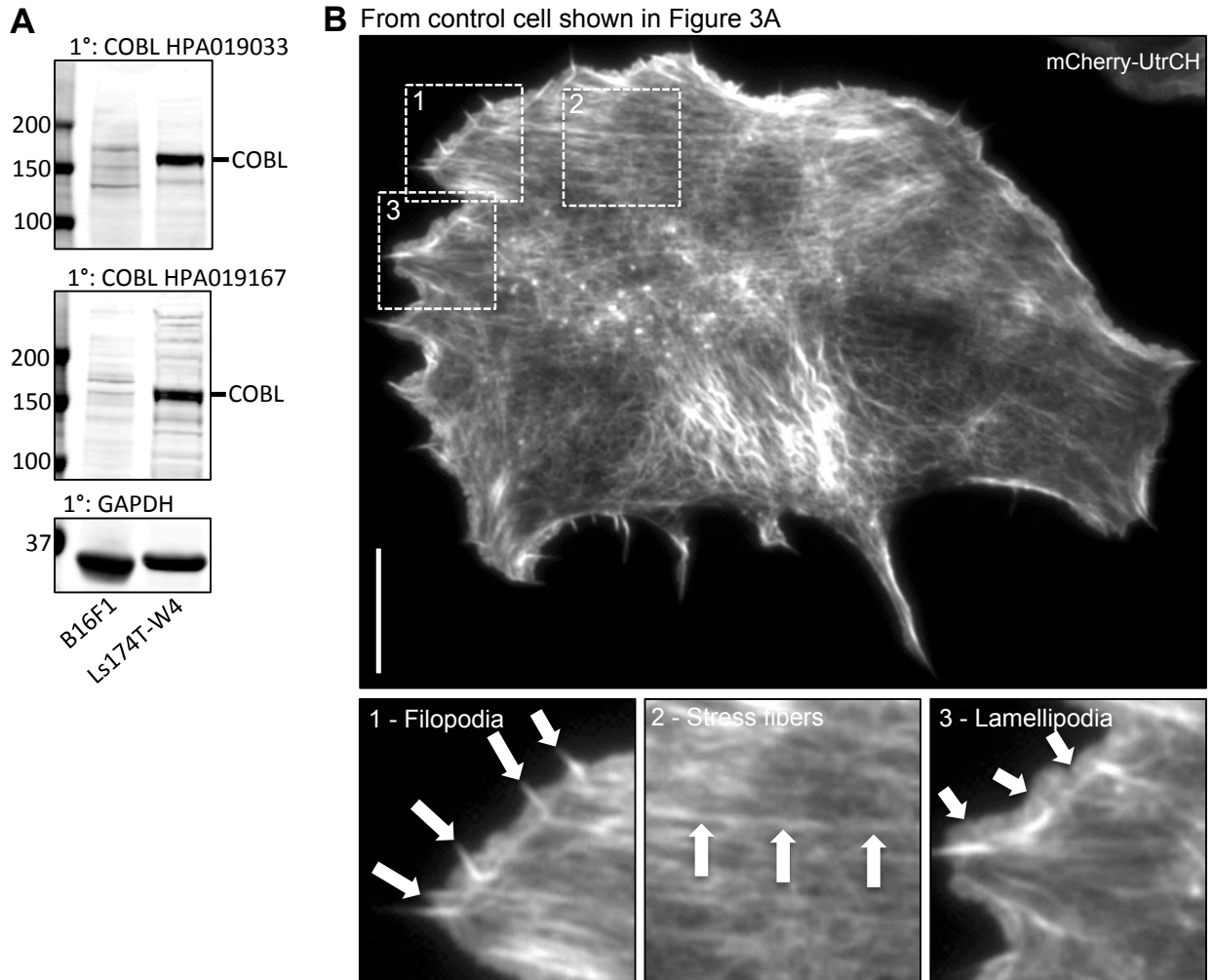
Figure 4-1: (A) Western blots of B16F1 and Ls174T-W4 (positive control) cell lysates using two antibodies against COBL showing lack of expression in B16F1 cells. GAPDH was used as a loading control. (B) B16F1 cell expressing mCherry-UtrCH with zoom panels highlight stress fibers, lamellipodium, and filopodia as indicated. Scale bar is 10 μm.

Results

COBL induces formation of dynamic linear actin structures in melanoma cells

Localization analysis, along with overexpression and KD studies, suggest that COBL is necessary and sufficient to drive microvillar growth on the apical surface of intestinal epithelial cells (Grega-Larson et al., 2015). If COBL is a key factor in microvillar assembly,
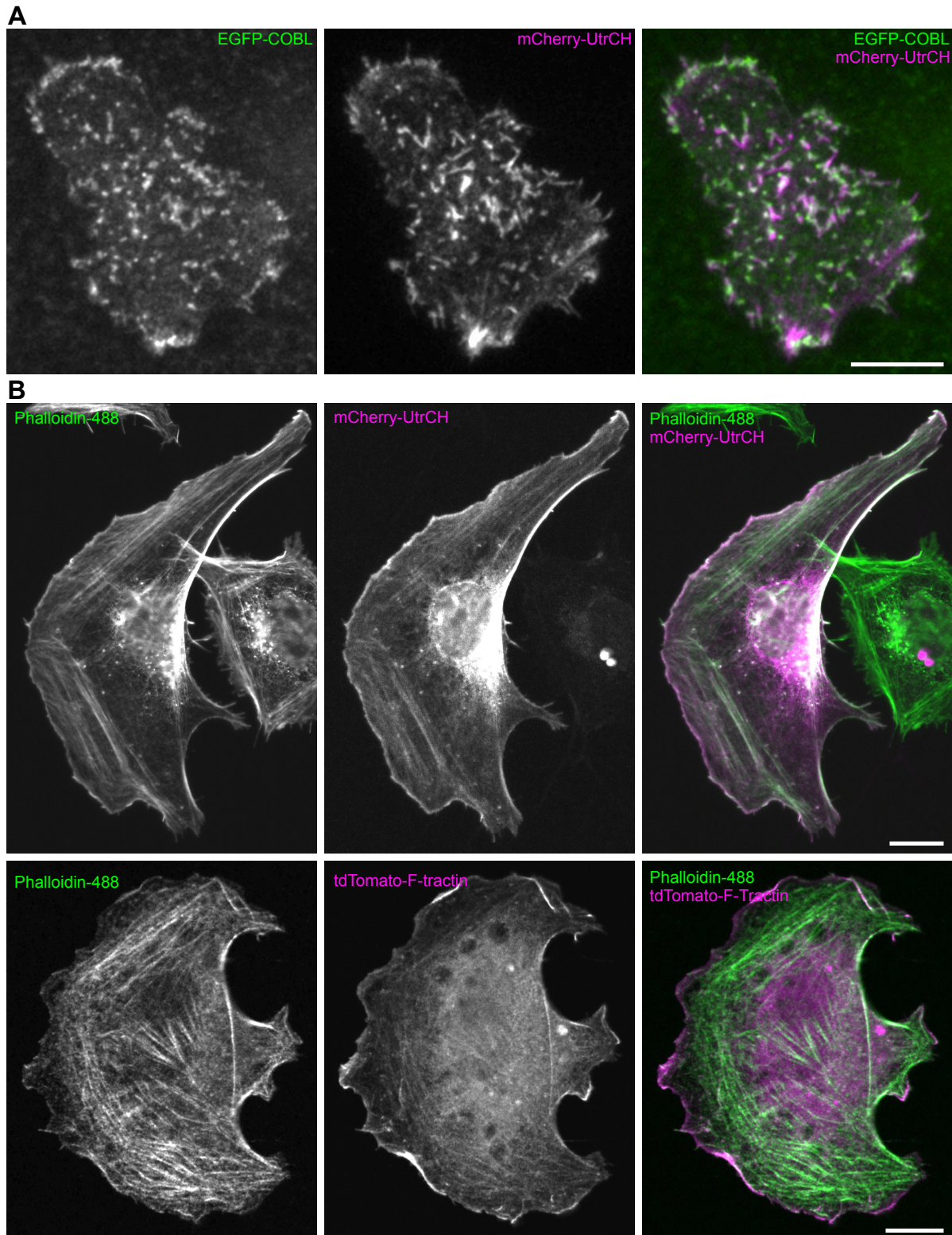
Figure 4-2: (A) A B16F1 cell expressing EGFP-COBL and mCherry-UtrCH reveals that the induction of linear actin structures does not dependent on the identity of the fluorescent protein tag. (B) B16F1 cells expressing either mCherry-UtrCH (upper row) or td-Tomato-F-tractin (lower row) and stained with Phalloidin-488. All scale bars are 10 µm.

we hypothesized that its expression in cells that do not normally make these protrusions would lead to the production of microvillus-like features. To test this hypothesis, we transfected B16F1 mouse melanoma cells with 3x-mCitrine-tagged COBL and mCherry-UtrCH (Burkel et al., 2007), and examined cells using near-TIRF microscopy. The 3x-mCitrine-tag enabled us to visualize low levels of COBL and avoid confounding dominant negative effects that can be associated with strong over-expression. B16F1 cells have been used in numerous previous studies on actin cytoskeleton dynamics (Mejillano et al., 2004; Schober et al., 2007; Starke et al., 2014; Svitkina et al., 2003; Vignjevic et al., 2006) and lack appreciable levels of endogenous COBL (Figure 4-1A). These cells assemble a broad range of actin-rich networks including stress fibers, filopodia, and lamellipodia (Figure 4-1B). Expression of 3x-mCitrine-COBL had little impact on the number of finger-like protrusions. However, we did note the aberrant formation of F-actin-rich structures throughout the cytoplasm (Figure 4-3B). Due to their high labeling intensity, we reasoned that these were composed of numerous actin filaments. Control experiments revealed that an EGFP-tagged variant of COBL produced an identical effect (Figure 4-2A). One end of each linear structure was capped by a prominent COBL punctum (Figure 4-3C, C'). COBL-induced structures were highly dynamic (Figure 4-3C, C'), growing (14.6 ± 1.5 nm/s) and shrinking (36 ± 5.3 nm/s) over the course of minutes (Figure 4-3D), with a mean lifetime of 162 ± 20 s. Interestingly, COBL appeared to accumulate along the length of the structure during the time leading up to disassembly (Figure 4-3C, C', E). Such oscillatory dynamics are consistent with the unique behavior exhibited by COBL in pyrene-actin assembly assays (Husson et al., 2011).

A mCherry-UtrCH

B 3x-mCitrine-COBL mCherry-UtrCH 3x-mCitrine-COBL mCherry-UtrCH

C 3x-mCitrine-COBL mCherry-UtrCH 0 s 35 80 115 130 165

C' 3x-mCitrine-COBL mCherry-UtrCH 0 s 15 65 80 100 110

D Rate (nm/sec) -60 -40 -20 0 20 40 60 Shortening Elongation

E COBL F-actin Length (μm) Time (sec)

F 3x-mCitrine-COBL mCherry-UtrCH 0 s 20 40 60 100 140 170 210

G 3x-mCitrine-COBL mCherry-UtrCH

H EGFP-COBL-WH2* mCherry-UtrCH

I EGFP-COBL-sever* mCherry-UtrCH

J Peak Length (μm) **** WT COBL COBL-sever*

Figure 4-3: COBL expression induces the formation of linear cytosolic actin structures in B16F1 cells. Live near-TIRF imaging of a B16F1 cell expressing mCherry-UtrCH alone (A) or 3x-mCitrine-COBL (green) and mCherry-UtrCH 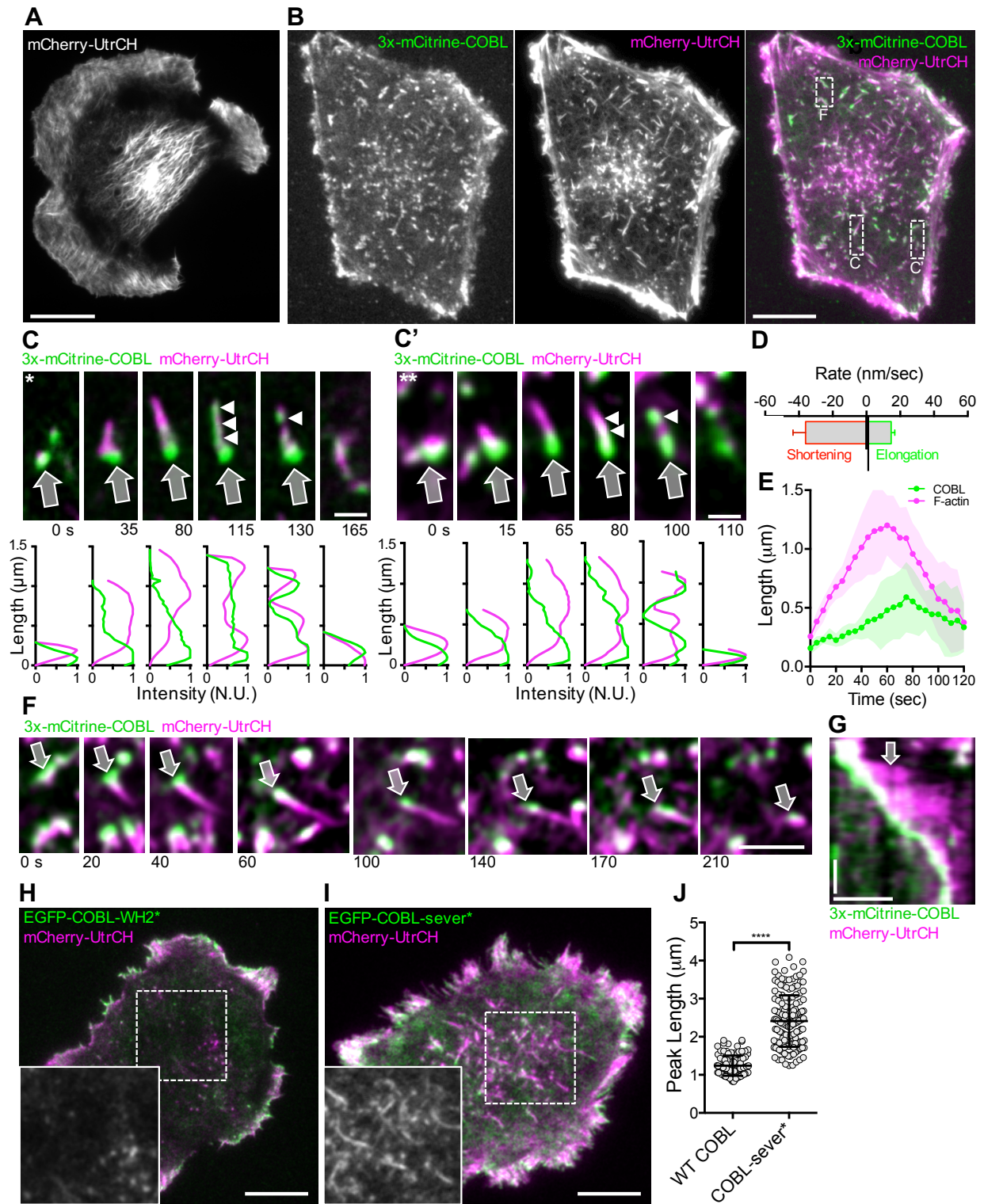(magenta) (B). Scale bar 5 μm. (C & C') Montages reveal the dynamics of single linear actin structures that form in the dashed boxes in merge image from A. Arrows highlight the initial COBL puncta, arrowheads highlight COBL signal along the structure at later time points. Line scans are shown below each image. Scale bar 1 μm. (D) Rates of assembly and disassembly measured for intracellular actin structures induced by COBL overexpression. n = 42 structures from 10 cells. (E) Graph depicting the ensemble averages of the length of COBL-induced structure (magenta) and the length of the structure occupied by COBL (green) relative to time for ten individual structures ~110-115 sec in duration. Shaded area represents the standard deviation at each time point (F) Montage of a single linear actin structure from the boxed region in (A) that grows and moves through the cytosol before disassembly. Arrow highlights the COBL-associated end of the structure. Scale bar 2 μm. (G) Kymograph of actin structure in (F). Scale bars are 2 μm (horizontal) and 60 seconds (vertical). (H) Near-TIRF image of a B16F1 cell co-expressing EGFP-COBL-WH2* and mCherry-UtrCH. Zoom in lower left-hand corner is of the mCherry-UtrCH channel alone from boxed region. Scale bar is 5 μm. (I) Near-TIRF image of a B16F1 cell co-expressing EGFP-COBL-sever* and mCherry-UtrCH. Zoom in lower left-hand corner is of the mCherry-UtrCH channel alone from boxed region. Scale bar is 5 μm. (J) Graph of peak linear structure length in COBL expressing cells vs. COBL-sever* expressing cells.

A subset of COBL-induced structures appeared to glide through the cytosol (Figure 4-3F, G). In these cases, actin grew from a COBL punctum to a steady state length. Fiduciary marks in kymographs revealed that after initial elongation, the COBL-associated end of the structure shortened whereas the opposite end continued growing, producing an effective translocation of the structure through the cytosol. After a period of time, the COBL-associated end began to shorten faster than growth at the opposite end, leading to complete disassembly of the structure. The observed linear F-actin structures did not form in cells expressing a COBL construct with WH2 domain mutations that abolish actin binding (Chen et al., 2013), although this mutant still appeared to co-localize with F-actin in small puncta (EGFP-COBL-WH2*; Figure 4-3H). Additionally, the peak length of these structures increased by almost two fold when cells were expressing EGFP-COBL-sever*, a COBL mutant predicted to exhibit normal nucleation but defective severing activity (1.24 ± 0.27 vs. 2.41 ± 0.68; Figure 4-3I, J) (Jiao et al., 2014). Together, these data suggest

that COBL can induce the formation of short-lived linear actin structures, that functional WH2 domains are required for this activity, and that the lengths of these structures are limited by COBL severing activity.

COBL localizes to the pointed ends of dynamic linear actin structures

We sought to determine the polarity of COBL-induced linear actin structures. To differentiate between barbed- and pointed-ends, we co-expressed COBL with Eps8, which is known to target to the tips of actin bundles that support microvilli, stereocilia, and filopodia, where barbed ends are located (Croce et al., 2004; Disanza et al., 2006). As expected for a WH2 domain-containing nucleator (Dominguez, 2009), the COBL-associated end of the structure was identified as the pointed-end based on the fact that Eps8 was enriched on the opposite end (Figure 4-4 A,B). This is also consistent with data from epithelial cells where COBL localizes near the pointed-ends of microvillar actin bundles (Grega-Larson et al., 2015; Wayt and Bretscher, 2014).

Co-expression of COBL and espin induces robust formation of finger-like protrusions

Although these results indicate that full length COBL can promote the assembly of linear actin structures, these features fail to protrude from the surface of B16F1 cells (Figure 4-3; Figure 4-5A). One reason could be that COBL/actin complexes are poorly anchored at the plasma membrane. Because syndapin-2 (also known as PACSIN2) has been shown to target COBL to sites of protrusion formation in epithelial cells (Grega-Larson et al., 2015), we reasoned that co-expression of COBL with syndapin-2 should promote
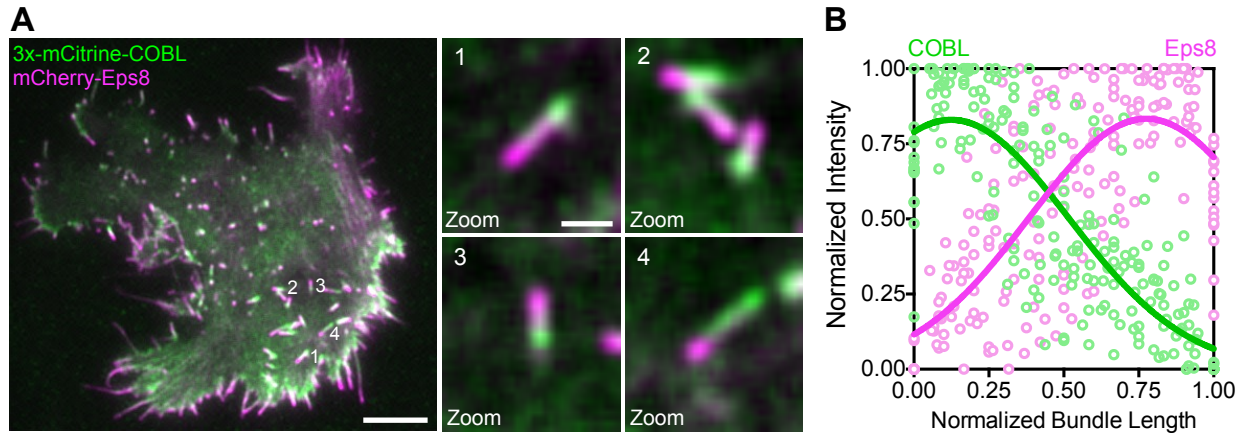
Figure 4-4: COBL localizes to the pointed ends of assembling linear actin structures. (A) Near-TIRF image of a B16F1 cell co-expressing 3x-mCitrine COBL and mCherry-Eps8. Zoom panels highlight intracellular structures with COBL and Eps8 on opposite sides. Numbers to the right of the structures in the first image correspond to the zoom numbers. Scale bar is 5 μm for left image and 1 μm for zoom images. (B) Line scans (n = 15 scans from 8 cells) along linear intracellular actin structures show the distribution of 3x-mCitrine-COBL (green) and mCherry-Eps8 (magenta) from cells co-expressing 3x-mCitrine-COBL and mCherry-Eps8.

anchoring of COBL-induced F-actin structures at the cell membrane. While we did observe prominent co-localization between these probes when co-expressed, we did not find a significant effect on protrusion *per se*; protrusion number was unchanged in co-expressing cells (Figure 4-5A,D). Thus, anchoring COBL at the membrane with syndapin-2 is not sufficient to generate finger-like protrusions in B16F1 cells.

We next explored the possibility that the rapid turnover dynamics and short lifetime of COBL-induced actin structures (162 ± 20 s) prevented their protrusion. To this end, we co-expressed 3x-mCitrine-COBL with factors that stabilize microvillar actin bundles including espin (Bartles et al., 1998), villin (Bretscher and Weber, 1979), and fimbrin (Bretscher and Weber, 1980) (Figure 4-5A). Interestingly, only co-expression of COBL with espin generated a significant increase in the number of protrusions as compared to each bundling protein tested alone (Figure 4-5A,D). Protrusions in COBL/espin co-expressing

A

UtrCH | Syndapin-2 / UtrCH | Fascin / UtrCH | Fimbrin / UtrCH | Villin / UtrCH | Espin / UtrCH

Zoom

COBL / UtrCH | COBL / Syndapin-2 | COBL / Fascin | COBL / Fimbrin | COBL / Villin | COBL / Espin

B

Normalized COBL Intensity vs Normalized Protrusion Length

C

Espin-WH2* / UtrCH | Espin-WH2* / COBL | EspinΔABD / UtrCH | EspinΔABD / COBL

D

Protrusions / 10 μm

* = vs. COBL
# = vs. Bundler alone

* vs. COBL + Espin
# vs. Espin alone

UtrCH, COBL, Syn2, COBL + Syn2, Fascin, COBL + Fascin, Fimbrin, COBL + Fimbrin, Villin, COBL + Villin, Espin, COBL + Espin, Espin-WH2*, COBL + Espin-WH2*, Espin-ΔABD, COBL + Espin-ΔABD

NS, ***, **, NS, NS, ****, ****, ****, ####, ****, ####, ****, ####, ****, ####, ****

79

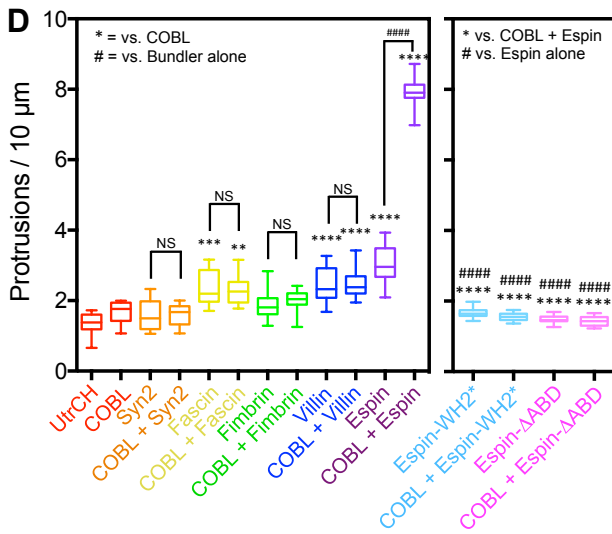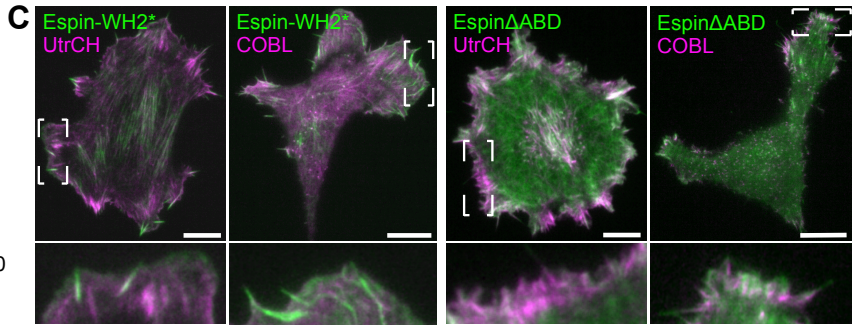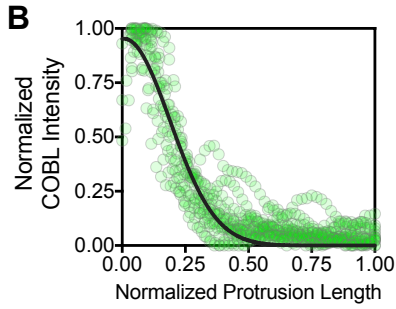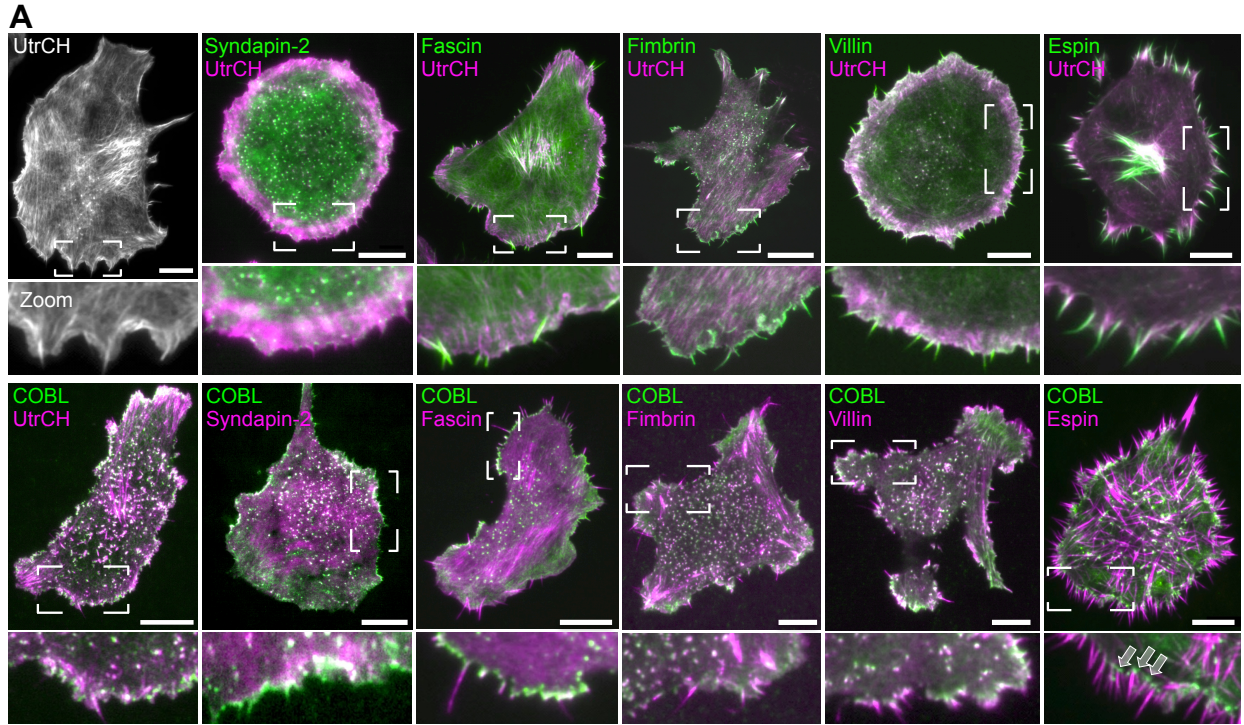**Figure 4-5: Espin stabilizes COBL-induced linear actin structures**. (A) Near-TIRF images of B16F1 cells expressing the constructs indicated, zoomed images highlight the morphology of the cell edge. All scale bars are 10 μm. Arrows in COBL/Espin zoom panel show COBL puncta at the base of peripheral protrusions, where the pointed-ends of actin filaments are expected to reside. (B) Line scans (n = 15 scans from 7 cells) along protrusions of cells co-expressing COBL and espin showing the distribution of 3x-mCitrine-COBL. (C) Near-TIRF images of B16F1 cells expressing the constructs indicated, zoomed images highlight the morphology of the cell edge. All scale bars are 10 μm. (D) Number of protrusions per 10 microns perimeter for cells expressing the constructs indicated. ANOVA with Tukey's multiple comparison's test was used for comparisons and to determine significance. (#### & **** p<0.0001). For both graphs, the boxes represent the 25th and 75th percentiles around the median, and the whiskers represent the 5th and 95th percentiles. n = 15 cells/condition.

cells were long-lived (874 ± 34 s in espin/COBL co-expressing cells vs. 162 ± 20 s with COBL alone), with many persisting for the full fifteen-minute duration of our time-lapse acquisitions. In COBL/espin co-expressing cells, we observed COBL puncta at the base of protrusions, where the pointed-ends of actin filaments are expected to reside (Figure 4-5A, COBL/espin; Figure 4-5B). Similar to villin and fimbrin, the actin bundling protein fascin, which is important for filopodial formation (Vignjevic et al., 2006), failed to increase protrusion number when co-expressed with COBL when compared to fascin alone (Figure 4-5A,D). Interestingly, COBL did not enrich on fascin-containing filopodia, suggesting that these factors segregate onto distinct populations of F-actin.

To investigate the domains of espin responsible for promoting robust protrusion when co-expressed with COBL, we generated two espin constructs, one with inactivating mutations in the WH2 domain (Espin-WH2*), and a second lacking the C-terminal actin bundling domain (EspinΔABD) (Figure 3C, D). Both of these constructs were unable to promote protrusion at levels comparable to wild-type espin, with protrusion numbers near control levels. Additionally, when these constructs were co-expressed with COBL, they were unable to induce the robust increase in protrusion formation that was observed with wild-type espin. Taken together, these data suggest that both the WH2 domain and C-
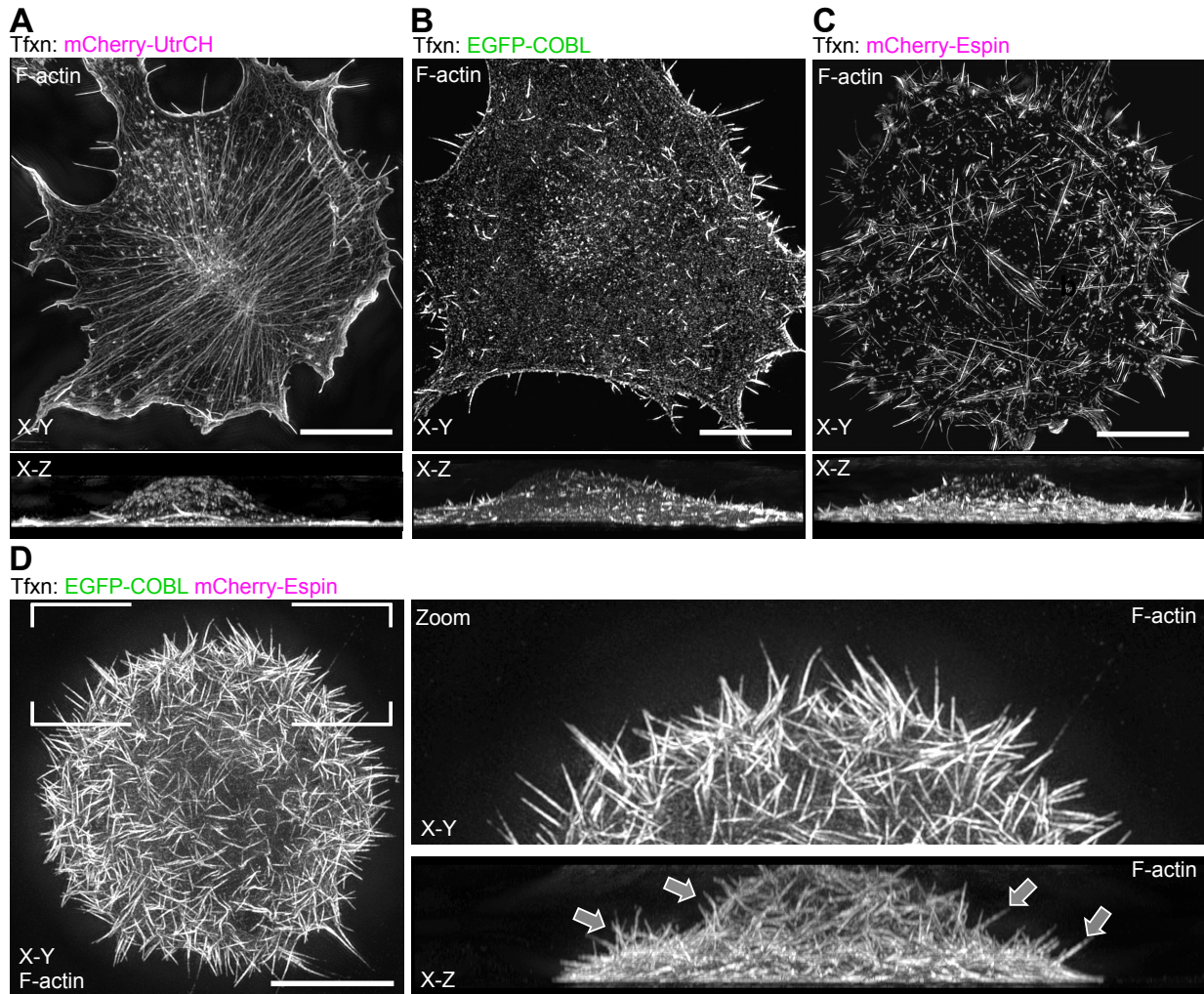
Figure 4-6: Espin and COBL co-expressing cells build microvillus-like protrusions. SIM X-Y and X-Z projections of phalloidin-stained cells transfected with mCherry-UtrCH alone (A), EGFP-COBL alone (B), or mCherry-espin alone (C) or co-transfected with EGFP-COBL and mCherry-espin (D). All scale bars are 5 μm.

terminal actin bundling domain of espin are required to synergize with COBL to drive the robust growth of finger-like protrusions.

Because the near-TIRF imaging approach used here only provides a limited view of the ventral cell surface, we turned to super-resolution structured-illumination microscopy (SIM) to assess how COBL co-expression with bundling proteins impacts the architecture of the actin cytoskeleton on a whole cell level (Figure 4). Strikingly, SIM

imaging of COBL/espin co-expressing cells revealed numerous self-supported protrusions extending from the dorsal surface (Figure 4D), structures that were largely absent from the surface of cells expressing either factor alone (Figure 4B, C). We also noted an apparent lack of ventral stress fibers in COBL/espin co-expressing cells, suggesting a significant re-allocation of actin into the induced surface protrusions. These data suggest that although COBL expression is capable of inducing linear actin based structures in both epithelial (Grega-Larson et al., 2015) and non-epithelial (Figure 1) cell types, COBL activity must be coordinated with bundlers such as espin to allow cells to assemble long-lived surface protrusions (Figure 3 & 4).

Discussion

In this report, we show that COBL expression in B16F1 mouse melanoma cells drives the formation of dynamic linear actin structures in the cytoplasm (Figure 1). These structures fail to give rise to plasma membrane protrusions, but they do exhibit COBL-enrichment at their pointed-ends and undergo dramatic cycles of elongation and shortening over the course of minutes (Figure 1B-F; Movies S2 & 3). Co-expression of COBL with the actin bundling protein espin was sufficient to drive the formation of long-lived finger-like protrusions on the dorsal surface of the cell, free from any substrate attachment (Figures 3A, COBL/espin; 4D). Thus, by expressing only these two factors, a cell type that does not normally make microvilli is induced to form microvillus-like protrusions on its surface.

The cycles of elongation and shortening observed here for COBL-induced actin structures are consistent with previous *in vitro* studies, which demonstrated that COBL drives oscillatory kinetics in pyrene-actin assembly assays (Husson et al., 2011). At a superficial level, the behavior of COBL-induced linear actin structures is reminiscent of

the dynamic instability originally described for microtubules (Mitchison and Kirschner, 1984). In this case, switching between elongation and shortening is controlled by subunit nucleotide hydrolysis and the concentration of free subunits available for incorporation into polymers. While these parameters may also impact the behavior of the COBL-induced structures we describe here, our live cell observations suggest some clear distinctions from classic dynamic instability. Most importantly, fiduciary marks in structure kymographs indicate that elongation is due to assembly at barbed-ends, whereas shortening is a consequence of disassembly at pointed-ends (COBL puncta-associated) or in some cases, severing along the length of the structure. Thus, the observed dynamics are more likely driven by a treadmilling mechanism, rather than classic dynamic instability, where assembly and disassembly take place at the same end of the polymer.

How does COBL contribute to the formation and subsequent dynamics of these linear actin structures? Given that COBL has been implicated as an actin nucleator (Ahuja et al., 2007; Chen et al., 2013; Husson et al., 2011), one straightforward scenario is that COBL puncta nucleate filaments that then elongate from their barbed ends. Here, COBL would remain behind at the pointed ends as filaments elongate, similar to what has been reported for filaments nucleated by APC (Breitsprecher et al., 2012; Okada et al., 2010). Such localization is consistent with the fact that COBL targets to the pointed ends of microvillar actin bundles on the surface of polarized epithelial cells (Grega-Larson et al., 2015; Wayt and Bretscher, 2014). Based on their strong labeling intensity, we suggest that COBL-induced structures are composed of numerous filaments. Given that Eps8, which enriches at the tips of the parallel actin bundles that support microvilli and stereocilia (Croce et al., 2004; Disanza et al., 2006), is also enriched at one end, we

suspect these structures are parallel actin bundles, but confirmation of this point will require ultrastructural analysis. After elongating for over a minute, COBL appears to accumulate along the structure's length, which is then followed by rapid shortening. Because expression of a COBL mutant deficient in severing (EGFP-COBL-sever*) (Jiao et al., 2014) leads to an increase in the length of these structures, COBL severing activity is likely involved in the disassembly phase. This proposal would be consistent with previous *in vitro* studies showing that COBL WH2 domains can bind to and sever ADP-actin (Husson et al., 2011).

Previous studies have shown that numerous cell types use syndapin family F-BAR proteins to target COBL to the plasma membrane (Grega-Larson et al., 2015; Schuler et al., 2013; Schwintzer et al., 2011). Somewhat unexpectedly, our co-expression experiments revealed that formation of COBL/syndapin-2 complexes at the membrane is not sufficient for persistent protrusion formation. However, we did find that co-expressing COBL with the filament bundling protein espin led to a dramatic increase in peripheral protrusion number relative to cells expressing COBL or espin alone. Additionally, co-expression of these factors allowed B16F1 cells to assemble microvillus-like protrusions on their dorsal surface. In intestinal epithelial cells, which express endogenous espin, expression of COBL alone is sufficient to promote the robust growth of finger-like protrusions (in this case microvilli) (Grega-Larson et al., 2015). The specificity of espin exerting this effect versus other bundling proteins in the current study is intriguing; espin is unique among actin bundlers in that it contains a WH2 domain in addition to its C-terminal actin-bundling domain (Loomis et al., 2003). Interestingly, we found that an espin construct with inactivating mutations in the WH2 domain, was unable to increase

protrusion number when expressed alone or co-expressed with COBL. Espin has been implicated in the early stages of stereocilia formation (Sekerkova et al., 2006), suggesting that this bundling protein is important for the initial assembly of actin-based protrusions. In line with our data, the actin bundling protein fimbrin has been shown to be important for maintenance but not formation of stereocilia (Taylor et al., 2015).

Whether COBL induces the formation of dynamic linear actin structures independently or in cooperation with other actin regulatory factors remains an open question. Other actin nucleators and elongation factors are known to synergize activities to form actin filaments. Indeed, the tandem WH2 domain nucleator spire cooperates with the formin cappuccino in actin meshwork assembly in developing *Drosophila* oocytes (Dahlgaard et al., 2007; Quinlan et al., 2007). Moreover, the nucleation promoting factor Bud6 works with the formin Bni1 in the assembly of actin cables in budding yeast (Graziano et al., 2011). Finally, actin nucleator APC and the formin mDia1 are known to cooperate in building the actin networks that drive normal directional cell motility (Breitsprecher et al., 2012; Okada et al., 2010). Future studies are needed to determine if COBL cooperates with formins or other elongation factors when building cellular actin features.

Another outstanding question relates to the role of dimerization/oligomerization in the regulation of COBL activity. COBL contains a weak coiled coil motif, but how this domain contributes to COBL activity remains unclear. Previous studies showed that dimerization is critical for boosting the activity of other WH2 domain nucleators including VopL and spire (Namgoong et al., 2011). Spire most likely dimerizes through its interaction with the formin cappuccino in *Drosophila* and formin-2 in mammals (Dahlgaard

et al., 2007; Montaville et al., 2014). Interestingly, while VopL and spire require dimerization for strong nucleation activity, COBL displays nucleation activity without dimerization (Ahuja et al., 2007; Husson et al., 2011). This may be related to the fundamental mechanism of nucleation in these different cases, i.e. stabilization of long pitch (VopL and spire) vs. short pitch (COBL) actin nuclei (Namgoong et al., 2011). Future investigations will need to determine if COBL dimerization/oligomerization is required for assembling the linear actin structures described here.

The data presented here provides insight on the mechanisms employed by COBL in the assembly of actin-based structures in cells. In concordance with *in vitro* kinetic studies of COBL fragments (Ahuja et al., 2007; Husson et al., 2011), our live cell imaging revealed the formation of dynamic linear actin structures, which emanate from COBL puncta. Based on findings presented here as well as results from previous studies (Grega-Larson et al., 2015), we propose that COBL/syndapin-2 complexes cooperate with actin bundling proteins such as espin, to drive the formation of persistent microvillus-like cell surface protrusions. Future studies using *in vitro* reconstitution approaches will be needed to test this concept directly.

CHAPTER V.

FUTURE DIRECTIONS PART I.

INITIAL CHARACTERIZATION OF THE INTESTINAL BRUSH BORDER OF THE

SYNDAPIN-2 KNOCKOUT MOUSE

Abstract

Coordinated interaction between the actin cytoskeleton and the plasma membrane is critical for the generation and maintenance of plasma membrane protrusions. Proteins belonging to the Bin-Amphiphysin-Rvs161/167 (BAR) domain family are critical for binding to membrane and stabilizing membrane curvature. Specifically, Fes-CIP4 homology-BAR (F-BAR) domain-containing proteins bind and stabilize membrane curvature. Here we present data showing that the F-BAR domain-containing protein syndapin-2 is required for maintaining normal microvillar structure. In mice lacking syndapin-2, microvilli are significantly shorter as compared to wild-type mice. The actin nucleator cordon-bleu (COBL), which we previously showed is targeted to the BB by syndapin-2, is still present in the BB in syndapin-2 knockout mice, suggesting that there are other mechanisms for targeting COBL to the BB. Finally, the increased presence of immune cells and segmented filamentous bacteria on the surface of the intestinal epithelium suggest that there may be a barrier defect in the syndapin-2 KO mice. The preliminary data presented here provide a strong rationale for continuing the characterization of the syndapin-2 KO mouse, and also generate new hypotheses behind the mechanisms of BB assembly and maintenance that remain to be tested.

Introduction

The intestinal brush border (BB) serves as the sole site of nutrient absorption in the body and also provides a physical barrier to prevent the translocation of bacteria and toxins into the organism. The BB is found on the surface of intestinal epithelial cells, termed enterocytes, and is made up of an array of tightly packed microvilli, finger-like membrane protrusions of uniform length supported by a core bundle of actin filaments (Crawley et al., 2014a). Microvilli serve to further increase the surface area of the intestinal epithelium to maximize nutrient absorption; to that end, microvilli are packed with enzymes and transporters responsible processing and absorbing the nutrients that pass through the small intestine (Goodman, 2010). At the same time, BB microvilli provide a barrier that on one end prevents infection of the host, but also plays a role in maintaining the niche that supports the intestinal microbiome (Delacour et al., 2016). Despite the importance of the BB in human health, the mechanisms employed by the enterocyte to assemble BB microvilli remain largely unclear.

Syndapins, also known as PACSINs (protein kinase C and casein kinase II interacting protein), contain an N-terminal Fes-CIP4 homology Bin-amphiphysin-Rvs161/167 (F-BAR) domain that binds to positive membrane curvature, and a C-terminal Src homology 3 domain that binds to dynamin and N-WASP. Through these interactions, syndapins link the actin cytoskeleton to the plasma membrane in dynamic processes such as clathrin-dependent and independent endocytosis, and neural spine formation (McDonald and Gould, 2016). The syndapin family is made of three genes that generate three main isoforms in mammals; syndapin-1 and 3 show tissue specific expression, with syndapin-1 being expressed in neurons and syndapin-3 in heart and skeletal tissues,

while syndapin-2 is ubiquitously expressed (Quan and Robinson, 2013). We have previously shown that syndapin-2 is expressed in enterocytes, is important for proper BB formation, and is critical for binding to and targeting the actin nucleator cordon-bleu (COBL) to the BB in Ls174T-W4 cells, a cell culture model system of BB assembly (Grega-Larson et al., 2015). However, whether or not this COBL/syndapin-2 complex is relevant *in vivo* is unclear. Here, we provide preliminary characterization of the intestinal BB from mice that are homozygous KO for the syndapin-2 gene using light and electron microscopy. These mice show significant defects in microvillar structure, suggesting that syndapin-2 is required for BB maintenance *in vivo.*

Results

Syndapin-2 localizes to the apical domain of enterocytes in the small intestine

To examine localization of syndapin-2 in the mouse small intestine, we stained intestinal tissue sections from wild-type and syndapin-2 KO mice with antibodies to syndapin-2 and villin, an actin bundling protein found throughout the BB (Bretscher and Weber, 1979). Although syndapin-2 displayed a significant cytoplasmic localization, it was highly enriched at the base of the BB in mature enterocytes on the villi of the small intestine, and the apical domain of immature enterocytes of the crypt, where the BB is initially formed (Figure 5-1 A-C). Importantly, no syndapin-2 protein was detected in the syndapin-2 KO mice as assessed by immunoblot of enterocyte whole cell lysates and immunofluorescence (Figure 5-1D,E). BB villin signal in the KO tissue also appeared lower, although this must still be confirmed quantitatively.
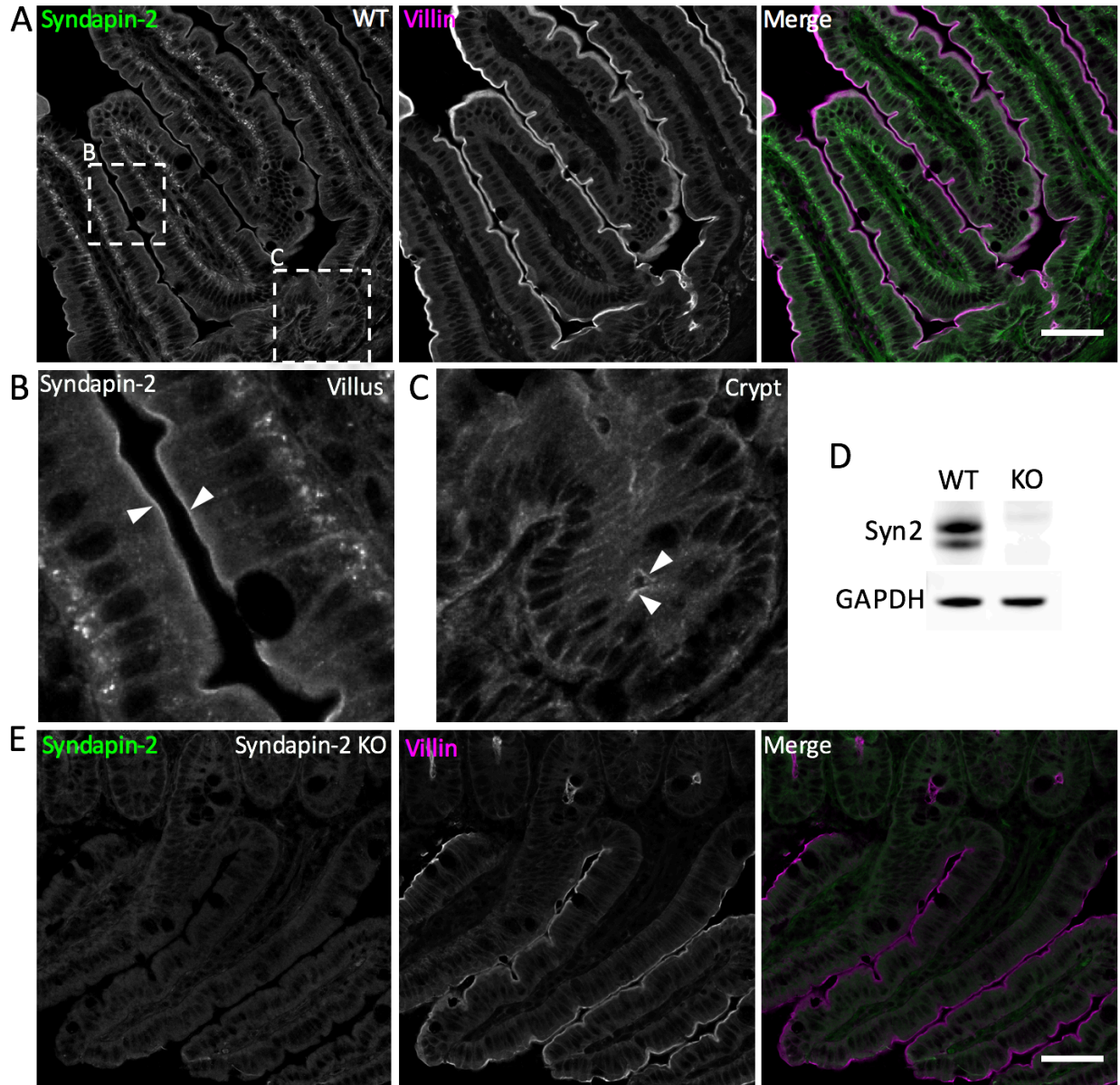
Figure 5-2: Syndapin-2 localizes to the apical domain of enterocytes in the small intestine.
A) Syndapin-2 (green) and Villin (magenta) localization in wild-type mouse small intestinal tissue. B) Zoom from A highlighting villar localization and C) crypt localization of syndapin-2. D) Immunoblot for syndapin-2 of enterocyte lysates from wild-type and syndapin-2 KO mice. GAPDH was used as a loading control. E) No syndapin-2 immunostaining above background observed in syndapin-2 KO mouse small intestinal tissue. Scale bars are 50 μm.

COBL BB enrichment is impaired but still present in syndapin-2 KO mice

Since we previously demonstrated that syndapin-2 is required for targeting the actin nucleator COBL to the BB in cultured cells (Grega-Larson et al., 2015), we next examined the localization of COBL in the syndapin-2 KO mouse intestine (Fig. 5-2). COBL was enriched at the base of the BB in syndapin-2 KO mice, but to a lesser extent than wild-type controls (BB:cytoplasmic ratio 2.83 ± 0.26 in WT vs. 1.52 ± 0.18 in KO, Fig. 5-2C), suggesting other mechanisms function to localize COBL to the BB if syndapin-2 is lost.
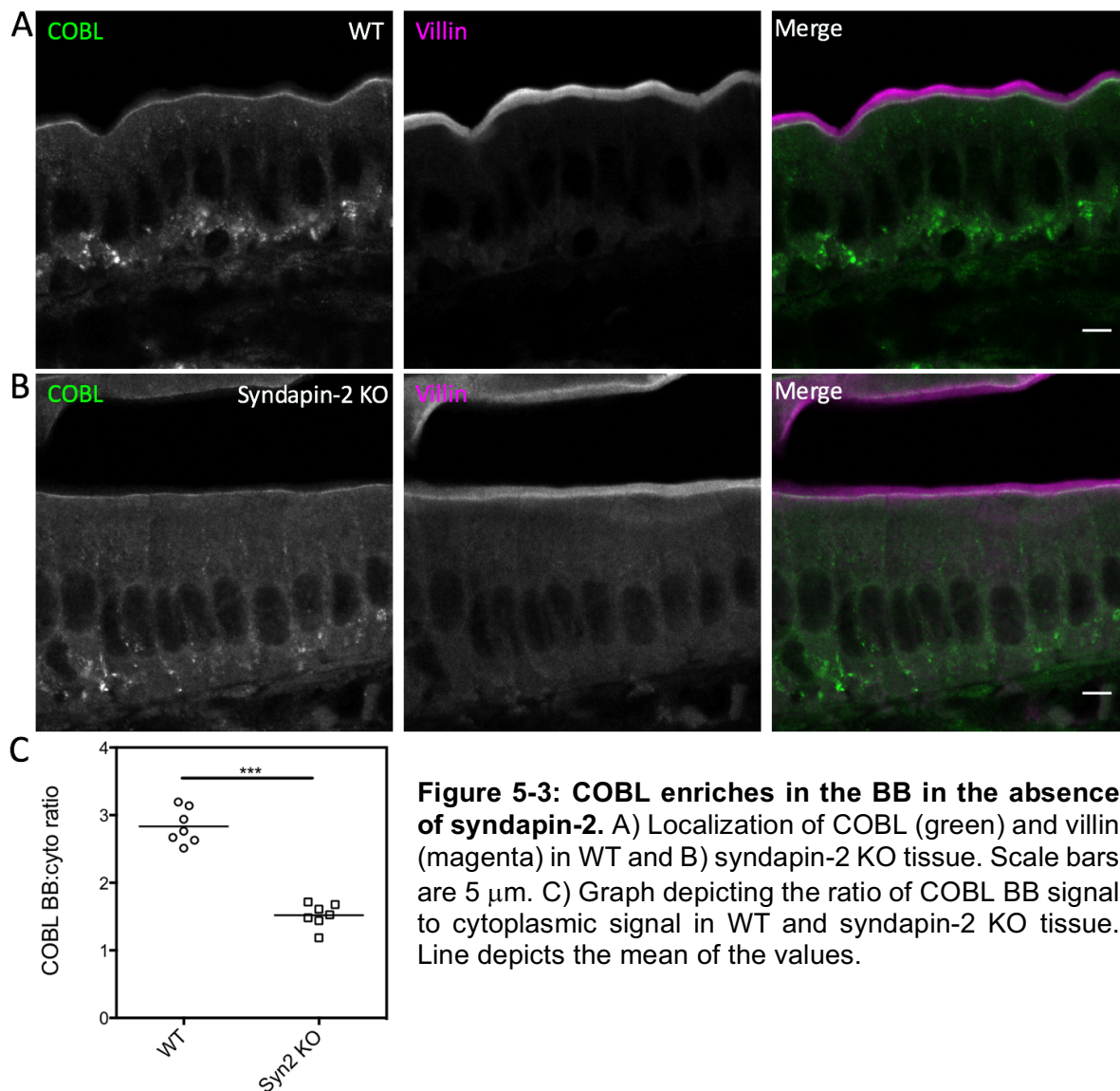
Figure 5-3: COBL enriches in the BB in the absence of syndapin-2. A) Localization of COBL (green) and villin (magenta) in WT and B) syndapin-2 KO tissue. Scale bars are 5 μm. C) Graph depicting the ratio of COBL BB signal to cytoplasmic signal in WT and syndapin-2 KO tissue. Line depicts the mean of the values.

BB ultrastructure is disrupted by the loss of syndapin-2

We next examined the ultrastructure of the syndapin-2 KO mouse by transmission electron microscopy (TEM). TEM of syndapin-2 KO mouse duodenum and proximal colon revealed several defects in BB microvilli architecture. Microvilli in wild-type cells displayed uniform length with neighboring microvilli, and approximately 20% of the actin bundles that support them are positioned below the plasma membrane (Fig. 5-3A,E). In the KO duodenum, while microvilli still displayed uniform length, KO microvilli were significantly shorter than WT (Fig. 5-3B,D). Lifting of the plasma membrane off the core actin bundle was also observed in the KO case, which we hypothesize contributes to the decrease in microvillar length (Fig. 5-3B, left image), although a decrease in core bundle length also may play a factor in decreased microvillar length (Fig. 5-3C). In severe cases, multiple microvilli were fused with one another, resulting in one protrusion encasing multiple core actin bundles. (Fig. 5-3B, right image). The result of these phenotypes is that the ratio of microvillar length to the core actin bundle length is significantly decreased in the KO mouse (Fig. 5-3E). For an unknown reason, the core actin bundles that are below the microvilli in the KO mouse often display high electron density (see Fig. 5-3B, left image). In the colon, pronounced length discrepancies between microvilli were observed, along plasma membrane lifting and microvillar fusion (Fig. 5-3F,G).

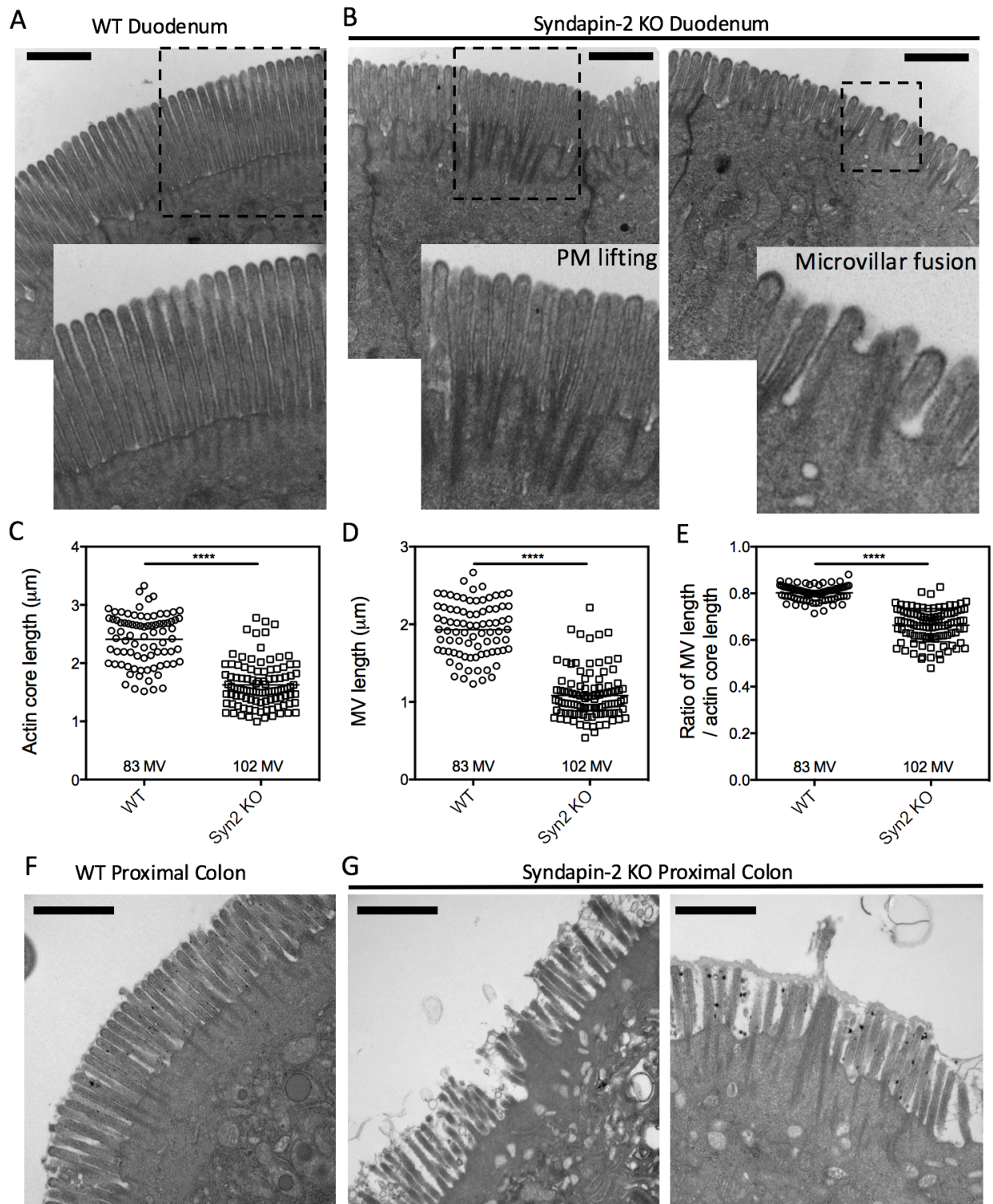**Figure 5-4: TEM of WT and syndapin-2 KO duodenal & proximal colon tissue.** A) WT and B)syndapin-2 KO duodenum sections. C-E) Quantification of the C) actin core length, D) microvilllar length, and E) ratio of microvillar length to actin core length in WT and syndapin-2 KO tissue. **** p<0.0001. F) WT and G) syndapin-2 KO proximal colon sections. All scale bars are 1 μm.

Syndapin-2 KO intestinal epithelium displays signs of defective barrier function

Next, we analyzed the intestinal surface using scanning electron microscopy (SEM). In the ileum we noted an increase in the number of segmented filamentous bacteria (SFBs) in syndapin-2 KO mice as compared to heterozygous animals (Fig. 5-4A,B). SFBs are commensal bacteria that colonize the ileum and are specialized to integrate into and attach to the intestinal BB (Ericsson et al., 2014). We also noted an increase in the number of what we believe are immune cells on the surface of the colonic epithelium, suggesting an increased inflammatory response from the immune system (Fig. 5-4C,D) (Tait Wojno and Artis, 2012), although this must be the focus of future studies. These data together are suggestive of a barrier defect in the intestinal epithelium of the syndapin-2 KO mice.

In addition to immune cells on the surface of the colonic epithelium, we noted differences in the colonic epithelial surface when comparing heterozygous and KO animals (Fig. 5-4C,D). The heterozygous animals displayed characteristic 'domes' in the epithelium, that were absent in the KO epithelium, giving the KO epithelium a flatter appearance. These data suggest that, because syndapin-2 is able to bind and bend membrane, syndapin-2 may play a role in generating this epithelial morphology.

Characterization of isolated brush borders from syndapin-2 KO mice

We next isolated the BBs from the syndapin-2 KO mice and WT controls. A protein gel loaded for equal total protein showed no obvious changes in the enterocyte whole cell lysate or the isolated BBs between the WT and syndapin-2 KO samples (Fig. 5-5A). Immunoblotting the whole cell lysate and the isolated BB sample for syndapin-2 revealed

A — Syndapin-2 +/-

B — Syndapin-2 -/-

Ileum
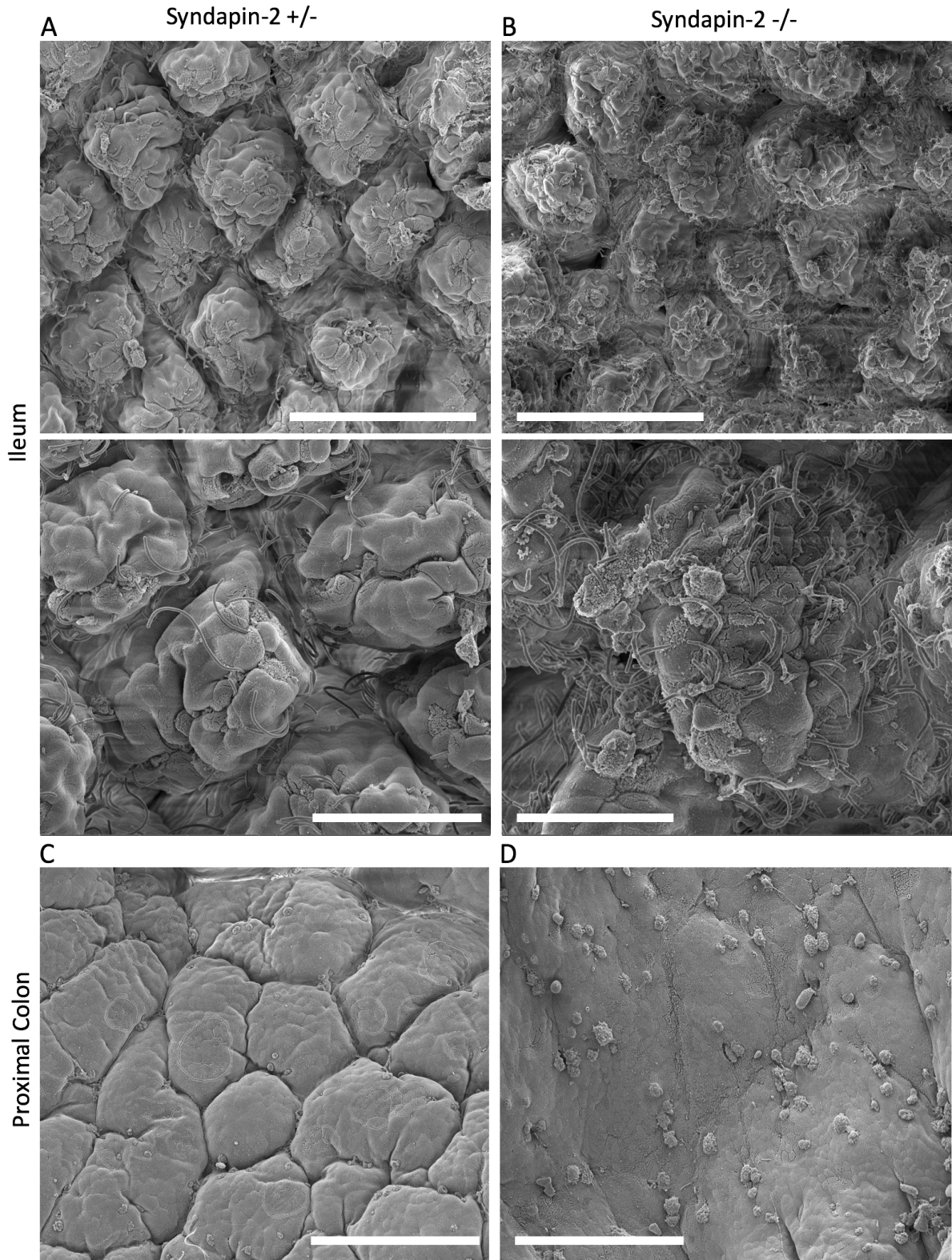
C — Proximal Colon

D

Figure 5-4: SEM of WT and syndapin-2 KO ileum & proximal colon tissue. A) WT and B) syndapin-2 KO ileal tissue looking down on villi. C & D) WT and B) syndapin-2 KO proximal colon tissue looking down on colonic surface. Scale bars are 100 μm for images in first and third rows and 50 μm in the second row.

that the whole cell lysate contained two species of syndapin-2, while the isolated BB sample contained only the lower molecular weight species (Fig 5-5B). This suggests that there are two splice isoforms of syndapin-2 in enterocytes and only the smaller species is present in the BB, or syndapin-2 is post-translationally modified (eg. phosphorylated and only the unphosphorylated form is found in the BB).

Staining of isolated BBs from each condition for F-actin and plasma membrane showed what was previously seen in TEM images of intact tissue sections; microvilli were significantly shorter in the syndapin-2 KO mice BBs, and actin bundles protruded below the membrane in each condition (Fig. 5-5C,D). However as opposed to the intact tissue TEM, the rootlets did not appear as prominent in TEM images of the syndapin-2 KO BBs as compared to WT BBs (Fig. 5-5E,F). TEM of isolated BBs from each condition did reveal that syndapin-2 KO microvilli in addition to being shorter, were also wider than WT control microvilli. The increased width was most prominent at the base, suggesting a defect in linking the plasma membrane at the base of the microvilli to the underlying actin bundle. Also, in the WT BBs, the spacing between the plasma membrane and the underlying terminal web was uniform. This uniformity was lost in the syndapin-2 KO BBs, which suggests that the terminal web is disorganized in the syndapin-2 KO mouse.

Conclusions and Future Directions

Here, we report a preliminary characterization of the intestinal BBs of mice lacking syndapin-2. The actin nucleator COBL still enriches in the BB of syndapin-2 KO mice, but to a lesser extent than in WT control mice, suggesting alternate mechanisms for targeting
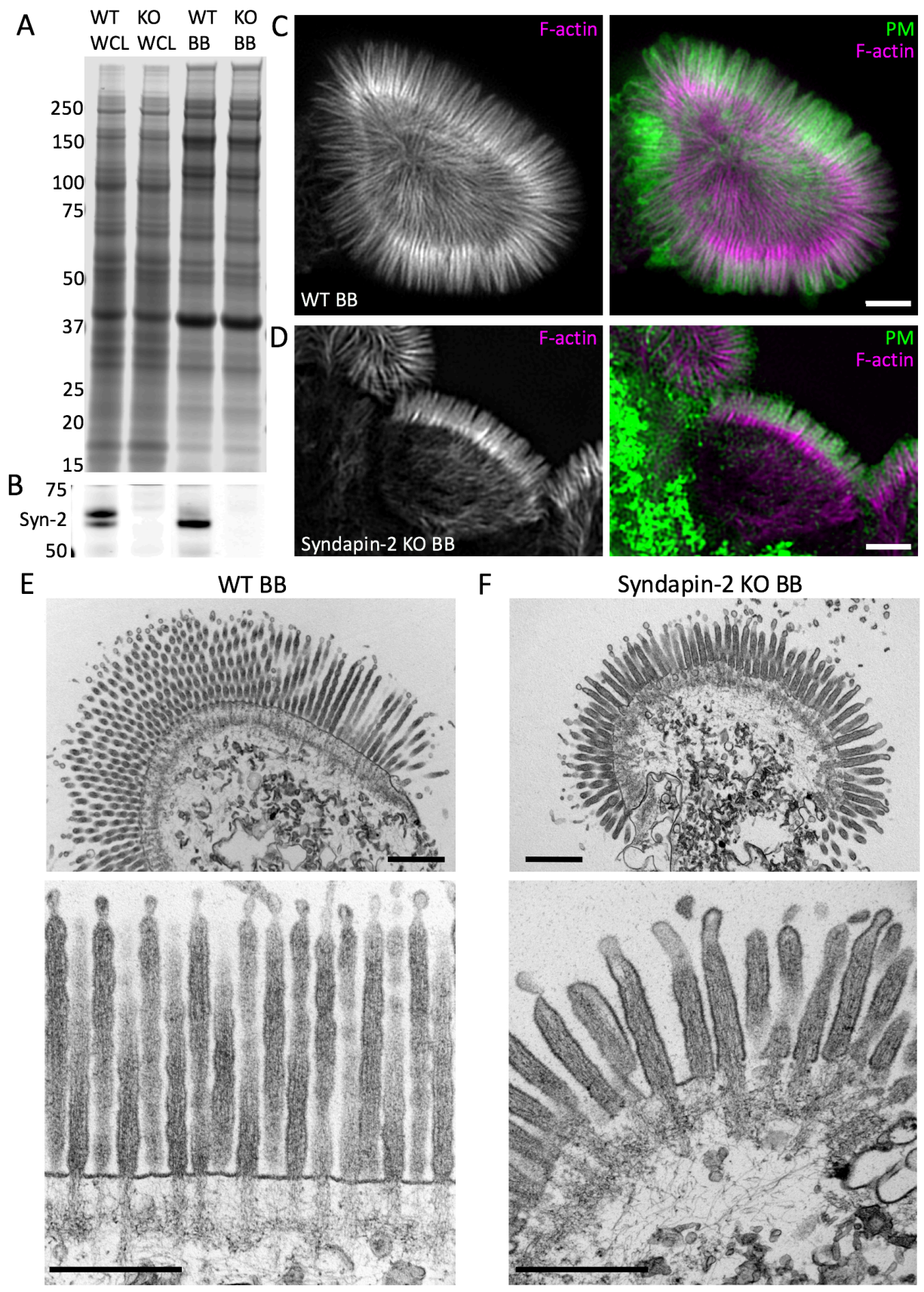
Figure 5-5: Characterization of isolated BBs from WT and syndapin-2 KO mice A) Coomassie Blue stained gel of whole cell lysates (WCL) and isolated BB samples from WT and syndapin-2 KO mice. B) Immunoblot for syndapin-2 in WT and KO WCL and BB samples. C & D)SIM of isolated WT and KO BBs stained for the plasma membrane (green, ConA) and F-actin (magenta). Scale bars are 2 μm. E) WT and F) syndapin-2 KO BBs imaged by TEM. Scale bars are 1 μm.

COBL to the BB. Syndapin-2 KO mice display short microvilli, which is due to a lifting of the plasma membrane off of the core actin bundle, and an increase in microvillar width. In addition to defects in microvillar morphology, the terminal web of syndapin-2 KO BBs also appears disorganized when compared to the terminal web in isolated WT BBs. Furthermore, the increased number of segmented filamentous bacteria on the ileal epithelium, along with the presence of immune cells on the colonic surface, suggests that there is a barrier defect in the syndapin-2 KO mice, which may be due to a decrease in microvillar length.

Mechanisms of BB targeting by COBL

What other mechanisms may target COBL to the base of the BB in the absence of syndapin-2? One possibility is that another syndapin family member, syndapin-1 or syndapin-3, may compensate for syndapin-2 in targeting COBL to the BB. Indeed, it has been shown that all syndapin isoforms are able to interact with COBL via an SH3/PxxP interaction (Schwintzer et al., 2011). Whether other isoforms of syndapin are playing a compensatory role in the syndapin-2 KO mouse remains to be tested, although it is known that syndapin-2 and 3 do not compensate in the syndapin-1 KO mouse (Koch et al., 2011). Immunostaining and immunoblotting for the other family members in KO and WT tissue sections and lysates is an obvious future direction.

Another possibility is that COBL is able to target to the apical membrane by a syndapin independent mechanism. The COBL linker domain localizes throughout the BB

when expressed in Ls174T-W4 cells (Chapter III)(Grega-Larson et al., 2015), and to the BB of JEG-3 placental epithelial cells (Wayt and Bretscher, 2014). However, its mechanism of targeting is completely unknown, and because there are no known protein domains that form from this polypeptide, determining the mechanism of targeting by this peptide would be an interesting future direction. More recently, a study suggested that the N-terminal 450 amino acids of COBL is able to bind lipids in *in vitro* liposome flotation assays (Hou et al., 2015). If this were a mechanism that was involved in targeting COBL to the BB, then we would expect to see some COBL targeting to the BB in the absence of syndapin-2 in Ls174T-W4 cells which is not the case. Thus, it is more likely that, if this domain does indeed bind membrane directly, it is a weaker interaction that serves to enhance COBL targeting by syndapin-2. Another possibility is that in the context of the full length protein, this lipid binding domain is masked and is only revealed upon some sort of activation of COBL.

Roles for syndapin-2 in the BB

It is straightforward to see how a syndapin-2/COBL complex acts as a static linker between the plasma membrane and the core actin bundle at the base of the BB by virtue of the membrane binding F-BAR domain of syndapin-2 and the actin-binding WH2 domains of COBL. A loss of this membrane link in syndapin-2 KO mice would give rise to the plasma membrane lifting off of the core F-actin bundle that we see in our TEM images (Fig. 5-3). However, it is known that syndapin-2 plays a critical role in endocytosis by linking the membrane with the NPF N-WASP (Kessels and Qualmann, 2002) and the GTPase dynamin (Anggono et al., 2006). Furthermore, the positive membrane curvature at the base of filopodia (Hines et al., 2012) and BB microvilli is a hotspot for endocytosis

99

(Soldati and Schliwa, 2006). Thus, an alternate hypothesis is that syndapin-2 provides an active link between the plasma membrane and the core actin bundle by using the downward force of endocytosis to constantly pull the membrane down around the core actin bundle; this downward force would counteract the upward force of actin polymerization at the tips of microvilli. This would suggest that the uniform length of microvilli is maintained by a balance of forces that must be tightly regulated in cells (Fig. 5-6).
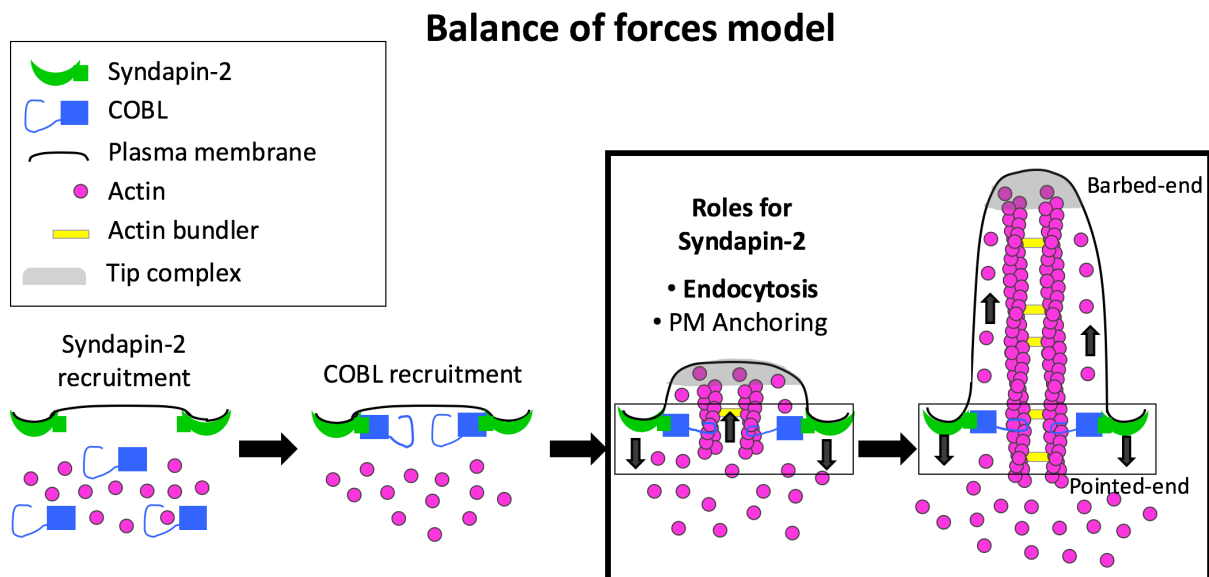
Figure 5-6: Balance of forces model for BB assembly and maintenance.

This model remains to be tested, but predicts that microvillar length can be modulated by inhibiting or increasing the rates of endocytosis or actin polymerization. One way to modulate the rate of endocytosis is by using the small molecule Dynasore, which blocks endocytosis by inhibiting the GTPase activity of dynamin required for vesicle scission (Macia et al., 2006). Using genetically encoded labels for or dyes for the plasma membrane and F-actin, Ls174T-W4 cells could be monitored by live cell imaging to see

the effect that inhibition of endocytosis by dynasore has on microvillar length and the coupling of the microvillar membrane to the core actin bundle. Similar experiments could also be performed with intravital imaging of mouse small intestine from Lifeact mice (Riedl et al., 2010), which we now have in the Tyska lab mouse colony, and a plasma membrane dye. Conversely, amphipathic molecules that decrease membrane tension have been shown to increase endocytosis rates (Raucher and Sheetz, 1999); thus, if this hypothesis is correct, incubation of cells or tissue with these molecules should increase the length of microvilli, and decrease the amount of the actin bundle that is not enveloped by microvillar membrane.

Barrier defects in the syndapin-2 KO mice

SEM of the ileum of syndapin-2 KO mice revealed an increased colonization by SFBs. SFBs have a hook shaped appendage called the holdfast on one of their ends that is used to burrow into the apical domain of enterocytes without penetrating the cell membrane (Blumershine and Savage, 1977). This induces localized displacement of the BB and actin polymerization underneath the holdfast, a region collectively known as the holdfast point. The most obvious reason for increased SFB colonization in the syndapin-2 KO mice is that due to a decrease in microvillar length, SFBs are able to gain easier access to the apical membrane underneath the BB for attachment. Another reason for increased colonization may be suboptimal packing density of microvilli in the syndapin-2 KO mice, a metric that must be scored using TEM images of sections cut orthogonally to the microvillar axis in the future. It is interesting to note that we see an increased colonization of SFBs in other KO mouse models in our lab for molecules important for BB assembly and maintenance (Tyska lab, unpublished data). In humans, SFBs are present

in early childhood but are usually cleared by three years of age (Yin et al., 2013). However, in a retrospective analysis, 6/6 patients with ulcerative colitis were found to be colonized with high levels of SFBs, whereas 3/6 patients without the disease displayed only low level colonization (Caselli et al., 2013). Thus, the relationship between molecules important for assembly of the BB and maintaining BB integrity, SFBs and the immune system, should be the focus of future work.

In the syndapin-2 colonic epithelium, the periodic dome shaped appearance of the monolayer was misshapen, giving the colonic epithelium a flatter appearance (Fig 5-4C,D). Interestingly, actin dynamics have been shown to be required for generating the characteristic folds present in the proximal colon during development, which are necessary for increasing the surface area of the colon by about three-fold (Colony and Conforti, 1993). Thus, syndapin-2 may play a role in coupling actin dynamics to the plasma membrane in this process during development.

Characterization of isolated BBs from syndapin-2 KO mice

Before discussing the syndapin-2 KO BBs, it is important to discuss the reasons for the two different size species of syndapin-2 detected in the whole cell lysates in Figure 5-5B, and the fact that only one of the species is detected in the BB. The first possibility is that these two bands represent two different splice isoforms of syndapin-2. There are four known splice isoforms of syndapin-2 between 52 and 65 kDa in size, with the 56 kDa isoform apparently being the most abundant (Qualmann and Kelly, 2000). It is unclear which isoform is present in our lysates, but this should be determined in the future.

The alternative explanation for the two bands present in the whole cell lysate is that only one isoform is present in enterocytes but it is post-translationally modified. For

example, it could exist in phosphorylated and unphosphorylated states, and only the unphosphorylated state is present in the BB. Syndapin-2 contains 23 annotated phosphorylation sites (http://www.phosphosite.org). Thus, it is possible that syndapin-2 is inactive in its phosphorylated state and that it is somehow dephosphorylated and thus activated in the BB. The regulation of syndapin-2 activity must be the subject of future work. The clear first experiment to determine if phosphorylation is playing a role is to treat the enterocyte lysate with lambda phosphatase and see if the two bands collapse to a single species or not.

TEM of isolated BBs from syndapin-2 and WT mice revealed greater detail in the organization of the terminal web in these animals, due to the extraction of cytoplasm that occurs during BB isolation. In syndapin-2 KO mouse, the intermediate filaments of the terminal web appeared disorganized when compared to WT controls, although at this point, we have no understanding of the mechanism behind this observation. Interestingly, in the myosin-1a KO mouse, cytokeratins 8 and 18, the major cytokeratins present in the terminal web, were significantly upregulated (Tyska et al., 2005). Thus, the disorganization of the terminal web seen in syndapin-2 KO mice may be due to an increase in intermediate filaments, which may be upregulated to provide more support when other core components maintaining microvillar structure are lost.

One method that our lab has utilized to gain insight into the WT mouse BB proteome, and the altered BB proteomes from KO mice that we study, is subjecting our isolated BB preparations to shotgun mass spectrometry to gain a comprehensive list of the proteins in the BB (Benesh et al., 2010; McConnell et al., 2011). We recently submitted equally treated WT and syndapin-2 KO BBs for two-dimensional liquid

chromatography tandem mass spectrometry. Analyzing changes in protein levels between the WT and KO samples shown by the mass spectrometry data will allow for the design of more directed experiments that will allow us to determine the molecular mechanisms underlying the BB defects in the syndapin-2 KO mouse.

CHAPTER VI.

FUTURE DIRECTIONS & CONCLUSION

In addition to the future directions to pursue with the syndapin-2 KO mouse discussed in Chapter V, there are several questions that can be the focus of future investigation that extend from our published studies of COBL presented in Chapters III and IV. Also, there are new technologies that can be employed to further our understanding of the role COBL plays in BB assembly.

Is the coiled coil of COBL required for actin nucleation and/or severing activity?

Our cell culture studies show that both nucleation and severing activities of COBL that have been observed *in vitro* (Husson et al., 2011) also function in cells (Chapters III and IV) (Grega-Larson et al., 2015; Grega-Larson et al., 2016). While our structure/function and mutagenesis studies have shown which WH2 domains of COBL are required for nucleation and severing in cells, it is still unknown if other domains of COBL are required for these functions. Many actin assembly factors, such as formins and the actin elongation factor VASP require oligomerization to be functional; specifically, formins function as dimers and VASP as a tetramer. In the case of VASP and some formins, a coiled coil is required for oligomerization. Coiled coils (CCs) are helices assembled from repeat heptad amino acid sequences that twist around each other to form a supercoil. COBL contains a putative CC, but a role in mediating oligomerization of COBL has never been tested. Furthermore, it is unknown if oligomerization influences COBL function.

Because we have readouts for COBL function in fixed and live cells, we can test the if the coiled coil is necessary for nucleation and severing by COBL by either deleting

the CC domain or replacing it with a linker with the same size as the CC unable to support oligomerization. By expressing these constructs in Ls174T-W4 and scoring microvillar length, straightness, F-actin amount and coverage with our SIM based assays (Fig. 3-4), we can determine whether or not the CC is required for inducing microvillar assembly by comparing these constructs to full length COBL. Additionally, by expressing these CC deleted constructs in B16F1 cells and imaging them live, future studies can assess whether or not these constructs induce the formation of dynamic intracellular actin structures in the cytoplasm of these cells. These readouts together will shed light on a role for the CC of COBL in controlling actin nucleation and severing in cells.

WH2 domain-containing COBL constructs lacking the CC are able to nucleate and sever filaments *in vitro* (Husson et al., 2011), however these constructs are weak nucleators as compared to the Arp 2/3 complex and formins (Dominguez, 2016). Thus one possibility is that the CC of COBL functions to bring multiple COBL molecules together to enhance its nucleation activity. The CC of COBL is relatively weak when compared with the CCs from VASP and formins, but COBL, unlike spire, has a predicted CC domain using Paircoil2 CC prediction algorithm (Fig. 6-1) (McDonnell et al., 2006). Thus, it is possible that COBL is able to homomultimerize unlike spire, which requires an interaction with formin dimers to dimerize and act in cells (Vizcarra et al., 2011). Alternatively, the CC of COBL may not be strong enough to induce multimerization alone, could help stabilize COBL/syndapin-2 complexes, which would multimerize due to the oligomerization of the syndapin-2 F-BAR domain (Wang et al., 2009). In this case, to determine if oligomerization is required for COBL function in cells, it would be important to mutate the N-terminal syndapin-2 binding domain of COBL in the context of the CC
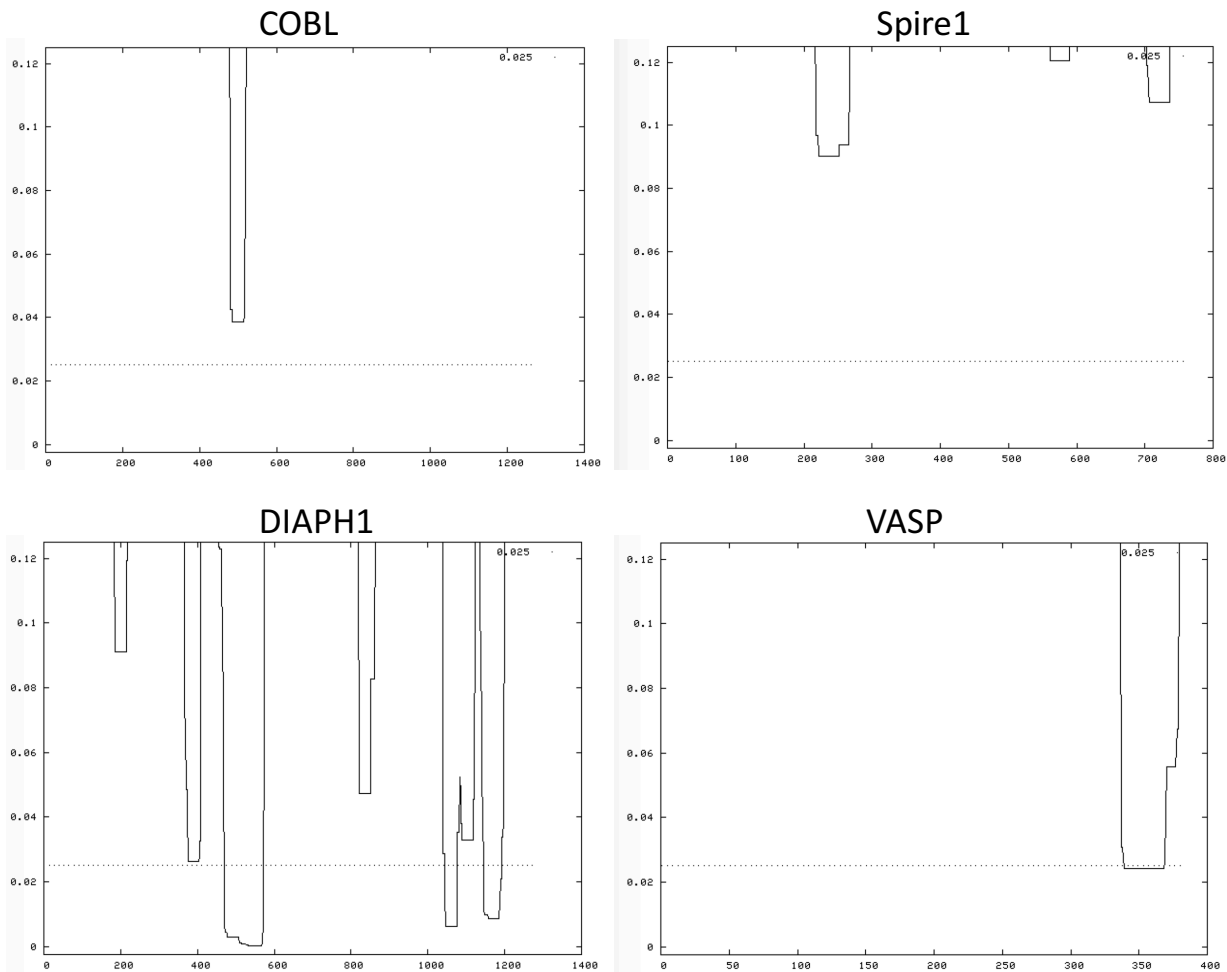
Figure 6-1. Paircoil2 coiled coil prediction software shows that COBL has a weak CC. COBL has a predicted CC (AA 486-515) but it does not achieve the confidence interval of 0.025 set by the prediction software. Spire has no predicted CC. DIAPH1 has two CCs (AA 460-562 and 1027-1179). VASP has a C-terminal CC (AA 336-380).

mutants. Investigating the function of the predicted CC of COBL will provide insight into its mechanism of action in cells and should be the focus of future work. If oligomerization is not required for COBL function in cells, COBL would be the first WH2 domain containing nucleator that did not need to oligomerize to function in cells.

What factors target the COBL/syndapin-2 complex to and activate it in the BB?

While we have identified that a COBL/syndapin-2 complex is necessary for proper BB formation, the molecules that act upstream to activate this complex are still unknown. It is known that Rho GTPases of the Ras superfamily, specifically Cdc42 and Rac1, bind and activate the Arp2/3 complex activator N-WASP and the I-BAR domain containing protein IRSp53, which are both critical factors in generating filopodia (Disanza et al., 2013; Ho et al., 2004; Miki et al., 2000). Thus, a focus of future studies in Ls174T-W4 cells should be to determine if members of the Rho family GTPases also function in microvillar assembly by impinging on COBL or syndapin-2 to drive BB assembly. Because we know that COBL and syndapin-2 are highly enriched in the BBs of these cells, KD of each rho family member could be performed in cells followed by immunostaining for COBL or syndapin-2 and F-actin. The percent of cells with BBs and with COBL and syndapin-2 enrichment in the BB could then be determined to see which of these GTPases are involved in Ls174T-W4 cell BB assembly. Identifying GTPase binding and activating sites on COBL or syndapin-2 would provide a significant advance in the field, as these sites have not been determined for either molecule as of yet. This shRNA screen could act as a pilot study to determine molecules to investigate further using the new technologies and more relevant model systems discussed below. Importantly, this type of screen has been successful in Ls174T-W4 cells for identifying a role for the GTPase Rap2a as a molecule involved in the initial establishment of polarity in these cells, further upstream of BB assembly (Gloerich et al., 2012).

CRISPR/Cas9 genome editing technology to generate COBL KO cells

One critique with our COBL KD studies (Chapter 3; Fig. 3-6)(Grega-Larson et al., 2015) is that, even though our KD is more than 95% effective globally, we cannot say for certain on a per cell basis if low levels of COBL are still present. Because COBL has such a powerful effect on actin cytoskeletal dynamics in cells, even at low levels it could have effects in our KD cells that make our data difficult to interpret. For example, when we show that, in COBL KD cells that still make BBs microvilli are shorter, we cannot say with certainty that this is due to alternative pathways for BB assembly, or due to low levels of COBL still present in these cells. Fortunately, the CRISPR/Cas9 system is now providing a way to get rid of the variability in KD cell lines due to expression differences on a per cell basis by simply creating a knock out cell line for a gene of interest (Jinek et al., 2012).

Ls174T-W4 cells are good candidates for generating clonal KO cell lines using CRISPR/Cas9 technology. Unlike other epithelial cells that we use in the lab, Ls174T-W4 cells are easily transfectable, grow quickly in culture, and because they grow as single cells, isolating single cells for clonal selection is simple. Generating a clonal COBL KO line of Ls174T-W4 cells would be a valuable tool for studying the process of BB assembly. First, we could determine with certainty if BBs forming in our COBL KD cell line are due to low levels of COBL or alternative mechanisms; because the BB is necessary for survival, it is likely that alternate mechanisms for BB assembly exist. The COBL KO cell line would provide a useful model system to interrogate these other pathways.
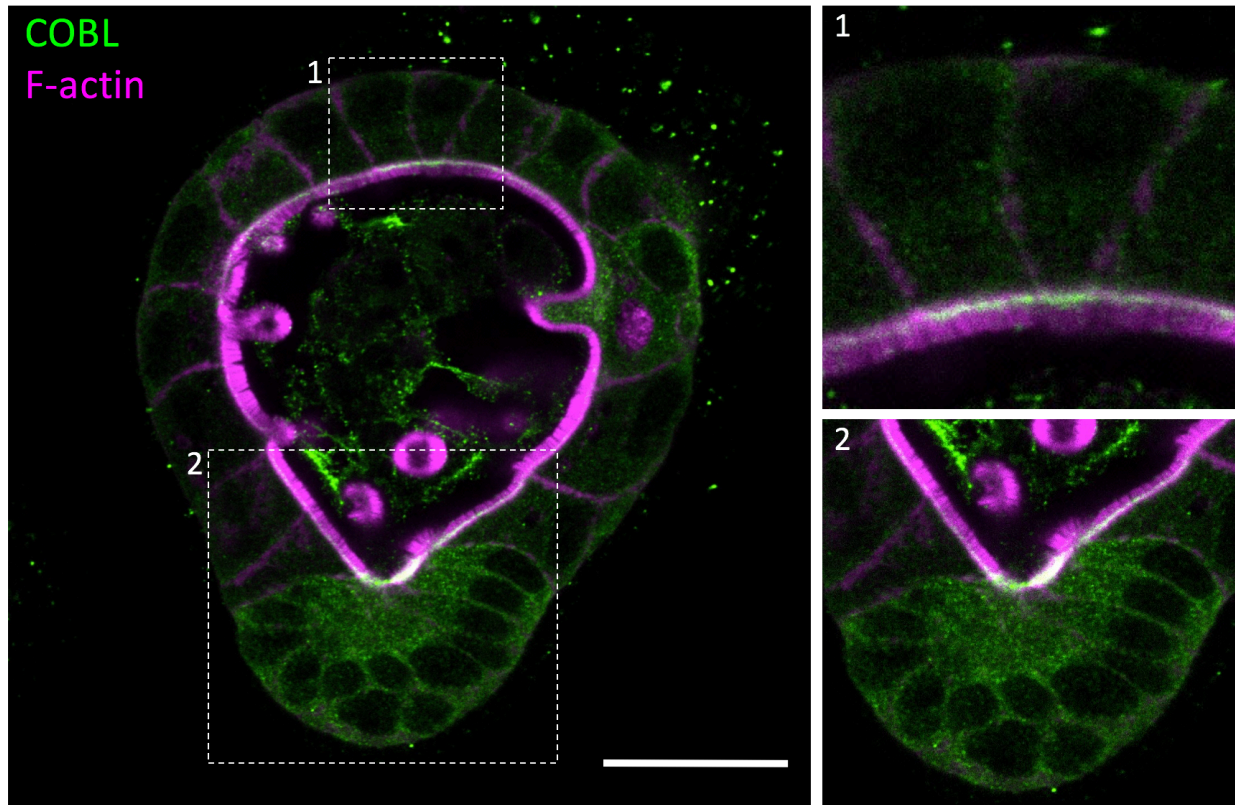
Figure 6-2: Immunostaining of COBL in an intestinal enteroid. COBL (green) and F-actin (magenta) staining in an enteroid. 1) Villar domain. 2) Crypt domain. Scale bar is 20 μm.

Intestinal enteroids as a cell culture model to study BB assembly

While Ls174T-W4 cells have been valuable for investigating the mechanisms employed by COBL for BB assembly, it is now important to study COBL function in BB assembly in a more relevant context. The intestinal enteroid cell culture system was developed by the Clevers' laboratory (Sato et al., 2009). Amazingly, by isolating crypts from young mice, embedding them in matrigel, and culturing them in the presence of the correct factors, the crypts will first seal and then expand into cysts with a lumen in the center of a single layer of epithelial cells, with a stem cell containing crypt domain giving rise to differentiated cells in the villar domain. Intestinal enteroids are an extremely powerful model system because they recapitulate an *in vivo* like setting but are amenable to all of the manipulations that

can be performed in cultured cells. To confirm that COBL localized similarly in enteroids as it does in intestinal tissue and Ls174T-W4 cells, we immunostained organoids cultured for three days after passaging with a COBL antibody. Interestingly, COBL was highly expressed in the crypt domain of organoids and expressed at lower levels in the villar domain where it localized to the base of the BB as in tissue (Fig. 6-2). The high expression of COBL in the crypt is expected for molecules that are involved in BB assembly, because BB assembly occurs as cells migrate up the crypt (Crawley et al., 2014a). Once out on the villar domain, BB assembly is complete as evidenced by the characteristic 'paint brush' appearance of the BB (Fig. 6-2, zoom 1).

Now that our lab has established the enteroid system as a model for studying BB assembly, there are several future directions with regard to COBL that should be pursued in enteroids. First, because our lab now has the mRuby-Lifeact mice, we can culture enteroids from these mice and make COBL KO lines from these enteroids using the CRISPR/Cas9 system. This will allow us to visualize actin dynamics that occur during BB assembly in wild-type and COBL KO enteroids. Additionally, using CRISPR/Cas9, endogenous COBL can be fluorescently tagged with EGFP in organoids from the mRuby-Lifeact mouse. This will allow for visualization of COBL localization while BB actin is assembling. If these studies are performed, it will be the first time BB assembly is visualized in an *in vivo*-like context.

The generation of an EGFP-COBL tagged enteroid line in mRuby-Lifeact organoids would also allow us to examine if some of the phenomena that we saw when visualizing cell polarization and BB assembly in Ls174T-W4 cells are relevant *in vivo.* One exciting observation that we made during these live cell imaging experiments was that
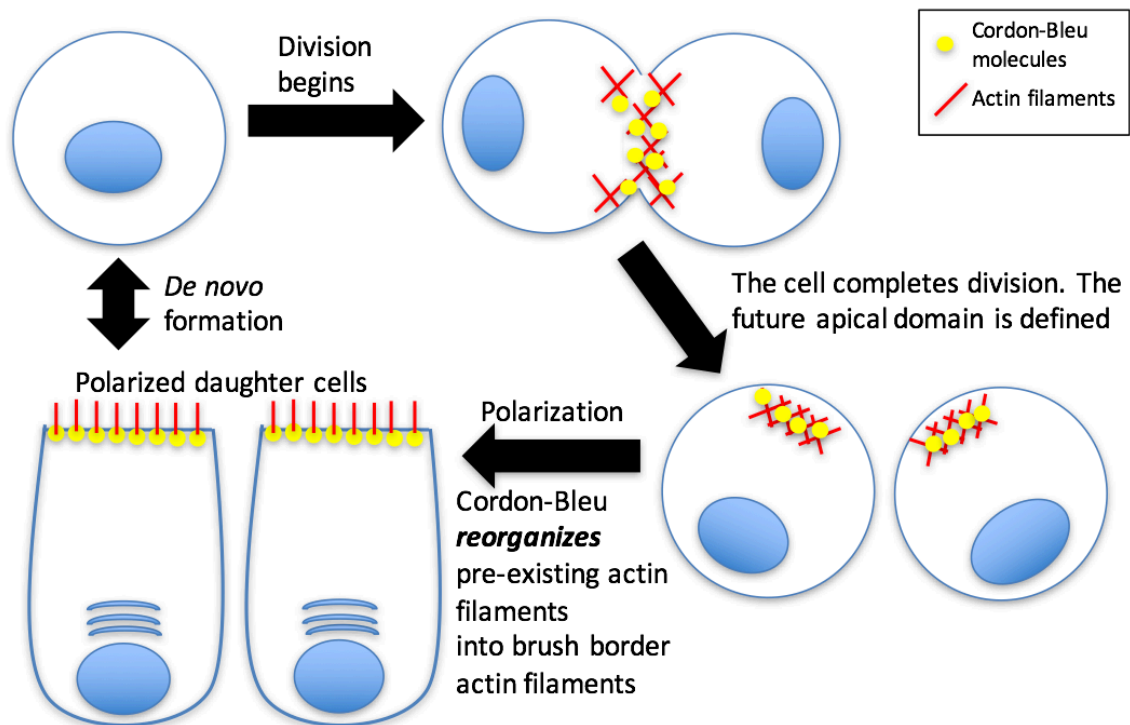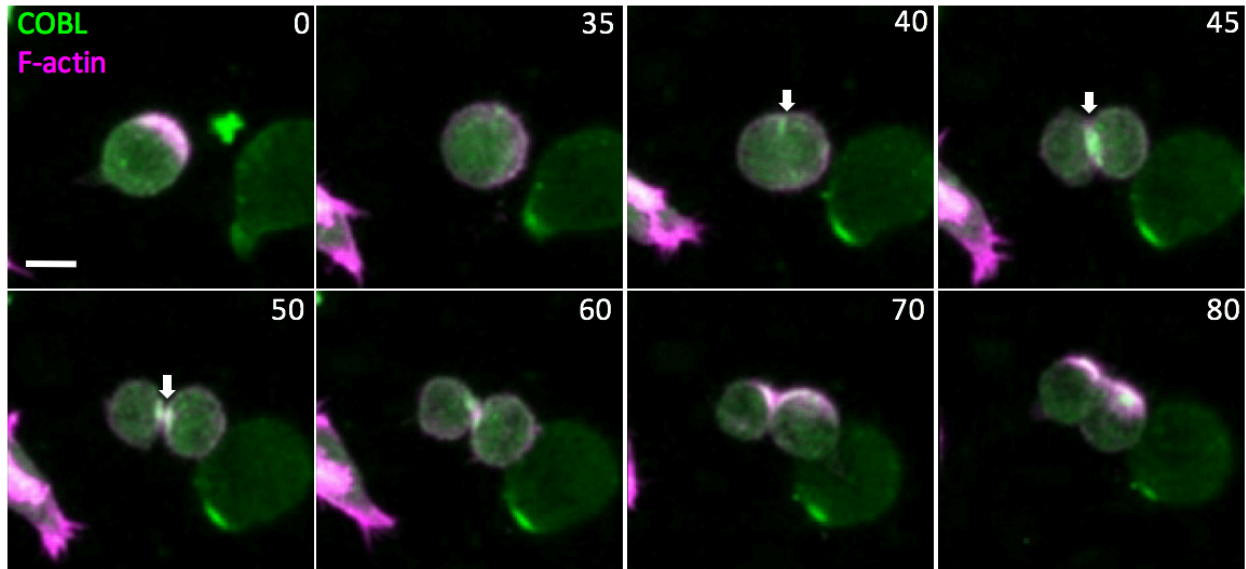
Figure 6-3: BB assembly, on occasion, is coupled with cell division in Ls174T-W4 cells: Live cell imaging of COBL (green) and F-actin (magenta, UtrCH). Arrow highlights the site of division. Time is minutes, scale bar is 5 μm. Cartoon depicting how cell division and BB assembly may be coupled in cells.

BB assembly may be coupled to cell division (Figs. 6-3 and 6-4). In this instance, COBL would polarize in a cell which corresponded to BB assembly. Then the cell would

depolarize and divide, and COBL would enrich at the cleavage furrow during cytokinesis. After division, the actin of the cytokinetic ring seemed to be repurposed to form BBs in the two daughter cells. Because cell division occurs in the transit amplifying zone of the crypt as cells migrate up the crypt-villus axis, we hypothesized that BB assembly and cell proliferation may be coupled *in vivo*, however until the mRuby-Lifeact enteroids, we did not have a good model system to test our hypothesis. Having COBL labeled in this system as well will allow us to see if COBL may play a role in repurposing the actin used for cytokinesis into BB actin filaments. This is an attractive model not only because cell division and BB assembly occur simultaneously in the intestine, but also because generating actin filaments *de novo* is energetically costly to the cell (Skau and Waterman, 2015); so, repurposing the actin from cytokinesis would be energetically favorable.

Conclusion

The work presented here highlights a role for a complex of the actin nucleator COBL and the F-BAR domain containing protein syndapin-2 in the assembly of the BB in cultured intestinal epithelial cells (Chapter III) and lends insight into the mechanism of actin filament assembly employed by COBL in cells (Chapter IV). Furthermore, preliminary data from the syndapin-2 KO mouse suggests that this protein complex is required for proper intestinal BB assembly *in vivo.* Future work using the newly available tools highlighted in this section to will be critical for further elucidating the mechanism employed by the COBL/syndapin-2 complex to promote intestinal BB assembly *in vivo.*

REFERENCES

Ahuja, R., Pinyol, R., Reichenbach, N., Custer, L., Klingensmith, J., Kessels, M.M., and Qualmann, B. (2007). Cordon-bleu is an actin nucleation factor and controls neuronal morphology. Cell *131*, 337-350.

Amann, K.J., and Pollard, T.D. (2001). Direct real-time observation of actin filament branching mediated by Arp2/3 complex using total internal reflection fluorescence microscopy. Proceedings of the National Academy of Sciences of the United States of America *98*, 15009-15013.

Anggono, V., Smillie, K.J., Graham, M.E., Valova, V.A., Cousin, M.A., and Robinson, P.J. (2006). Syndapin I is the phosphorylation-regulated dynamin I partner in synaptic vesicle endocytosis. Nature neuroscience *9*, 752-760.

Antonellis, P.J., Pollock, L.M., Chou, S.W., Hassan, A., Geng, R., Chen, X., Fuchs, E., Alagramam, K.N., Auer, M., and McDermott, B.M., Jr. (2014). ACF7 is a hair-bundle antecedent, positioned to integrate cuticular plate actin and somatic tubulin. The Journal of neuroscience : the official journal of the Society for Neuroscience *34*, 305-312.

Applewhite, D.A., Barzik, M., Kojima, S., Svitkina, T.M., Gertler, F.B., and Borisy, G.G. (2007). Ena/VASP proteins have an anti-capping independent function in filopodia formation. Molecular biology of the cell *18*, 2579-2591.

Aspenstrom, P. (2010). Formin-binding proteins: modulators of formin-dependent actin polymerization. Biochimica et biophysica acta *1803*, 174-182.

Baas, A.F., Boudeau, J., Sapkota, G.P., Smit, L., Medema, R., Morrice, N.A., Alessi, D.R., and Clevers, H.C. (2003). Activation of the tumour suppressor kinase LKB1 by the STE20-like pseudokinase STRAD. The EMBO journal *22*, 3062-3072.

Baas, A.F., Kuipers, J., van der Wel, N.N., Batlle, E., Koerten, H.K., Peters, P.J., and Clevers, H.C. (2004). Complete polarization of single intestinal epithelial cells upon activation of LKB1 by STRAD. Cell *116*, 457-466.

Bartles, J.R., Zheng, L., Li, A., Wierda, A., and Chen, B. (1998). Small espin: a third actin-bundling protein and potential forked protein ortholog in brush border microvilli. The Journal of cell biology *143*, 107-119.

Belin, B.J., Lee, T., and Mullins, R.D. (2015). DNA damage induces nuclear actin filament assembly by Formin -2 and Spire-(1/2) that promotes efficient DNA repair. [corrected]. eLife *4*, e07735.

Benesh, A.E., Nambiar, R., McConnell, R.E., Mao, S., Tabb, D.L., and Tyska, M.J. (2010). Differential localization and dynamics of class I myosins in the enterocyte microvillus. Molecular biology of the cell *21*, 970-978.

Blanchoin, L., and Pollard, T.D. (2002). Hydrolysis of ATP by polymerized actin depends on the bound divalent cation but not profilin. Biochemistry *41*, 597-602.

Blumershine, R.V., and Savage, D.C. (1977). Filamentous microbes indigenous to the murine small bowel: A scanning electron microscopic study of their morphology and attachment to the epithelium. Microbial ecology *4*, 95-103.

Breitsprecher, D., Jaiswal, R., Bombardier, J.P., Gould, C.J., Gelles, J., and Goode, B.L. (2012). Rocket launcher mechanism of collaborative actin assembly defined by single-molecule imaging. Science *336*, 1164-1168.

Breitsprecher, D., Koestler, S.A., Chizhov, I., Nemethova, M., Mueller, J., Goode, B.L., Small, J.V., Rottner, K., and Faix, J. (2011). Cofilin cooperates with fascin to disassemble filopodial actin filaments. Journal of cell science *124*, 3305-3318.

Bretscher, A. (1989). Rapid phosphorylation and reorganization of ezrin and spectrin accompany morphological changes induced in A-431 cells by epidermal growth factor. The Journal of cell biology *108*, 921-930.

Bretscher, A., and Weber, K. (1979). Villin: the major microfilament-associated protein of the intestinal microvillus. Proceedings of the National Academy of Sciences of the United States of America *76*, 2321-2325.

Bretscher, A., and Weber, K. (1980). Fimbrin, a new microfilament-associated protein present in microvilli and other cell surface structures. The Journal of cell biology *86*, 335-340.

Burgess, D.R., and Grey, R.D. (1974). Alterations in morphology of developing microvilli elicited by cytochalasin B. Studies of embryonic chick intestine in organ culture. The Journal of cell biology *62*, 566-574.

Burke, T.A., Christensen, J.R., Barone, E., Suarez, C., Sirotkin, V., and Kovar, D.R. (2014). Homeostatic actin cytoskeleton networks are regulated by assembly factor competition for monomers. Current biology : CB *24*, 579-585.

Burkel, B.M., von Dassow, G., and Bement, W.M. (2007). Versatile fluorescent probes for actin filaments based on the actin-binding domain of utrophin. Cell motility and the cytoskeleton *64*, 822-832.

Campellone, K.G., and Welch, M.D. (2010). A nucleator arms race: cellular control of actin assembly. Nature reviews Molecular cell biology *11*, 237-251.

Carlier, M.F., Husson, C., Renault, L., and Didry, D. (2011). Control of actin assembly by the WH2 domains and their multifunctional tandem repeats in Spire and Cordon-Bleu. International review of cell and molecular biology *290*, 55-85.

Carlsson, L., Nystrom, L.E., Sundkvist, I., Markey, F., and Lindberg, U. (1977). Actin polymerizability is influenced by profilin, a low molecular weight protein in non-muscle cells. Journal of molecular biology *115*, 465-483.

Carroll, E.A., Gerrelli, D., Gasca, S., Berg, E., Beier, D.R., Copp, A.J., and Klingensmith, J. (2003). Cordon-bleu is a conserved gene involved in neural tube formation. Developmental biology *262*, 16-31.

Caselli, M., Tosini, D., Gafa, R., Gasbarrini, A., and Lanza, G. (2013). Segmented filamentous bacteria-like organisms in histological slides of ileo-cecal valves in patients with ulcerative colitis. The American journal of gastroenterology *108*, 860-861.

Chaudhry, F., Little, K., Talarico, L., Quintero-Monzon, O., and Goode, B.L. (2010). A central role for the WH2 domain of Srv2/CAP in recharging actin monomers to drive actin turnover in vitro and in vivo. Cytoskeleton (Hoboken) *67*, 120-133.

Chen, X., Ni, F., Tian, X., Kondrashkina, E., Wang, Q., and Ma, J. (2013). Structural basis of actin filament nucleation by tandem W domains. Cell reports *3*, 1910-1920.

Chesarone, M.A., DuPage, A.G., and Goode, B.L. (2010). Unleashing formins to remodel the actin and microtubule cytoskeletons. Nature reviews Molecular cell biology *11*, 62-74.

Chesarone, M.A., and Goode, B.L. (2009). Actin nucleation and elongation factors: mechanisms and interplay. Current opinion in cell biology *21*, 28-37.

Chhabra, E.S., and Higgs, H.N. (2007). The many faces of actin: matching assembly factors with cellular structures. Nature cell biology *9*, 1110-1121.

Chou, S.W., Hwang, P., Gomez, G., Fernando, C.A., West, M.C., Pollock, L.M., Lin-Jones, J., Burnside, B., and McDermott, B.M., Jr. (2011). Fascin 2b is a component of stereocilia that lengthens actin-based protrusions. PloS one *6*, e14807.

Colony, P.C., and Conforti, J.C. (1993). Morphogenesis in the fetal rat proximal colon: effects of cytochalasin D. The Anatomical record *235*, 241-252.

Crawley, S.W., Mooseker, M.S., and Tyska, M.J. (2014a). Shaping the intestinal brush border. The Journal of cell biology *207*, 441-451.

Crawley, S.W., Shifrin, D.A., Jr., Grega-Larson, N.E., McConnell, R.E., Benesh, A.E., Mao, S., Zheng, Y., Zheng, Q.Y., Nam, K.T., Millis, B.A.*, et al.* (2014b). Intestinal brush border assembly driven by protocadherin-based intermicrovillar adhesion. Cell *157*, 433-446.

Crawley, S.W., Weck, M.L., Grega-Larson, N.E., Shifrin, D.A., Jr., and Tyska, M.J. (2016). ANKS4B Is Essential for Intermicrovillar Adhesion Complex Formation. Developmental cell *36*, 190-200.

Croce, A., Cassata, G., Disanza, A., Gagliani, M.C., Tacchetti, C., Malabarba, M.G., Carlier, M.F., Scita, G., Baumeister, R., and Di Fiore, P.P. (2004). A novel actin barbed-end-capping activity in EPS-8 regulates apical morphogenesis in intestinal cells of Caenorhabditis elegans. Nature cell biology *6*, 1173-1179.

Dahlgaard, K., Raposo, A.A., Niccoli, T., and St Johnston, D. (2007). Capu and Spire assemble a cytoplasmic actin mesh that maintains microtubule organization in the Drosophila oocyte. Developmental cell *13*, 539-553.

Davidson, G.P., Cutz, E., Hamilton, J.R., and Gall, D.G. (1978). Familial enteropathy: a syndrome of protracted diarrhea from birth, failure to thrive, and hypoplastic villus atrophy. Gastroenterology *75*, 783-790.

Delacour, D., Salomon, J., Robine, S., and Louvard, D. (2016). Plasticity of the brush border - the yin and yang of intestinal homeostasis. Nature reviews Gastroenterology & hepatology *13*, 161-174.

Didry, D., Cantrelle, F.X., Husson, C., Roblin, P., Moorthy, A.M., Perez, J., Le Clainche, C., Hertzog, M., Guittet, E., Carlier, M.F.*, et al.* (2012). How a single residue in individual beta-thymosin/WH2 domains controls their functions in actin assembly. The EMBO journal *31*, 1000-1013.

Dietrich, S., Weiss, S., Pleiser, S., and Kerkhoff, E. (2013). Structural and functional insights into the Spir/formin actin nucleator complex. Biological chemistry *394*, 1649-1660.

Disanza, A., Bisi, S., Winterhoff, M., Milanesi, F., Ushakov, D.S., Kast, D., Marighetti, P., Romet-Lemonne, G., Muller, H.M., Nickel, W.*, et al.* (2013). CDC42 switches IRSp53 from inhibition of actin growth to elongation by clustering of VASP. The EMBO journal *32*, 2735-2750.

Disanza, A., Mantoani, S., Hertzog, M., Gerboth, S., Frittoli, E., Steffen, A., Berhoerster, K., Kreienkamp, H.J., Milanesi, F., Di Fiore, P.P.*, et al.* (2006). Regulation of cell shape by Cdc42 is mediated by the synergic actin-bundling activity of the Eps8-IRSp53 complex. Nature cell biology *8*, 1337-1347.

Dominguez, R. (2009). Actin filament nucleation and elongation factors--structure-function relationships. Critical reviews in biochemistry and molecular biology *44*, 351-366.

Dominguez, R. (2016). The WH2 Domain and Actin Nucleation: Necessary but Insufficient. Trends in biochemical sciences *41*, 478-490.

Drummond, M.C., Barzik, M., Bird, J.E., Zhang, D.S., Lechene, C.P., Corey, D.P., Cunningham, L.L., and Friedman, T.B. (2015). Live-cell imaging of actin dynamics reveals mechanisms of stereocilia length regulation in the inner ear. Nature communications *6*, 6873.

Ericsson, A.C., Hagan, C.E., Davis, D.J., and Franklin, C.L. (2014). Segmented filamentous bacteria: commensal microbes with potential effects on research. Comparative medicine *64*, 90-98.

Faix, J., Breitsprecher, D., Stradal, T.E., and Rottner, K. (2009). Filopodia: Complex models for simple rods. The international journal of biochemistry & cell biology *41*, 1656-1664.

Fawley, J., and Gourlay, D.M. (2016). Intestinal alkaline phosphatase: a summary of its role in clinical disease. The Journal of surgical research *202*, 225-234.

Francis, S.P., Krey, J.F., Krystofiak, E.S., Cui, R., Nanda, S., Xu, W., Kachar, B., Barr-Gillespie, P.G., and Shin, J.B. (2015). A short splice form of Xin-actin binding repeat containing 2 (XIRP2) lacking the Xin repeats is required for maintenance of stereocilia morphology and hearing function. The Journal of neuroscience : the official journal of the Society for Neuroscience *35*, 1999-2014.

Gasca, S., Hill, D.P., Klingensmith, J., and Rossant, J. (1995). Characterization of a gene trap insertion into a novel gene, cordon-bleu, expressed in axial structures of the gastrulating mouse embryo. Developmental genetics *17*, 141-154.

Gittes, F., Mickey, B., Nettleton, J., and Howard, J. (1993). Flexural rigidity of microtubules and actin filaments measured from thermal fluctuations in shape. The Journal of cell biology *120*, 923-934.

Gloerich, M., Ten Klooster, J.P., Vliem, M.J., Koorman, T., Zwartkruis, F.J., Clevers, H., and Bos, J.L. (2012). Rap2A links intestinal cell polarity to brush border formation. Nature cell biology *14*, 793-801.

Goodman, B.E. (2010). Insights into digestion and absorption of major nutrients in humans. Advances in physiology education *34*, 44-53.

Graziano, B.R., DuPage, A.G., Michelot, A., Breitsprecher, D., Moseley, J.B., Sagot, I., Blanchoin, L., and Goode, B.L. (2011). Mechanism and cellular function of Bud6 as an actin nucleation-promoting factor. Molecular biology of the cell *22*, 4016-4028.

Grega-Larson, N.E., Crawley, S.W., Erwin, A.L., and Tyska, M.J. (2015). Cordon bleu promotes the assembly of brush border microvilli. Molecular biology of the cell *26*, 3803-3815.

Grega-Larson, N.E., Crawley, S.W., and Tyska, M.J. (2016). Impact of cordon-bleu expression on actin cytoskeleton architecture and dynamics. Cytoskeleton (Hoboken).

Grimm-Gunter, E.M., Revenu, C., Ramos, S., Hurbain, I., Smyth, N., Ferrary, E., Louvard, D., Robine, S., and Rivero, F. (2009). Plastin 1 binds to keratin and is required for terminal web assembly in the intestinal epithelium. Molecular biology of the cell *20*, 2549-2562.

Guillot, C., and Lecuit, T. (2013). Mechanics of epithelial tissue homeostasis and morphogenesis. Science *340*, 1185-1189.

Haag, N., Schwintzer, L., Ahuja, R., Koch, N., Grimm, J., Heuer, H., Qualmann, B., and Kessels, M.M. (2012). The actin nucleator Cobl is crucial for Purkinje cell development and works in close conjunction with the F-actin binding protein Abp1. The Journal of neuroscience : the official journal of the Society for Neuroscience *32*, 17842-17856.

Hansen, S.D., and Mullins, R.D. (2010). VASP is a processive actin polymerase that requires monomeric actin for barbed end association. The Journal of cell biology *191*, 571-584.

Helander, H.F., and Fandriks, L. (2014). Surface area of the digestive tract - revisited. Scandinavian journal of gastroenterology *49*, 681-689.

Henty-Ridilla, J.L., Rankova, A., Eskin, J.A., Kenny, K., and Goode, B.L. (2016). Accelerated actin filament polymerization from microtubule plus ends. Science *352*, 1004-1009.

Hertzog, M., Milanesi, F., Hazelwood, L., Disanza, A., Liu, H., Perlade, E., Malabarba, M.G., Pasqualato, S., Maiolica, A., Confalonieri, S*., et al.* (2010). Molecular basis for the dual function of Eps8 on actin dynamics: bundling and capping. PLoS biology *8*, e1000387.

Higgs, H.N., and Pollard, T.D. (1999). Regulation of actin polymerization by Arp2/3 complex and WASp/Scar proteins. The Journal of biological chemistry *274*, 32531-32534.

Hines, J.H., Henle, S.J., Carlstrom, L.P., Abu-Rub, M., and Henley, J.R. (2012). Single vesicle imaging indicates distinct modes of rapid membrane retrieval during nerve growth. BMC biology *10*, 4.

Hirokawa, N., Tilney, L.G., Fujiwara, K., and Heuser, J.E. (1982). Organization of actin, myosin, and intermediate filaments in the brush border of intestinal epithelial cells. The Journal of cell biology *94*, 425-443.

Ho, H.Y., Rohatgi, R., Lebensohn, A.M., Le, M., Li, J., Gygi, S.P., and Kirschner, M.W. (2004). Toca-1 mediates Cdc42-dependent actin nucleation by activating the N-WASP-WIP complex. Cell *118*, 203-216.

Hou, W., Izadi, M., Nemitz, S., Haag, N., Kessels, M.M., and Qualmann, B. (2015). The Actin Nucleator Cobl Is Controlled by Calcium and Calmodulin. PLoS biology *13*, e1002233.

Howard, J., and Hyman, A.A. (2003). Dynamics and mechanics of the microtubule plus end. Nature *422*, 753-758.

Husson, C., Renault, L., Didry, D., Pantaloni, D., and Carlier, M.F. (2011). Cordon-Bleu uses WH2 domains as multifunctional dynamizers of actin filament assembly. Molecular cell *43*, 464-477.

Jiao, Y., Walker, M., Trinick, J., Pernier, J., Montaville, P., and Carlier, M.F. (2014). Mutagenetic and electron microscopy analysis of actin filament severing by Cordon-Bleu, a WH2 domain protein. Cytoskeleton (Hoboken) *71*, 170-183.

Jinek, M., Chylinski, K., Fonfara, I., Hauer, M., Doudna, J.A., and Charpentier, E. (2012). A programmable dual-RNA-guided DNA endonuclease in adaptive bacterial immunity. Science *337*, 816-821.

Kang, F., Purich, D.L., and Southwick, F.S. (1999). Profilin promotes barbed-end actin filament assembly without lowering the critical concentration. The Journal of biological chemistry *274*, 36963-36972.

Kessels, M.M., and Qualmann, B. (2002). Syndapins integrate N-WASP in receptor-mediated endocytosis. The EMBO journal *21*, 6083-6094.

Kitajiri, S., Sakamoto, T., Belyantseva, I.A., Goodyear, R.J., Stepanyan, R., Fujiwara, I., Bird, J.E., Riazuddin, S., Riazuddin, S., Ahmed, Z.M.*, et al.* (2010). Actin-bundling protein TRIOBP forms resilient rootlets of hair cell stereocilia essential for hearing. Cell *141*, 786-798.

Koch, D., Spiwoks-Becker, I., Sabanov, V., Sinning, A., Dugladze, T., Stellmacher, A., Ahuja, R., Grimm, J., Schuler, S., Muller, A.*, et al.* (2011). Proper synaptic vesicle formation and neuronal network activity critically rely on syndapin I. The EMBO journal *30*, 4955-4969.

Lebrand, C., Dent, E.W., Strasser, G.A., Lanier, L.M., Krause, M., Svitkina, T.M., Borisy, G.G., and Gertler, F.B. (2004). Critical role of Ena/VASP proteins for filopodia formation in neurons and in function downstream of netrin-1. Neuron *42*, 37-49.

Lee, S.H., and Dominguez, R. (2010). Regulation of actin cytoskeleton dynamics in cells. Molecules and cells *29*, 311-325.

Liu, R., Abreu-Blanco, M.T., Barry, K.C., Linardopoulou, E.V., Osborn, G.E., and Parkhurst, S.M. (2009). Wash functions downstream of Rho and links linear and branched actin nucleation factors. Development *136*, 2849-2860.

Liu, X.P., Koehler, K.R., Mikosz, A.M., Hashino, E., and Holt, J.R. (2016). Functional development of mechanosensitive hair cells in stem cell-derived organoids parallels native vestibular hair cells. Nature communications *7*, 11508.

Loomis, P.A., Zheng, L., Sekerkova, G., Changyaleket, B., Mugnaini, E., and Bartles, J.R. (2003). Espin cross-links cause the elongation of microvillus-type parallel actin bundles in vivo. The Journal of cell biology *163*, 1045-1055.

Lu, J., Meng, W., Poy, F., Maiti, S., Goode, B.L., and Eck, M.J. (2007). Structure of the FH2 domain of Daam1: implications for formin regulation of actin assembly. Journal of molecular biology *369*, 1258-1269.

Machesky, L.M., Reeves, E., Wientjes, F., Mattheyse, F.J., Grogan, A., Totty, N.F., Burlingame, A.L., Hsuan, J.J., and Segal, A.W. (1997). Mammalian actin-related protein 2/3 complex localizes to regions of lamellipodial protrusion and is composed of evolutionarily conserved proteins. The Biochemical journal *328 (Pt 1)*, 105-112.

Macia, E., Ehrlich, M., Massol, R., Boucrot, E., Brunner, C., and Kirchhausen, T. (2006). Dynasore, a cell-permeable inhibitor of dynamin. Developmental cell *10*, 839-850.

Majstoravich, S., Zhang, J., Nicholson-Dykstra, S., Linder, S., Friedrich, W., Siminovitch, K.A., and Higgs, H.N. (2004). Lymphocyte microvilli are dynamic, actin-dependent structures that do not require Wiskott-Aldrich syndrome protein (WASp) for their morphology. Blood *104*, 1396-1403.

Mallavarapu, A., and Mitchison, T. (1999). Regulated actin cytoskeleton assembly at filopodium tips controls their extension and retraction. The Journal of cell biology *146*, 1097-1106.

Manor, U., Bartholomew, S., Golani, G., Christenson, E., Kozlov, M., Higgs, H., Spudich, J., and Lippincott-Schwartz, J. (2015). A mitochondria-anchored isoform of the actin-nucleating spire protein regulates mitochondrial division. eLife *4*.

Manor, U., Disanza, A., Grati, M., Andrade, L., Lin, H., Di Fiore, P.P., Scita, G., and Kachar, B. (2011). Regulation of stereocilia length by myosin XVa and whirlin depends on the actin-regulatory protein Eps8. Current biology : CB *21*, 167-172.

Manseau, L.J., and Schupbach, T. (1989). cappuccino and spire: two unique maternal-effect loci required for both the anteroposterior and dorsoventral patterns of the Drosophila embryo. Genes & development *3*, 1437-1452.

Maroux, S., Coudrier, E., Feracci, H., Gorvel, J.P., and Louvard, D. (1988). Molecular organization of the intestinal brush border. Biochimie *70*, 1297-1306.

Martin-Belmonte, F., Gassama, A., Datta, A., Yu, W., Rescher, U., Gerke, V., and Mostov, K. (2007). PTEN-mediated apical segregation of phosphoinositides controls epithelial morphogenesis through Cdc42. Cell *128*, 383-397.

Mburu, P., Romero, M.R., Hilton, H., Parker, A., Townsend, S., Kikkawa, Y., and Brown, S.D. (2010). Gelsolin plays a role in the actin polymerization complex of hair cell stereocilia. PloS one *5*, e11627.

McConnell, R.E., Benesh, A.E., Mao, S., Tabb, D.L., and Tyska, M.J. (2011). Proteomic analysis of the enterocyte brush border. American journal of physiology Gastrointestinal and liver physiology *300*, G914-926.

McConnell, R.E., Higginbotham, J.N., Shifrin, D.A., Jr., Tabb, D.L., Coffey, R.J., and Tyska, M.J. (2009). The enterocyte microvillus is a vesicle-generating organelle. The Journal of cell biology *185*, 1285-1298.

McDonald, N.A., and Gould, K.L. (2016). Linking up at the BAR: Oligomerization and F-BAR protein function. Cell Cycle *15*, 1977-1985.

McDonnell, A.V., Jiang, T., Keating, A.E., and Berger, B. (2006). Paircoil2: improved prediction of coiled coils from sequence. Bioinformatics *22*, 356-358.

Mejillano, M.R., Kojima, S., Applewhite, D.A., Gertler, F.B., Svitkina, T.M., and Borisy, G.G. (2004). Lamellipodial versus filopodial mode of the actin nanomachinery: pivotal role of the filament barbed end. Cell *118*, 363-373.

Miki, H., Yamaguchi, H., Suetsugu, S., and Takenawa, T. (2000). IRSp53 is an essential intermediate between Rac and WAVE in the regulation of membrane ruffling. Nature *408*, 732-735.

Mitchison, T., and Kirschner, M. (1984). Dynamic instability of microtubule growth. Nature *312*, 237-242.

Mogilner, A., and Rubinstein, B. (2005). The physics of filopodial protrusion. Biophysical journal *89*, 782-795.

Montaville, P., Jegou, A., Pernier, J., Compper, C., Guichard, B., Mogessie, B., Schuh, M., Romet-Lemonne, G., and Carlier, M.F. (2014). Spire and Formin 2 synergize and antagonize in regulating actin assembly in meiosis by a ping-pong mechanism. PLoS biology *12*, e1001795.

Mooseker, M.S., and Howe, C.L. (1982). The brush border of intestinal epithelium: a model system for analysis of cell-surface architecture and motility. Methods in cell biology *25 Pt B*, 143-174.

Mooseker, M.S., Pollard, T.D., and Wharton, K.A. (1982). Nucleated polymerization of actin from the membrane-associated ends of microvillar filaments in the intestinal brush border. The Journal of cell biology *95*, 223-233.

Morgan, C.P., Krey, J.F., Grati, M., Zhao, B., Fallen, S., Kannan-Sundhari, A., Liu, X.Z., Choi, D., Muller, U., and Barr-Gillespie, P.G. (2016). PDZD7-MYO7A complex identified in enriched stereocilia membranes. eLife *5*.

Namgoong, S., Boczkowska, M., Glista, M.J., Winkelman, J.D., Rebowski, G., Kovar, D.R., and Dominguez, R. (2011). Mechanism of actin filament nucleation by Vibrio VopL and implications for tandem W domain nucleation. Nature structural & molecular biology *18*, 1060-1067.

Narayanan, P., Chatterton, P., Ikeda, A., Ikeda, S., Corey, D.P., Ervasti, J.M., and Perrin, B.J. (2015). Length regulation of mechanosensitive stereocilia depends on very slow actin dynamics and filament-severing proteins. Nature communications *6*, 6855.

Nicholson-Dykstra, S.M., and Higgs, H.N. (2008). Arp2 depletion inhibits sheet-like protrusions but not linear protrusions of fibroblasts and lymphocytes. Cell motility and the cytoskeleton *65*, 904-922.

Nolen, B.J., Tomasevic, N., Russell, A., Pierce, D.W., Jia, Z., McCormick, C.D., Hartman, J., Sakowicz, R., and Pollard, T.D. (2009). Characterization of two classes of small molecule inhibitors of Arp2/3 complex. Nature *460*, 1031-1034.

Ohta, K., Higashi, R., Sawaguchi, A., and Nakamura, K. (2012). Helical arrangement of filaments in microvillar actin bundles. Journal of structural biology *177*, 513-519.

Okada, K., Bartolini, F., Deaconescu, A.M., Moseley, J.B., Dogic, Z., Grigorieff, N., Gundersen, G.G., and Goode, B.L. (2010). Adenomatous polyposis coli protein nucleates actin assembly and synergizes with the formin mDia1. The Journal of cell biology *189*, 1087-1096.

Olt, J., Mburu, P., Johnson, S.L., Parker, A., Kuhn, S., Bowl, M., Marcotti, W., and Brown, S.D. (2014). The actin-binding proteins eps8 and gelsolin have complementary roles in regulating the growth and stability of mechanosensory hair bundles of mammalian cochlear outer hair cells. PloS one *9*, e87331.

Paul, A.S., and Pollard, T.D. (2008). The role of the FH1 domain and profilin in formin-mediated actin-filament elongation and nucleation. Current biology : CB *18*, 9-19.

Pellegrin, S., and Mellor, H. (2005). The Rho family GTPase Rif induces filopodia through mDia2. Current biology : CB *15*, 129-133.

Peng, A.W., Belyantseva, I.A., Hsu, P.D., Friedman, T.B., and Heller, S. (2009). Twinfilin 2 regulates actin filament lengths in cochlear stereocilia. The Journal of neuroscience : the official journal of the Society for Neuroscience *29*, 15083-15088.

Peng, J., Wallar, B.J., Flanders, A., Swiatek, P.J., and Alberts, A.S. (2003). Disruption of the Diaphanous-related formin Drf1 gene encoding mDia1 reveals a role for Drf3 as an effector for Cdc42. Current biology : CB *13*, 534-545.

Perrin, B.J., Strandjord, D.M., Narayanan, P., Henderson, D.M., Johnson, K.R., and Ervasti, J.M. (2013). beta-Actin and fascin-2 cooperate to maintain stereocilia length. The Journal of neuroscience : the official journal of the Society for Neuroscience *33*, 8114-8121.

Peter, B.J., Kent, H.M., Mills, I.G., Vallis, Y., Butler, P.J., Evans, P.R., and McMahon, H.T. (2004). BAR domains as sensors of membrane curvature: the amphiphysin BAR structure. Science *303*, 495-499.

Peterson, L.W., and Artis, D. (2014). Intestinal epithelial cells: regulators of barrier function and immune homeostasis. Nature reviews Immunology *14*, 141-153.

Pollard, T.D. (1986). Rate constants for the reactions of ATP- and ADP-actin with the ends of actin filaments. The Journal of cell biology *103*, 2747-2754.

Pollard, T.D. (2007). Regulation of actin filament assembly by Arp2/3 complex and formins. Annual review of biophysics and biomolecular structure *36*, 451-477.

Pollard, T.D. (2016). Actin and Actin-Binding Proteins. Cold Spring Harbor perspectives in biology *8*.

Pollard, T.D., Blanchoin, L., and Mullins, R.D. (2000). Molecular mechanisms controlling actin filament dynamics in nonmuscle cells. Annual review of biophysics and biomolecular structure *29*, 545-576.

Pollard, T.D., and Borisy, G.G. (2003). Cellular motility driven by assembly and disassembly of actin filaments. Cell *112*, 453-465.

Pollard, T.D., and Mooseker, M.S. (1981). Direct measurement of actin polymerization rate constants by electron microscopy of actin filaments nucleated by isolated microvillus cores. The Journal of cell biology *88*, 654-659.

Pollock, L.M., and McDermott, B.M., Jr. (2015). The cuticular plate: a riddle, wrapped in a mystery, inside a hair cell. Birth defects research Part C, Embryo today : reviews *105*, 126-139.

Prost, J., Barbetta, C., and Joanny, J.F. (2007). Dynamical control of the shape and size of stereocilia and microvilli. Biophysical journal *93*, 1124-1133.

Pylypenko, O., Welz, T., Tittel, J., Kollmar, M., Chardon, F., Malherbe, G., Weiss, S., Michel, C.I., Samol-Wolf, A., Grasskamp, A.T.*, et al.* (2016). Coordinated recruitment of Spir actin nucleators and myosin V motors to Rab11 vesicle membranes. eLife *5*.

Qualmann, B., and Kelly, R.B. (2000). Syndapin isoforms participate in receptor-mediated endocytosis and actin organization. The Journal of cell biology *148*, 1047-1062.

Qualmann, B., and Kessels, M.M. (2009). New players in actin polymerization--WH2-domain-containing actin nucleators. Trends in cell biology *19*, 276-285.

Quan, A., and Robinson, P.J. (2013). Syndapin--a membrane remodelling and endocytic F-BAR protein. The FEBS journal *280*, 5198-5212.

Quinlan, M.E., Heuser, J.E., Kerkhoff, E., and Mullins, R.D. (2005). Drosophila Spire is an actin nucleation factor. Nature *433*, 382-388.

Quinlan, M.E., Hilgert, S., Bedrossian, A., Mullins, R.D., and Kerkhoff, E. (2007). Regulatory interactions between two actin nucleators, Spire and Cappuccino. The Journal of cell biology *179*, 117-128.

Raucher, D., and Sheetz, M.P. (1999). Membrane expansion increases endocytosis rate during mitosis. The Journal of cell biology *144*, 497-506.

Ravanelli, A.M., and Klingensmith, J. (2011). The actin nucleator Cordon-bleu is required for development of motile cilia in zebrafish. Developmental biology *350*, 101-111.

Rebowski, G., Boczkowska, M., Hayes, D.B., Guo, L., Irving, T.C., and Dominguez, R. (2008). X-ray scattering study of actin polymerization nuclei assembled by tandem W domains. Proceedings of the National Academy of Sciences of the United States of America *105*, 10785-10790.

Renault, L., Bugyi, B., and Carlier, M.F. (2008). Spire and Cordon-bleu: multifunctional regulators of actin dynamics. Trends in cell biology *18*, 494-504.

Revenu, C., Ubelmann, F., Hurbain, I., El-Marjou, F., Dingli, F., Loew, D., Delacour, D., Gilet, J., Brot-Laroche, E., Rivero, F.*, et al.* (2012). A new role for the architecture of microvillar actin bundles in apical retention of membrane proteins. Molecular biology of the cell *23*, 324-336.

Riedl, J., Flynn, K.C., Raducanu, A., Gartner, F., Beck, G., Bosl, M., Bradke, F., Massberg, S., Aszodi, A., Sixt, M.*, et al.* (2010). Lifeact mice for studying F-actin dynamics. Nature methods *7*, 168-169.

Rizvi, S.A., Neidt, E.M., Cui, J., Feiger, Z., Skau, C.T., Gardel, M.L., Kozmin, S.A., and Kovar, D.R. (2009). Identification and characterization of a small molecule inhibitor of formin-mediated actin assembly. Chemistry & biology *16*, 1158-1168.

Rodriguez, O.C., Schaefer, A.W., Mandato, C.A., Forscher, P., Bement, W.M., and Waterman-Storer, C.M. (2003). Conserved microtubule-actin interactions in cell movement and morphogenesis. Nature cell biology *5*, 599-609.

Rohatgi, R., Ma, L., Miki, H., Lopez, M., Kirchhausen, T., Takenawa, T., and Kirschner, M.W. (1999). The interaction between N-WASP and the Arp2/3 complex links Cdc42-dependent signals to actin assembly. Cell *97*, 221-231.

Roignot, J., Peng, X., and Mostov, K. (2013). Polarity in mammalian epithelial morphogenesis. Cold Spring Harbor perspectives in biology *5*.

Rosales-Nieves, A.E., Johndrow, J.E., Keller, L.C., Magie, C.R., Pinto-Santini, D.M., and Parkhurst, S.M. (2006). Coordination of microtubule and microfilament dynamics by Drosophila Rho1, Spire and Cappuccino. Nature cell biology *8*, 367-376.

Rotty, J.D., Wu, C., and Bear, J.E. (2013). New insights into the regulation and cellular functions of the ARP2/3 complex. Nature reviews Molecular cell biology *14*, 7-12.

Rotty, J.D., Wu, C., Haynes, E.M., Suarez, C., Winkelman, J.D., Johnson, H.E., Haugh, J.M., Kovar, D.R., and Bear, J.E. (2015). Profilin-1 serves as a gatekeeper for actin assembly by Arp2/3-dependent and -independent pathways. Developmental cell *32*, 54-67.

Rould, M.A., Wan, Q., Joel, P.B., Lowey, S., and Trybus, K.M. (2006). Crystal structures of expressed non-polymerizable monomeric actin in the ADP and ATP states. The Journal of biological chemistry *281*, 31909-31919.

Rzadzinska, A.K., Schneider, M.E., Davies, C., Riordan, G.P., and Kachar, B. (2004). An actin molecular treadmill and myosins maintain stereocilia functional architecture and self-renewal. The Journal of cell biology *164*, 887-897.

Safer, D., and Nachmias, V.T. (1994). Beta thymosins as actin binding peptides. BioEssays : news and reviews in molecular, cellular and developmental biology *16*, 590.

Sagot, I., Rodal, A.A., Moseley, J., Goode, B.L., and Pellman, D. (2002). An actin nucleation mechanism mediated by Bni1 and profilin. Nature cell biology *4*, 626-631.

Salles, F.T., Merritt, R.C., Jr., Manor, U., Dougherty, G.W., Sousa, A.D., Moore, J.E., Yengo, C.M., Dose, A.C., and Kachar, B. (2009). Myosin IIIa boosts elongation of stereocilia by transporting espin 1 to the plus ends of actin filaments. Nature cell biology *11*, 443-450.

Saotome, I., Curto, M., and McClatchey, A.I. (2004). Ezrin is essential for epithelial organization and villus morphogenesis in the developing intestine. Developmental cell *6*, 855-864.

Sato, T., Vries, R.G., Snippert, H.J., van de Wetering, M., Barker, N., Stange, D.E., van Es, J.H., Abo, A., Kujala, P., Peters, P.J., *et al.* (2009). Single Lgr5 stem cells build crypt-villus structures in vitro without a mesenchymal niche. Nature *459*, 262-265.

Scheffer, D.I., Zhang, D.S., Shen, J., Indzhykulian, A., Karavitaki, K.D., Xu, Y.J., Wang, Q., Lin, J.J., Chen, Z.Y., and Corey, D.P. (2015). XIRP2, an actin-binding protein essential for inner ear hair-cell stereocilia. Cell reports *10*, 1811-1818.

Schirenbeck, A., Arasada, R., Bretschneider, T., Schleicher, M., and Faix, J. (2005a). Formins and VASPs may co-operate in the formation of filopodia. Biochemical Society transactions *33*, 1256-1259.

Schirenbeck, A., Bretschneider, T., Arasada, R., Schleicher, M., and Faix, J. (2005b). The Diaphanous-related formin dDia2 is required for the formation and maintenance of filopodia. Nature cell biology *7*, 619-625.

Schober, J.M., Komarova, Y.A., Chaga, O.Y., Akhmanova, A., and Borisy, G.G. (2007). Microtubule-targeting-dependent reorganization of filopodia. Journal of cell science *120*, 1235-1244.

Schuler, S., Hauptmann, J., Perner, B., Kessels, M.M., Englert, C., and Qualmann, B. (2013). Ciliated sensory hair cell formation and function require the F-BAR protein syndapin I and the WH2 domain-based actin nucleator Cobl. Journal of cell science *126*, 196-208.

Schumacher, N., Borawski, J.M., Leberfinger, C.B., Gessler, M., and Kerkhoff, E. (2004). Overlapping expression pattern of the actin organizers Spir-1 and formin-2 in the developing mouse nervous system and the adult brain. Gene expression patterns : GEP *4*, 249-255.

Schwintzer, L., Koch, N., Ahuja, R., Grimm, J., Kessels, M.M., and Qualmann, B. (2011). The functions of the actin nucleator Cobl in cellular morphogenesis critically depend on syndapin I. The EMBO journal *30*, 3147-3159.

Sekerkova, G., Zheng, L., Mugnaini, E., and Bartles, J.R. (2006). Differential expression of espin isoforms during epithelial morphogenesis, stereociliogenesis and postnatal maturation in the developing inner ear. Developmental biology *291*, 83-95.

Sept, D., and McCammon, J.A. (2001). Thermodynamics and kinetics of actin filament nucleation. Biophysical journal *81*, 667-674.

Shifrin, D.A., Jr., McConnell, R.E., Nambiar, R., Higginbotham, J.N., Coffey, R.J., and Tyska, M.J. (2012). Enterocyte microvillus-derived vesicles detoxify bacterial products and regulate epithelial-microbial interactions. Current biology : CB *22*, 627-631.

Shin, J.B., Longo-Guess, C.M., Gagnon, L.H., Saylor, K.W., Dumont, R.A., Spinelli, K.J., Pagana, J.M., Wilmarth, P.A., David, L.L., Gillespie, P.G.*, et al.* (2010). The R109H variant of fascin-2, a developmentally regulated actin crosslinker in hair-cell stereocilia, underlies early-onset hearing loss of DBA/2J mice. The Journal of neuroscience : the official journal of the Society for Neuroscience *30*, 9683-9694.

Skau, C.T., and Waterman, C.M. (2015). Specification of Architecture and Function of Actin Structures by Actin Nucleation Factors. Annual review of biophysics *44*, 285-310.

Slepecky, N., and Chamberlain, S.C. (1985). Immunoelectron microscopic and immunofluorescent localization of cytoskeletal and muscle-like contractile proteins in inner ear sensory hair cells. Hearing research *20*, 245-260.

Soldati, T., and Schliwa, M. (2006). Powering membrane traffic in endocytosis and recycling. Nature reviews Molecular cell biology *7*, 897-908.

Starke, J., Wehrle-Haller, B., and Friedl, P. (2014). Plasticity of the actin cytoskeleton in response to extracellular matrix nanostructure and dimensionality. Biochemical Society transactions *42*, 1356-1366.

Steffen, A., Faix, J., Resch, G.P., Linkner, J., Wehland, J., Small, J.V., Rottner, K., and Stradal, T.E. (2006). Filopodia formation in the absence of functional WAVE- and Arp2/3-complexes. Molecular biology of the cell *17*, 2581-2591.

Suarez, C., Carroll, R.T., Burke, T.A., Christensen, J.R., Bestul, A.J., Sees, J.A., James, M.L., Sirotkin, V., and Kovar, D.R. (2015). Profilin regulates F-actin network homeostasis by favoring formin over Arp2/3 complex. Developmental cell *32*, 43-53.

Svitkina, T.M., Bulanova, E.A., Chaga, O.Y., Vignjevic, D.M., Kojima, S., Vasiliev, J.M., and Borisy, G.G. (2003). Mechanism of filopodia initiation by reorganization of a dendritic network. The Journal of cell biology *160*, 409-421.

Tait Wojno, E.D., and Artis, D. (2012). Innate lymphoid cells: balancing immunity, inflammation, and tissue repair in the intestine. Cell host & microbe *12*, 445-457.

Taylor, M.J., Perrais, D., and Merrifield, C.J. (2011). A high precision survey of the molecular dynamics of mammalian clathrin-mediated endocytosis. PLoS biology *9*, e1000604.

Taylor, R., Bullen, A., Johnson, S.L., Grimm-Gunter, E.M., Rivero, F., Marcotti, W., Forge, A., and Daudet, N. (2015). Absence of plastin 1 causes abnormal maintenance of hair cell stereocilia and a moderate form of hearing loss in mice. Human molecular genetics *24*, 37-49.

ten Klooster, J.P., Jansen, M., Yuan, J., Oorschot, V., Begthel, H., Di Giacomo, V., Colland, F., de Koning, J., Maurice, M.M., Hornbeck, P*., et al.* (2009). Mst4 and Ezrin induce brush borders downstream of the Lkb1/Strad/Mo25 polarization complex. Developmental cell *16*, 551-562.

Tilney, L.G., and Cardell, R.R. (1970). Factors controlling the reassembly of the microvillous border of the small intestine of the salamander. The Journal of cell biology *47*, 408-422.

Tilney, L.G., Cotanche, D.A., and Tilney, M.S. (1992). Actin filaments, stereocilia and hair cells of the bird cochlea. VI. How the number and arrangement of stereocilia are determined. Development *116*, 213-226.

Tilney, L.G., and DeRosier, D.J. (1986). Actin filaments, stereocilia, and hair cells of the bird cochlea. IV. How the actin filaments become organized in developing stereocilia and in the cuticular plate. Developmental biology *116*, 119-129.

Tilney, L.G., Egelman, E.H., DeRosier, D.J., and Saunder, J.C. (1983). Actin filaments, stereocilia, and hair cells of the bird cochlea. II. Packing of actin filaments in the stereocilia and in the cuticular plate and what happens to the organization when the stereocilia are bent. The Journal of cell biology *96*, 822-834.

Tilney, L.G., and Saunders, J.C. (1983). Actin filaments, stereocilia, and hair cells of the bird cochlea. I. Length, number, width, and distribution of stereocilia of each hair cell are

related to the position of the hair cell on the cochlea. The Journal of cell biology *96*, 807-821.

Tilney, L.G., Tilney, M.S., and Cotanche, D.A. (1988). Actin filaments, stereocilia, and hair cells of the bird cochlea. V. How the staircase pattern of stereociliary lengths is generated. The Journal of cell biology *106*, 355-365.

Tilney, L.G., Tilney, M.S., Saunders, J.S., and DeRosier, D.J. (1986). Actin filaments, stereocilia, and hair cells of the bird cochlea. III. The development and differentiation of hair cells and stereocilia. Developmental biology *116*, 100-118.

Tittel, J., Welz, T., Czogalla, A., Dietrich, S., Samol-Wolf, A., Schulte, M., Schwille, P., Weidemann, T., and Kerkhoff, E. (2015). Membrane targeting of the Spir.formin actin nucleator complex requires a sequential handshake of polar interactions. The Journal of biological chemistry *290*, 6428-6444.

Tocchetti, A., Soppo, C.B., Zani, F., Bianchi, F., Gagliani, M.C., Pozzi, B., Rozman, J., Elvert, R., Ehrhardt, N., Rathkolb, B.*, et al.* (2010). Loss of the actin remodeler Eps8 causes intestinal defects and improved metabolic status in mice. PloS one *5*, e9468.

Tokuo, H., Mabuchi, K., and Ikebe, M. (2007). The motor activity of myosin-X promotes actin fiber convergence at the cell periphery to initiate filopodia formation. The Journal of cell biology *179*, 229-238.

Tolias, K.F., Hartwig, J.H., Ishihara, H., Shibasaki, Y., Cantley, L.C., and Carpenter, C.L. (2000). Type Ialpha phosphatidylinositol-4-phosphate 5-kinase mediates Rac-dependent actin assembly. Current biology : CB *10*, 153-156.

Tyska, M.J., Mackey, A.T., Huang, J.D., Copeland, N.G., Jenkins, N.A., and Mooseker, M.S. (2005). Myosin-1a is critical for normal brush border structure and composition. Molecular biology of the cell *16*, 2443-2457.

Tyska, M.J., and Mooseker, M.S. (2002). MYO1A (brush border myosin I) dynamics in the brush border of LLC-PK1-CL4 cells. Biophysical journal *82*, 1869-1883.

Vallance, B.A., Chan, C., Robertson, M.L., and Finlay, B.B. (2002). Enteropathogenic and enterohemorrhagic Escherichia coli infections: emerging themes in pathogenesis and prevention. Canadian journal of gastroenterology = Journal canadien de gastroenterologie *16*, 771-778.

van der Flier, L.G., and Clevers, H. (2009). Stem cells, self-renewal, and differentiation in the intestinal epithelium. Annual review of physiology *71*, 241-260.

Verner, K., and Bretscher, A. (1985). Microvillus 110K-calmodulin: effects of nucleotides on isolated cytoskeletons and the interaction of the purified complex with F-actin. The Journal of cell biology *100*, 1455-1465.

Vignjevic, D., Kojima, S., Aratyn, Y., Danciu, O., Svitkina, T., and Borisy, G.G. (2006). Role of fascin in filopodial protrusion. The Journal of cell biology *174*, 863-875.

Vizcarra, C.L., Kreutz, B., Rodal, A.A., Toms, A.V., Lu, J., Zheng, W., Quinlan, M.E., and Eck, M.J. (2011). Structure and function of the interacting domains of Spire and Fmn-family formins. Proceedings of the National Academy of Sciences of the United States of America *108*, 11884-11889.

Wang, Q., Navarro, M.V., Peng, G., Molinelli, E., Goh, S.L., Judson, B.L., Rajashankar, K.R., and Sondermann, H. (2009). Molecular mechanism of membrane constriction and tubulation mediated by the F-BAR protein Pacsin/Syndapin. Proceedings of the National Academy of Sciences of the United States of America *106*, 12700-12705.

Wayt, J., and Bretscher, A. (2014). Cordon Bleu serves as a platform at the basal region of microvilli, where it regulates microvillar length through its WH2 domains. Molecular biology of the cell *25*, 2817-2827.

Weck, M.L.C., S. W.; Stone, C. R.; Tyska, M. J. (2016). Myosin-7b Promotes Distal Tip Localization of the Intermicrovillar Adhesion Complex. Current biology : CB.

Welch, M.D., Iwamatsu, A., and Mitchison, T.J. (1997). Actin polymerization is induced by Arp2/3 protein complex at the surface of Listeria monocytogenes. Nature *385*, 265-269.

Wellington, A., Emmons, S., James, B., Calley, J., Grover, M., Tolias, P., and Manseau, L. (1999). Spire contains actin binding domains and is related to ascidian posterior end mark-5. Development *126*, 5267-5274.

Woodrum, D.T., Rich, S.A., and Pollard, T.D. (1975). Evidence for biased bidirectional polymerization of actin filaments using heavy meromyosin prepared by an improved method. The Journal of cell biology *67*, 231-237.

Yae, K., Keng, V.W., Koike, M., Yusa, K., Kouno, M., Uno, Y., Kondoh, G., Gotow, T., Uchiyama, Y., Horie, K.*, et al.* (2006). Sleeping beauty transposon-based phenotypic analysis of mice: lack of Arpc3 results in defective trophoblast outgrowth. Molecular and cellular biology *26*, 6185-6196.

Yang, C., and Svitkina, T. (2011). Filopodia initiation: focus on the Arp2/3 complex and formins. Cell adhesion & migration *5*, 402-408.

Yang, Q., Zhang, X.F., Pollard, T.D., and Forscher, P. (2012). Arp2/3 complex-dependent actin networks constrain myosin II function in driving retrograde actin flow. The Journal of cell biology *197*, 939-956.

Yi, K., Unruh, J.R., Deng, M., Slaughter, B.D., Rubinstein, B., and Li, R. (2011). Dynamic maintenance of asymmetric meiotic spindle position through Arp2/3-complex-driven cytoplasmic streaming in mouse oocytes. Nature cell biology *13*, 1252-1258.

Yin, Y., Wang, Y., Zhu, L., Liu, W., Liao, N., Jiang, M., Zhu, B., Yu, H.D., Xiang, C., and Wang, X. (2013). Comparative analysis of the distribution of segmented filamentous bacteria in humans, mice and chickens. The ISME journal *7*, 615-621.

Zampini, V., Ruttiger, L., Johnson, S.L., Franz, C., Furness, D.N., Waldhaus, J., Xiong, H., Hackney, C.M., Holley, M.C., Offenhauser, N.*, et al.* (2011). Eps8 regulates hair bundle length and functional maturation of mammalian auditory hair cells. PLoS biology *9*, e1001048.

Zhao, B., Wu, Z., and Muller, U. (2016). Murine Fam65b forms ring-like structures at the base of stereocilia critical for mechanosensory hair cell function. eLife *5*.

Zhou, K., Sumigray, K.D., and Lechler, T. (2015). The Arp2/3 complex has essential roles in vesicle trafficking and transcytosis in the mammalian small intestine. Molecular biology of the cell.

Zuchero, J.B., Coutts, A.S., Quinlan, M.E., Thangue, N.B., and Mullins, R.D. (2009). p53-cofactor JMY is a multifunctional actin nucleation factor. Nature cell biology *11*, 451-459.